SAND2022-6598

SANDIA REPORT
SAND20XX-XXXX
Printed May 2022

Sandia National Laboratories

GaAs Neutron Response Functions and Radiation Damage Metrics

Patrick J. Griffin, Nicholas Asper, William Charlton

Prepared by
Sandia National Laboratories
Albuquerque, New Mexico
87185 and Livermore,
California 94550

Issued by Sandia National Laboratories, operated for the United States Department of Energy by National Technology & Engineering Solutions of Sandia, LLC.

Available to DOE and DOE contractors from
U.S. Department of Energy
Office of Scientific and Technical Information
P.O. Box 62
Oak Ridge, TN 37831

Telephone: (865) 576-8401
Facsimile: (865) 576-5728
E-Mail: reports@osti.gov
Online ordering: http://www.osti.gov/scitech

Available to the public from
U.S. Department of Commerce
National Technical Information Service
5301 Shawnee Rd
Alexandria, VA 22312

Telephone: (800) 553-6847
Facsimile: (703) 605-6900
E-Mail: orders@ntis.gov
Online order: https://classic.ntis.gov/help/order-methods/

ABSTRACT

The radiation effects community needs clear, well-documented, neutron energy-dependent responses that can be used in assessing radiation-induced material damage to GaAs semiconductors and for correlating observed radiation-induced changes in the GaAs electronic properties with computed damage metrics. In support of the objective, this document provides: a) a clearly defined set of relevant neutron response functions for use in dosimetry applications; b) clear mathematical expressions for the defined response functions; and c) updated quantitative values for the energy-dependent response functions that reflect the best current nuclear data and modelling. This document recaps the legacy response functions. It then surveys the latest nuclear data and updates the recommended response function to support current GaAs damage studies. A detailed tabulation for six of the energy-dependent response functions is provided in an Appendix.

CONTENTS

LIST OF FIGURES

LIST OF TABLES

This page left blank

ACRONYMS AND DEFINITIONS

Abbreviation	Definition
arc-dpa	athermal recombination-corrected dpa
AWE	Atomic Weapon Establishment – a U.K. Ministry of Defense research facility
BCA	Binary collision approximation – a code that treats interactions between an atom and a lattice using single collision approximations for the scattering
cdf	Cumulative distribution function
CIAAW	Commission on Isotopic Abundances and Atomic Weights
dof	Degree of freedom
dpa	Displacement per atom
DD	Deuterium-deuterium – an accelerator-produced reaction that produces ~2.5-MeV neutrons
DFT	Density Functional Theory
DT	Deuterium-tritium – an accelerator-produced reaction that produces ~14-MeV neutrons
ENDF	Evaluated Nuclear Data File
FP	Frenkel pair
FWHM	Full width at half maximum
HBT	Heterojunction bipolar transistor
IUPAC	International Union of Pure and Applied Chemistry
IV	Interstitial-vacancy
kerma	Kinetic Energy Released per unit MAss
kMC	Kinetic Monte Carlo – a type of calculation that addresses defect interactions for times beyond what can be treated in MD codes
KP	Kinchin-Pease
LAMMPS	Large-scale Atomic/Molecular Massively Parallel Simulator – an example of a MD code
LED	Light emitting diode
LET	Linear energy transfer
LSS	Lindhard, Scharff, Schiott
MC	Monte Carlo
MD	Molecular Dynamics – a high fidelity code for modeling the interactions of atoms and molecules bases on the interatomic potentials
NIEL	Non-Ionizing Energy Loss
NRT	Norgett-Robinson-Torrens
pdf	Probability distribution function

Abbreviation	Definition
PKA	Primary knock-on atom – used to describe the primary residual atom emitted in a reaction
rpa	Replacement per atom
SEE	Single event effect
SIA	Self-interstitial atom
SNL	Sandia National Laboratories
ZBL	Zeigler, Biersack, Littmark

1. PURPOSE

The radiation effects community needs clear, well-documented, neutron energy-dependent responses that can be used in assessing radiation-induced material damage to GaAs semiconductors and for correlating observed radiation-induced changes in the GaAs electronic properties with computed damage metrics. The purpose of this document is to: a) clearly define a set of relevant neutron response functions; b) provide clear mathematical expressions for the defined response functions; and c) provide updated quantitative values for the energy-dependent response functions that reflect the best current nuclear data and modelling. In addition, this report details the assumptions and methodology that went into the determination of the characterization. This background data provides an evidence package that the mathematical expressions were correctly implemented. The details provided in this report should also enable others to rederive the values for verification purposes or to easily update the derivation of these response functions in the future as the underlying nuclear data evaluations are further refined by the nuclear data community.

2. FORMALISM FOR DAMAGE METRICS

There are a wide range of metrics used to characterize radiation damage. Table 2-1 summarizes some of the most commonly used metrics within the radiation damage and dosimetry communities. In this table the "calculated" metrics are identified separate from the "applied" metrics and some context is given for the application of each of the damage metrics. In this report we address all seven of the calculated damage metrics described in the table. We provide recommended energy-dependent functional representations for the first five responses. We discuss issues associated with the sixth response and ongoing activity to update this function. We also provide representative calculations for the seventh damage metric – which is a distribution, rather than a scalar quantity, that varies with the incident neutron energy. The "applied" metrics are typically associated with an experimental observable and are often correlated with a calculated metric. An approximation for all of the "applied" metrics can be obtained from a consideration of the calculated metrics, e.g., in the case of dose, by assuming that the dimensions of the material of interest are large enough that charged particle equilibrium can be assumed to exist in the relevant volumes so that the calculated kerma can be used as an approximation of the measured dose.

Most common radiation metrics are described by scalars that represent macroscopic integral quantities, which can be expressed as the convolution of the neutron source term over an energy-dependent microscopic damage response function, $\Re_{type}(E)$. The macroscopic observable, ${}^{facility}D_{type}$, can be expressed as:

$$ {}^{facility}D_{type} = {}^{type}\pounds \cdot {}^{facility}\Phi \cdot \int_0^\infty \phi^{facility}(E) \cdot \Re_{type}(E) \cdot dE \tag{1} $$

In this equation: ${}^{type}\pounds$ is a response unit conversion factor that varies with the selected microscopic damage response; ${}^{facility}\Phi$ is the scalar neutron fluence for the indicated radiation environment; and $\phi^{facility}(E)$ is the unit-normalized energy-dependent neutron spectrum – a probability distribution function that integrates to unity.

The response function for these scalar damage metrics can be further decomposed to better highlight the physics that supports the representation of the damage. As discussed in reference [Gri19], a general formulation of these response functions for neutron damage often takes the form:

$$ \Re_{type}(E) = \sum_{i,j_i} \sigma_{i,j_i}(E) \int_0^\infty dT_{R,j_i} \int_{-1}^{1} d\mu \cdot f\left(E, \mu, T_{R,j_i}\right) \cdot {}^{type-A}\Lambda\left(E_d, {}^{ion}_{type-B/D} T_{R,j_i}\right) \cdot $$

$$ {}^{type-B}\zeta\left(E_d, T_{R,j_i}, {}^{type-D}T_{dam}\right) \cdot {}^{type-C}\xi\left(T_{R,j_i}\right) \tag{2} $$

In this expression the summation is over all reaction channels, *i*, and over all residual charged particles in the outgoing reaction channel, j_i. $\sigma_{i,j_i}(E)$ is the reaction-specific energy-dependent cross section. The two integrals are over the recoil particle energy, T_{R,j_i}, and the angle of particle emission $\mu = cos(\theta)$. $f\left(E, \mu, T_{R,j_i}\right)$ is the energy/angle distribution for the emitted recoil particles. ${}^{type-A}\Lambda\left(E_d, {}^{ion}_{type-B/D} T_{R,j_i}\right)$ is a function that treats the efficiency of the damage near the displacement threshold energy, E_d, e.g., the Norgett-Robinson-Torrens (NRT) treatment [Nor75, Rob82].

${}^{type-B}\zeta\left(E_d, T_{R,j_i}, {}^{type-D}T_{dam}\right)$ is an "effective" generation correction term, e.g., it can take the form of the Robinson damage partition function for displacement damage [Rob69]. ${}^{type-C}\xi\left(T_{R,j_i}\right)$ is a residual damage efficiency correction or defect survival term, e.g., the arcdpa treatment [Nor18a, OECD] which is often applied over the NRT damage energy to account for the physics of athermal recombination corrections to the dpa (arcdpa). The details of the "type" of these various distributions in the respective damage metrics is addressed in Section 4 along with a more detailed discussion of the specific damage metrics in GaAs.

In Equation 2, we also refer to the term, ${}^{ion}_{type-B/D}T_{R,j_i}$. This is a shorthand notation for the functional expression, ${}^{type-B}\zeta\left(E_d, T_{R,j_i}, {}^{type-D}T_{dam}\right)$, the effective damage/defect generation component. We define this shorthand notation to support a more compact representation of the equation since this term appears as a dependent parameter in the ${}^{type-A}\Lambda\left(E_d, {}^{ion}_{type-B/D}T_{R,j_i}\right)$ term.

Some damage metrics represent distributions rather than scalar quantities and must be characterized as a vector or function. Example of this include the recoil energy distribution and the linear energy transfer (LET) metric that are used to characterize single event effects (SEE) in electronics. The incident neutron energy-dependent quantity, the recoil spectrum for the different atoms in the outgoing reaction channel, is a distribution or a vector quantity since there is a different recoil atom energy distribution for every incident neutron energy. The heaviest atom in the outgoing reaction channel is typically called the primary knock-on atom (PKA), but the recoil spectrum can be defined for every incident neutron energy, E, and for each type of outgoing particle in a given reaction channel, here notated as $O_{i,x}$. In this notation, i represents the reaction channel and x represents the outgoing particle in that channel. This probability distribution, ${}^{O_{i,x}}\Theta(T_{R,i,x}, E)$, is a function of the outgoing particle energy, $T_{R,i,x}$, as well as the incident neutron energy, and is defined as:

$$ {}^{O_{i,x}}\Theta(T_{R,i,x}, E) = \sum_{i,j_i} \delta\left[j_i, O_{i,x}\right] \cdot \phi(E) \cdot \sigma_{i,j_i}(E) \cdot \int_{-1}^{1} d\mu \cdot f\left(E, \mu, T_{R,j_i}\right) \tag{3} $$

where, $\delta\left[j_i, O_{i,x}\right]$ is the Kronecker delta function that is zero except when the summation index, j_i, for the outgoing particles in a given reaction channel matches the defined outgoing particle from the indicated reaction channel, $O_{i,x}$, in which case the Kronecker delta value is unity. Note that the Kronecker delta establishes a correspondence between j_i and $O_{i,x}$. In this formulation, identical outgoing particles from <u>different</u> reactions channels are not combined, but identical types of outgoing particles in a <u>given reaction channel</u> are combined, e.g., the alpha particles from the (n, α) and the (n,pα) channel are not combined, but the two alpha particles in a (n,2α) channel are combined.

An LET distribution, for a given incident neutron with energy, E, is used to model single event damage in electronics and is then defined as:

$$ L(E) = \sum_{i,j_i} {}^{GaAs}S\left[T_{R,j_i} \Rightarrow LET\left({}^{A^{j_i}}_{Z^{j_i}}P\right)\right] \mathrm{g}^{O_{i,j_i}}\Theta(T_{R,j_i}) \tag{4} $$

where ${}^{GaAs}S\left[T_{R,j_i} \Rightarrow LET\left({}^{A^{j_i}}_{Z^{j_i}}P\right)\right]$ is the electronic stopping power for a recoil product, P (with atomic mass A^{j_i}, atomic number Z^{j_i}, and recoil energy T_{R,j_i}) in a GaAs lattice. Unlike the recoil particle spectrum (which is particle type specific), this LET metric does reflect an explicit summation over all reaction channels and over all outgoing particles in a given reaction channel, i.e., the LET of different particles in the outgoing channel are added.

Table 2-1. Common Neutron Damage Metrics

Metrics	Units	Comments / Description / Application
Calculated Metrics		
Total Cross Section	b	Quantity captured in the nuclear data file that describes the reaction probability.
Total Kerma	rad(GaAs)	NJOY-2016 quantity [NJOY2016] for the locally-deposited energy produced from reactions described in the nuclear data file and constrained by the kinematics of the reactions.
Displacement Kerma	rad(GaAs)	NJOY-2016 quantity for the local energy deposited in the lattice (broken bonds and lattice phonons) and produced from the reactions described in the nuclear data file using a threshold displacement energy of zero.
Ionizing Kerma	rad(GaAs)	Quantity for the local energy deposition into electrons that is obtained by subtracting the displacement kerma from the total kerma.
NRT Damage Energy	MeV-mb	NJOY-2016 quantity for the damage energy produced from the nuclear data file using the NRT threshold treatment that corrects to reflect the recombination of low energy Frenkel pairs (vacancy/interstial).
1-MeV(GaAs)-Equivalent Damage Energy	MeV-mb	Derived from NJOY-2016 [ASTM722] using an empirically derived efficiency function that is proportional to the recoil atom energy and/or the NRT damage energy for the recoil atom and reflects a normalization of the value of the damage energy in the 1-MeV region to a reference value.
Recoil Atom Distribution	---	A unit normalized probability distribution function (pdf) where the dependent parameter is the energy of the primary recoil atom. This metric is used in the burst generation model for single event effects [Nor98].
Applied Metrics		
Total Dose	rad(GaAs)	Used to measure the response of GaAs calorimeters. Approximated by the calculated total kerma under the assumption that charged particle equilibrium exists.
Displacement Dose	rad(GaAs)	Approximated by the calculated displacement kerma.
NIEL	keV-cm^2/g	Proportional to displacement dose; defined for all incident particles; at high incident energies, includes the effect from nuclear interactions.
1-MeV(GaAs)-Equivalent 1-MeV(GaAs) Fluence	1-MeV(GaAs)-n/cm^2	Derived from 1-MeV(GaAs) damage energy by dividing the damage energy by the reference 1-MeV damage energy, 70 MeV-mb for GaAs.
Ionizing Dose	rad(GaAs)	Used to measure transient response of some GaAs detectors, e.g., photoconductive detectors (PCDs) [Kha09]. Approximated by the calculated ionizing kerma.

Frenkel Pair Density	FP/μ^3	Proportional to the NRT damage energy. Computed using $2*E_d/\beta$, where β is an atomic scattering correction term, to account for the energy per Frenkel pair.
Track Density	Tracks/μ	Used as a fluence monitor. Proportional to the total cross section.
Minority Carrier Recombination Lifetime	μsec	An experimental metric derived from carrier removal rates in bulk materials, lifetime changes in optoelectronics, or gain degradation in heterojunction bipolar transistors (HBTs). Used to unfold the efficiency term that is used to establish the 1-MeV(GaAs) metric.
Displacement per Atom	dpa	Used to correlate with material embrittlement. Proportional to the NRT damage energy.
LET Distribution	[MeV-cm^2/mg] /[particle/cm^2]	Used as a metric in single event damage modes to electronics, e.g., upset, latch-up, and gate rupture. A normalized distribution derived from the recoil atom energy distribution multiplied by the electronic stopping power. The dependent parameter is the LET, typically with units of MeV-cm^2/mg.

3. NEUTRON DATA SELECTION

The legacy ASTM E722 displacement damage response function was developed in 1991 and used the "then current" ^{nat}Ga cross section files as characterized in the ENDF/B-VI library [ENDF6] and the ^{75}As cross section as characterized in the ENDL-84 library [ENDL84]. The absence of photon production files (MF12/MF13/MF14/MF15) and product energy/angle distributions files (MF6) for the residual atom spectra in these legacy evaluations limited the fidelity in the modeling for the displacement damage metrics. In this 2022 update to the response functions, we sought to use the highest-fidelity community-consensus values for all components of the underlying nuclear data. The following subsections: a) address the various underlying components of the nuclear data that were selected; b) address the rationale for the selection of the recommended values; and c) document the recommended sources for the selection of the nuclear data.

3.1. Natural Abundance and Atomic Weights

Table 3-1 shows the latest natural abundance and isotopic mass data for the constituents of GaAs and indicates the recommended sources for this data.

Table 3-1. GaAs Isotopic Composition Data

Isotope	Natural Abundance [atom %] [CIAAW]	Isotopic Atomic Mass Excess [μamu] [AME2020]	Isotopic Atomic Mass [amu] [AME2020]	Elemental weight value or range [amu] [Abn16, CIAAW]
^{69}Ga	60.108 (50)	-69327.8 (12)	68.9255735 (13)	69.723 (1)
^{71}Ga	39.892 (50)	-70139.1 (8)	70.9247026 (9)	
^{75}As	1.00	-73034.2 (9)	74.9215946 (9)	74.921595 (6)
Numbers in parentheses indicate the absolute uncertainties in the trailing digits, e.g., 60.1079 (62) corresponds to 60.1079 ± 0.0062.				

The recommended elemental atomic weights are taken from the International Union of Pure and Applied Chemistry (IUPAC) Commission on Isotopic Abundances and Atomic Weights (CIAAW) [CIAAW]. These data represent revisions made by the CIAAW in 2020 and published in the Pure and Applied Chemistry. The recommended atomic weights for individual isotopes are taken from the recommendations of the Atomic Mass Data Center and are represented by the Atomic Mass evaluation 2020 (AME2020) [AME2020]. The natural isotopic abundance data are also required in order to convert the densities of target materials into the number densities of the constituting isotopes. The recommended natural abundance data come from the CIAAW recommendations that are documented in the IUPAC Technical Report. Since the natural abundance data can reflect a range depending upon the location where the sample was taken, the values cited here represent what the IUPAC indicates represents the best measurement of isotopic abundances from a single terrestrial source.

3.2. Displacement Threshold Energy

The **displacement threshold energy**, E_d, is defined to be the minimum kinetic energy, imparted to the primary recoil atom, that will result in the enduring displacement of the resulting lattice atom (identical to the target lattice atom in the case of an elastic or inelastic event). Since there is an angle-dependence to this value, the quoted value often corresponds to an angle-averaged value.

3.2.1. Literature Values

Table 3-2 shows some values for the displacement threshold energy as drawn from various sources in the literature. Values are divided into two categories, those derived from experiments and those developed from modeling. The OECD Primary Damage report [OECD] summarizes the status of the displacement threshold energy for GaAs as:

> "In GaAs experiments indicated that the minimum threshold energy is about 10 eV on both the Ga and As sublattices [Lehmann, 1993; Hausmann, 1996]. Classical MD simulations gave exactly the same result, and also indicated that single recoils of 15 eV can produce directly antisite defects in the material [Mattila, 1995]."

It should also be noted that a displacement threshold energy of 10 eV was used in the legacy ASTM E722 damage function.

Table 3-2. GaAs Displacement Threshold Energy Data

Lattice Atom	Experimental Range (eV)		Calculated Range (eV)	
	Value	Reference	Value	Reference
either	9	[Sa95] from DLTS measurements	13 ± 1 (avg) [8 – 28]	[Ch17]
either	10 ± 0.7	[Ba90]		
Ga			13.75	[Ga17]
As	7 - 11	[Po81]	14.3	[Ga17]
As			[10 – 20]	[Sa95]

3.2.2. Effective Displacement Energy for Polyatomic Materials

The recommended method for setting a displacement threshold energy for polyatomic materials is described by Ghoniem and Chou [Gh88] as: $E_d^{eff} = \left[\sum_i \frac{S_i}{E_d^i} \right]^{-1}$ where S_i and E_d^i are the stoichiometric fraction and threshold displacement energy for the i^{th} atomic species.

3.2.3. Adopted Value for the Displacement Threshold Energy

Given this background data on calculations and measurements, and in view of the variability seen in the literature, the angle-dependence of this quantity based upon the lattice atom positions, and the role that this quantity plays in the modeling of the damage metrics, we have elected to use a value of 10 eV for E_d in this development of recommended response functions.

3.3. Neutron Cross Section Evaluations

One of the most critical decisions in the development of the neutron response functions is the selection of the cross-section library used to characterize the neutron interaction with the lattice atoms. Whereas the legacy cross sections used in the 1991 work, and as reported in ASTM E722 [ASTM722], only had elemental evaluations available, and the nuclear data evaluations at that time did not typically provide the MF6 files that characterize the residual atom energy spectra, the newer evaluations now available represent isotopic evaluations and provide us with much higher fidelity nuclear data evaluations that we can use in the generation of the response functions.

Table 3-3 shows the nuclear data evaluations that we have selected as a result of our investigation. The following subsections address the nuclear data evaluations that were available and considered for the three isotopes of interest in GaAs and provide the details that supported this cross section recommendation.

Table 3-3. Selected GaAs Cross Section Data

Isotope	Selected Cross Section Evaluation
^{69}Ga	TENDL-2019
^{71}Ga	TENDL-2019
^{75}As	ENDF/B-VIII.0

Note that some modern nuclear data evaluations, such as the TENDL-2019 evaluations, cover an incident neutron energy range up to 200 MeV. However, in evaluations that go up to these high neutron energies, the discrete reaction channels are often only defined below ~20-MeV or ~30-MeV. Above that energy, the various reaction channels are lumped into a composite MF=3/MT=5 cross section and the MF=6/MT=5 entries provide composite representations the resulting recoil atom energies in this composite outgoing reaction channel. Because of this change in the format in which nuclear data is provided, and because of the modeling approaches/assumptions used in the nuclear data processing codes to capture the relevant physics for the response functions, some damage metrics can show an artificial discontinuity at this ~20-30 MeV boundary. This artifact, that can arise in the processed damage metrics, does not necessarily reflect an error in the nuclear data provided within the evaluation. Rather, it reflects an insufficiency in the level of details provided in the nuclear data evaluation or an inadequacy in the fidelity of the processing model used to convert the underlying nuclear data into the desired damage metric, e.g., lack of information on the correlation of outgoing particles in a given reaction channel.

While the TENDL-2019 ^{69}Ga and ^{71}Ga evaluations go up to 200 MeV, the ^{75}As ENDF/B-VIII.0 evaluation only goes up to 20-MeV. In our analysis, we use a 770-group SAND-IV energy group structure for a multigroup representation of the response functions and the SNL-NJOY-2016 code to process the nuclear data evaluations. This 770-group structure is an extended version of the 640-group SAND-II energy structure that went up to 20-MeV and this extended energy group structure goes up to 150 MeV. However, since the ENDF/B-VIII.0 ^{75}As evaluation only goes up to 20-MeV, the GaAs response functions presented here are not valid above the 20-MeV supported for the ^{75}As interactions. In general, the ^{69,71}Ga supplied data in figures and tables are truncated to reflect this upper 20-MeV energy limit for the composite response functions.

3.3.1. ^{69}Ga

Isotopic ^{69}Ga cross sections are found in recent ENDF/B-VIII.0, JEFF 3.3, JENDL 4.0, and TENDL-2019 libraries. The ENDF/B-VIII.0, which uses a January 2005 evaluation, and JENDL 4.0 evaluation, which uses a March 1994 evaluation, are both based on evaluations by Watanabe and are very similar in detail. A major issue with both of these evaluations is that they do not have any MF=6 energy/angle distributions nor MF=12/14 photon production files and, hence, forces our SNL-NJOY-2016 [SNLNJOY16] response metric analysis to rely upon the use of the kinematic-based models rather than the use a more detailed direct reaction-dependent kerma calculation. Older versions of the ENDF/B library were considered, but, in addition to the lack of MF=6/12/14 files,

they were also found to only have an elemental evaluation rather than an isotopic evaluation and, hence, were also deemed unacceptable. The TENDL nuclear data evaluations rely almost exclusively upon calculations, but, due to this model-based derivation, they do include MF=6 energy/angle product distributions and MF=12/14 photon production files as a well as MF=33 reaction covariance files. The TENDL-2019 library [Kon19] represents the most recent release of this library. The TENDL-2019 library was based upon calculations using the TALYS code [Kon12]. The JEFF 3.3 cross section (a January 2018 release) [JEFF3] is found to be taken from the earlier TENDL-2015 library. JEFF's adoption of this library implies that some detailed comparison of the calculated cross sections with available experimental data has been performed.

In order to evaluate the sensitivity of the damage metrics to the source of the cross sections, Figure 3-1 compares the neutron energy-dependent displacement kerma, as calculated with the SNL-NJOY-2016 code using the 770-group SAND-IV energy structure (an extended version of the 640-group SAND-II energy structure that goes up to 150 MeV). The nuclear data evaluations compared during this evaluation included ENDF/B-VIII.0, JENDL 4.0, TENDL-2019, and JEFF 3.3 ^{69}Ga isotopic nuclear data evaluations. For comparison with the legacy work, a comparison was also included with the ^{nat}Ga elemental ENDF/B-VI nuclear data evaluation. Since the ^{nat}Ga ENDF/B-VI displacement kerma is an elemental kerma and not a ^{69}Ga isotopic kerma as are the other curves, this curve was only included in this figure to permit a comparison with legacy work reflected in the ASTM E722 response. One cannot draw any firm conclusion regarding differences observed between the new isotopic ^{69}Ga displacement kerma and the elemental ^{nat}Ga legacy kerma. A valid comparison requires a comparison of like quantities and must be based upon a comparison of the composite of the new isotopic Ga displacement kerma. This comparison is presented in Section 8.

Since the logarithmic scale of the y-axis in Figure 3-1 makes it difficult to see small differences in the curves, we adopted the TENDL-2010 evaluation as the reference baseline evaluation and Figure 3-2 shows ratios of the other displacement kerma, as derived from the other new nuclear data evaluations, to the baseline TENDL-2019 displacement kerma. The variation in the displacement kerma for neutron energies greater than 1 keV is seen to be relatively small. However, considerable variation can be seen in the (n,γ) capture displacement kerma contribution that dominates the displacement kerma ratio at low neutron energies.

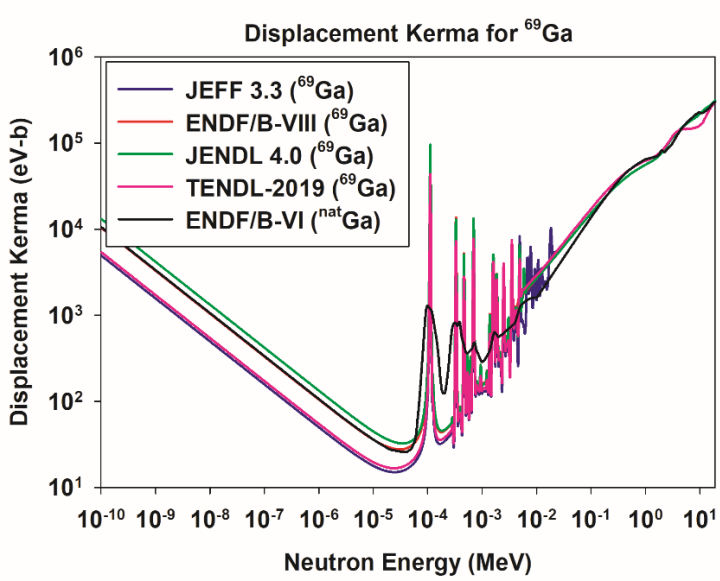

Figure 3-1. ^{69}Ga Displacement Kerma from Various Nuclear Data Evaluations

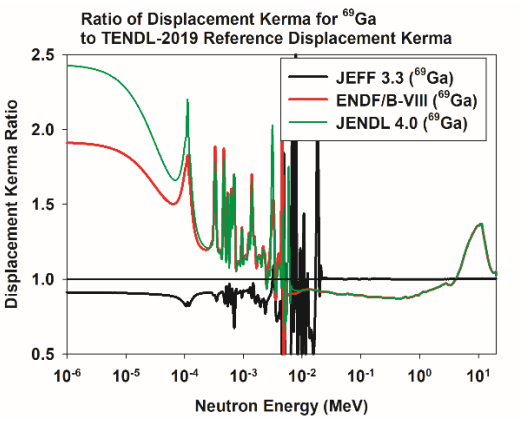

a) Total Energy Range

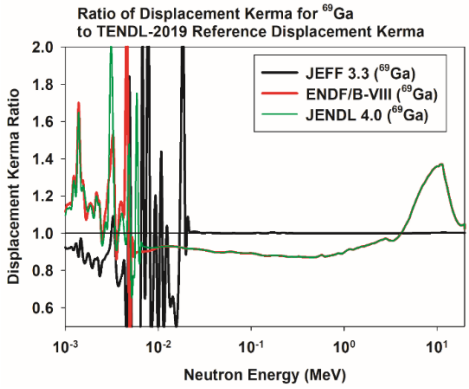

b) High Energy Region

Figure 3-2. Ratio of ^{69}Ga Displacement Kerma for Various Nuclear Data Evaluations to a Baseline Reference from TENDL-2019 Evaluation

The reference baseline nuclear data evaluation that we adopted for the ^{69}Ga cross section was the TENDL-2019 evaluation. Considerations supporting this selection included:

- It has MF=6 energy/angle distributions and MF=12/14 photon production files;
- The TENDL-2015 version was adopted in the JEFF 3.3 evaluation. Figure 3-2 shows that it is in excellent agreement with the adopted TENDL-2019 reference evaluation. The JEFF evaluation process is presumed to have had an evaluator compare the detailed nuclear data calculations with the available experimental database found in EXFOR [Otu14], but comments in the nuclear data evaluation and in the cited references are not typically sufficient to define the extend of the data comparison. This addresses some of the concern about using an evaluation that was derived solely based upon nuclear model calculations and lends credence to the position that an evaluator has made adequate comparisons between calculations and available experimental data.
- The TENDL-2019 represents an improvement/refinement over the TENDL-2015 library.

Using this TENDL-2019 nuclear data evaluation as the reference cross section evaluation, we next verify that this selection did not reflect any unexpected issues by examining some of the more detailed aspects of the data consistency.

3.3.1.1. Characterization of the Completeness and Fidelity of the Reaction Channels Considered

One element of a verification of the data processing is an examination of the contributions from various reaction channels to the total cross section. Figure 3-3 shows the energy-dependence of the main reaction channels. The figure is divided into two plots so that the total energy dependence can be illustrated while also providing a detailed comparison of the high energy reactions in the 1 – 20 MeV region. Figure 3-4 shows the same information, but here, to more clearly illustrate the importance of the different reaction channels, the cross sections are represented as a fraction of the total cross section, as a function of the incident neutron energy, and are depicted with a linear rather than a logarithmic y-axis.

The reaction channels addressed in the figures can be broken into four categories: elastic, inelastic, disappearance, and "other". The difference between the disappearance and the "other" reaction categories is that the disappearance category does not have a neutron in the outgoing reaction channel along with residual ions. This classification of reaction channels is used because it is reflected in the classification of the kerma components as processed by the NJOY-2016 code. The main ^{69}Ga reaction channels, along with the corresponding threshold energy, are:

- Elastic, MT2
- Inelastic, MT4 (sum of MF51-90 discrete and MF91 continuum)
- Disappearance channels:
  - Capture, MT102, (n,γ)
  - MT103, (n,p), E_{th} = 0.129478 MeV
  - MT107, (n, α), E_{th} = 0 MeV {the first datapoint is at 10^{-11} MeV}
  - MT22, (n,2α), E_{th} = 4.55475 MeV
- Other channels:
  - MT16, (n,2n) , E_{th} = 10.4641 MeV
  - MT28, (n,np) , E_{th} = 6.70641 MeV

Other high threshold energy reaction channels (within the disappearance and "other" category) are represented in the TENDL-2019 nuclear data evaluation, but, in order to help the reader differentiate between the set of curves, and because these channels either have a small cross section or a high threshold energy, they are not placed in the plots below. The high threshold reaction channels excluded from the plot, along with the corresponding reaction threshold energy, include:

- MT5, a sum of reactions not given explicitly in another MT. This reaction channel is used to capture the very high threshold channels, E_{th} = 30. MeV. It is also often used to capture the content of reactions, other than the elastic and total cross section, in the energy region > 30 MeV.
- MT11, (n,2nd), E_{th} = 21.9523 MeV
- MT17, (n,3n), E_{th} = 18.8635 MeV
- MT24, (n,2nα), E_{th} = 14.6102 MeV
- MT25, (n,3nα), E_{th} = 22.6422 MeV
- MT29, (n,n2a), E_{th} = 11.4446 MeV
- MT32, (n,nd), E_{th} = 14.7966. MeV
- MT33, (n,nt), E_{th} = 15.6035 MeV
- MT34, (n,n^{3}He), E_{th} = 18.2642 MeV
- MT41, (n,2np), E_{th} = 17.0538 MeV
- MT42, (n,3np), E_{th} = 24.2094 MeV
- MT44, (n,n2p), E_{th} = 16.829 MeV
- MT45, (n,npα), E_{th} = 12.1175 MeV
- MT104, (n,d), E_{th} = 4.44929 MeV
- MT105, (n,t), E_{th} = 8.44781 MeV
- MT108, (n,2α), E_{th} = 4.75055 MeV
- MT111, (n,2p), E_{th} = 10.4176 MeV
- MT112, (n,pα), E_{th} = 5.93021 MeV

- MT115, (n,pd), E_{th} = 14.5718 MeV
- MT116, (n,pt), E_{th} = 17.4892 MeV
- MT117, (n,dα), E_{th} = 9.86041 MeV

The above threshold energies for the reactions refer to a discrete cross section entry in the nuclear data file, typically associated with a zero cross section, but a point that serves as the lowest energy for interpolation purposes of non-zero cross sections at higher energies.

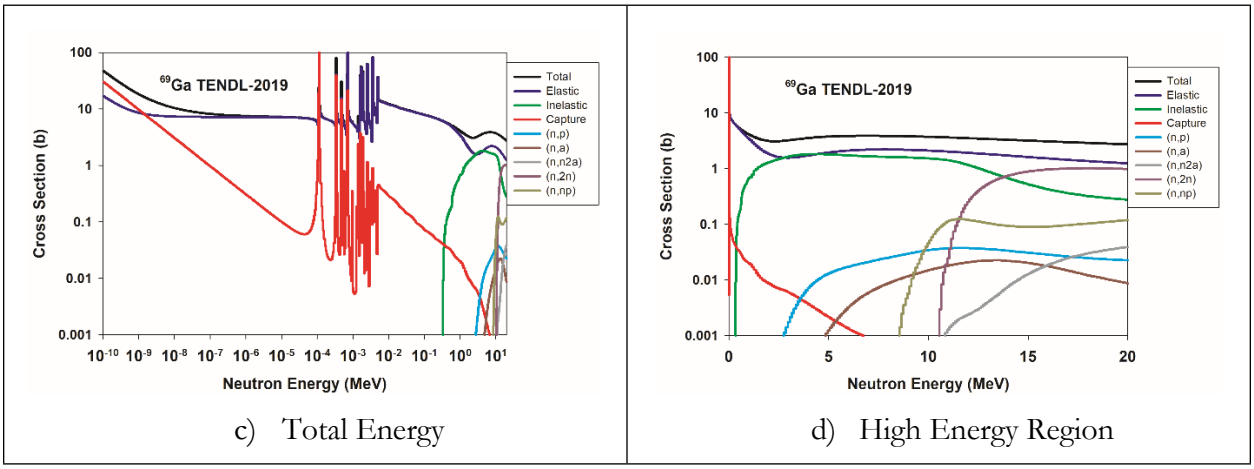

Figure 3-3. Contributions of Reaction Channels to the ^{69}Ga TENDL-2019 Cross Section

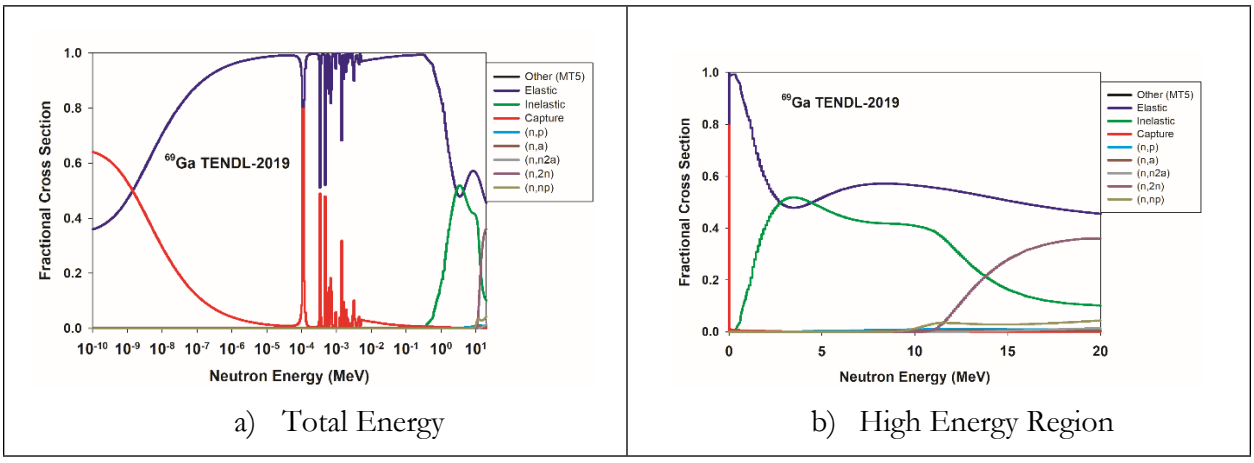

Figure 3-4. Fractional Contributions of Reaction Channels to the ^{69}Ga TENDL-2019 Cross Section

3.3.1.2. Characterization of the Photon Energy Emission

We next examine the consistence of the photon emission representation for this TENDL-2019 nuclear data evaluation. Figure 3-5 compares the ratio of the total kerma to the kinematic kerma limit. This provides a test of the energy conservation found within the nuclear data evaluation. If the ratio is greater than unity, then there is an issue with the energy balance – an issue that is probably due to a poor representation of the emitted photon spectrum for some reaction channels. Here, for the TENDL-2019 evaluation, we see a fairly good energy balance, i.e., the kerma never significantly exceeds the kinematic kerma limits, but it does show some moderate energy conservation violations in the 5 – 30 MeV region. Because of these energy conservation violations, and in light of the fact that the calculated kerma should never be greater than the SNL-NJOY-2016 calculated kinematic

kerma limit, we elected to over-ride the total kerma with the kinematic kerma limit in our development of the various response functions that depend upon the total kerma.

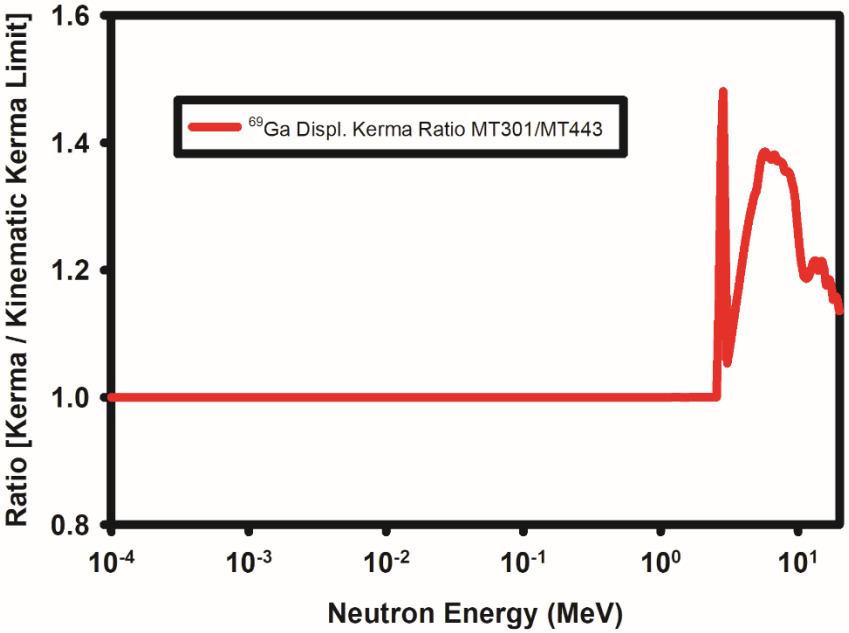

Figure 3-5. Ratio of ^{69}Ga Total kerma (MT=301) to the Kinematic Kerma Limit (MT=443) Using the Reference TENDL-2019 Evaluation

3.3.1.3. Representation of the Recoil Spectra

Another criterion that influences the selection of the nuclear data evaluation used for the cross section selection is the fidelity and consistency of the recoil atom spectra. While the TENDL-2019 nuclear data evaluation has a MF6 file characterization of the recoil atom spectra – an attribute that is desired in modeling the displacement damage metrics, an inspection of the properties and trends in the recoil spectra is a good verification step in accepting a recommended cross section. The following subsections document some of the inspection steps for the recoil atom spectra that were carried out.

3.3.1.3.1. *Elastic Scattering*

A useful verification test of the nuclear data evaluation's characterization of the recoil spectrum is to examine the recoil spectrum from the elastic scattering channel. For elastic scattering, conservation of momentum and energy results in a maximum energy transfer to a lattice atom given by:

$$E_{recoil} = \frac{4 \cdot A \cdot E_n}{(A+1)^2} \tag{5}$$

where E_n is the energy of the incident neutron and A is the atomic weight of the lattice atom when expressed in units of the neutron mass. ^{69}Ga has an atomic mass of 68.9255735 amu and the neutron mass is 1.008664916 amu, so the appropriate value of A to use in the formula is 68.33346973.

Table 3-4 shows the maximum recoil energy that should result from elastic scattering for various incident neutron energies. A requirement for the creation of a Frenkel pair under the Kinchin-Pease [Kin55] threshold treatment is for the lattice recoil damage energy in ^{69}Ga to be equal to the displacement threshold energy of 10 eV. Note that, according to the Kinchin-Pease treatment of the threshold displacement, this 10 eV is the damage energy and not the minimum recoil atom energy. Since, within the Kinchin-Pease formalism, the recoil energy is related to the damage energy by the expression $(2gE_d)/\beta$, where β=0.8 represents an atomic scattering correction term, the 10-eV damage energy corresponds to a minimum recoil atom energy of 25-eV. For an elastic scattering reaction this corresponds to a minimum incident neutron energy of ~440 eV in order to create a Frenkel pair (assuming use of the NRT displacement threshold treatment, which is addressed in Section 5.3).

Table 3-4. Maximum Recoil Energy for Neutron Elastic Scattering on ^{69}Ga

Incident Neutron Energy	Maximum Elastic PKA Recoil Energy
100 eV	5.68601 eV
175.87 eV	10. eV
439.7 eV	25. eV
1 keV	56.8601 eV
10 keV	568.601 eV
100 keV	5.68601 keV
1 MeV	56.8601 keV
10 MeV	568.601 keV
14 MeV	796.0414 keV
20 MeV	1.1372 MeV

Figure 3-6 shows the elastic recoil spectrum for several incident neutron energies. The shapes for the normalized recoil spectra are seen to be consistent with a sharp high energy cut-off energy – as expected from equation 5 and the conservation of energy and momentum in the kinematics from this reaction.

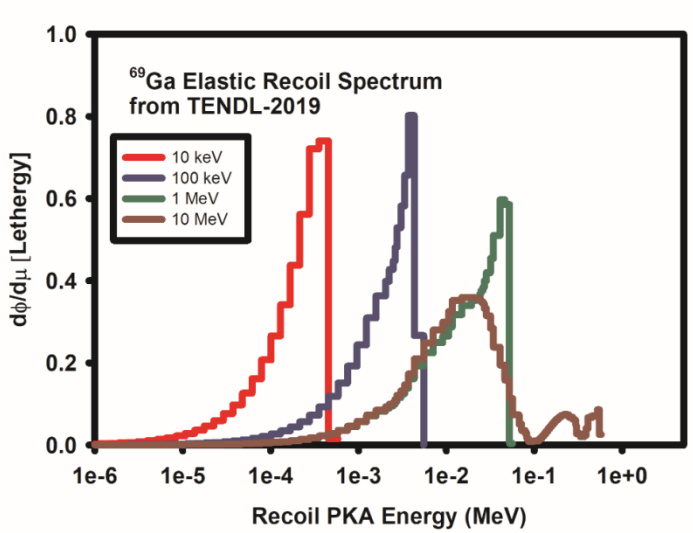

Figure 3-6. TENDL-2019 Characterization of the Recoil Spectrum for Elastic Scattering on ^{69}Ga

An inspection of the 10-MeV recoil spectrum in Figure 3-6 shows that it has a much more complex energy-dependent shape than is seen in the lower energy neutron recoil distributions. It still shows the expected upper sharp maximum, but it also shows much more structure in the lower energy recoil distribution. This is probably attributed to the more forward peaked angular distribution for elastic scattering seen in the high energy elastic scattering. Figure 3-7 shows the elastic scattering angular distribution. At low energy the recoils are fairly isotropic. However, at high incident neutron energies, the angular distribution shows a sharp forward peak (cosine is 1 at 0 degrees). The multiple peaks in the angular distribution can be mapped into the energy-dependent structure seen in the recoil distribution.

Figure 3-7. TENDL-2019 Characterization of the Total Angular Distribution for Elastic Scattering on ^{69}Ga

3.3.1.3.2. *Total Recoil Spectrum*

In addition to looking at the elastic channel, it is also useful to inspect the behavior of the total recoil atom energy distribution. Figure 3-8 shows the ^{69}Ga total recoil spectrum at several incident neutron energies. At low energies, the elastic scattering is the dominant reaction channel and the recoil spectra are similar to those seen in Figure 3-6 for elastic scattering. However, the multiple reaction channels that are open at high incident neutron energies give rise to a much more complex PKA recoil spectrum. A comparison of the total recoil spectra with those shown for just the elastic scattering channel is consistent with the expected magnitude of the various reaction channels addressed in the previous section.

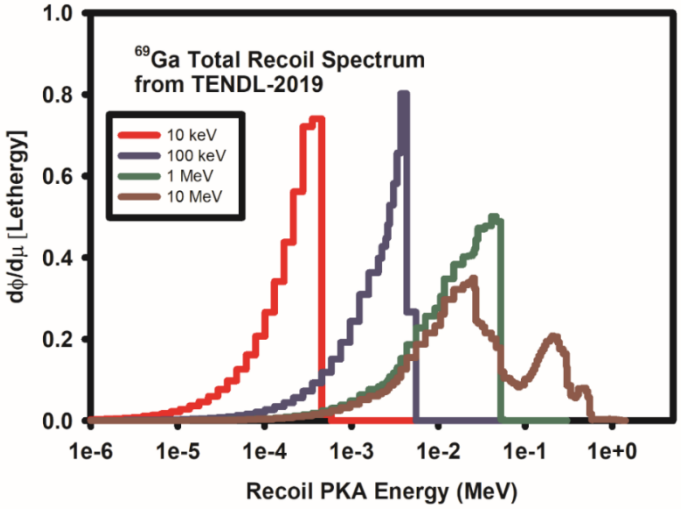

Figure 3-8. TENDL-2019 Characterization of the Total Recoil Spectrum on ^{69}Ga

3.3.1.3.3. *Average Recoil Energy*

Another verification step for the nuclear data evaluation is an examination of the recoil atom energies for the separate reaction channels. One approach to examining the reaction-dependent recoil spectra is to use the SNL-NJOY-2016 code with an interface to the SPKA-2020 code (which represents a minor modification of the SPKA6C code developed by S. Simakov [Sim07). This approach basically processes the NJOY-produced multigroup information which, in turn, is based upon the information found in the MF6 file for the various reaction channels. Table 3-5 shows the average recoil energy for different reaction channels at selected incident neutron energies.

The only drawback in this approach is that the processing only works for reactions where there is a MF6 entry in the nuclear data evaluation. This approach cannot typically be directly applied to the gamma capture reaction since, for this reaction channel, only the emitted photon spectrum is directly characterized in MF6 and reaction kinematics considerations must be used to derive an approximation of the recoil atom energy spectrum for the capture gamma reaction. Furthermore, when multiple photons are emitted, a rigorous derivation of the consistent recoil atom spectrum requires that information is also supplied on the angular correlation between the emitted photons. This angular correlation data is not supported by the present ENDF-6 format used to characterize the nuclear reaction data.

Table 3-5. Average Recoil Energy for Different Reaction Channels from Neutrons Incident on ^{69}Ga

Incident Neutron Energy	PKA Recoil Energy (keV)								
	Reaction Channel								
	Total (MT1)	Elastic (MT2)	Total Inelastic (MT4)	Continuum Inelastic (MT91)	(n,p) (MT103)	(n,α) (MT107)	(n,nα) (MT22)	(n,np) (MT28)	(n,d) (MT104)
10 keV	0.282	0.282	--	--	--	136.0	--	--	--
100 keV	2.95	2.95	--	--	--	150.0	--	--	--
1 MeV	22.59	21.8	20.45	---	22.0	206.2	---	---	---
10 MeV	75.46	43.0	106.1	99.1	214.1	655.2	433.7	188.4	188.6

One alternate approach to examining the reaction-dependent recoil energy, an approach that allows us to verify the interpretation of the recoil spectra, is to over-ride the damage partition function so that all of the energy in the outgoing reaction products is reported in the SNL-NJOY-2016 damage energy computation and then to extract the "averaged" PKA recoil energy by dividing the modified MT444 damage energy, which now captures all of the recoil energy, by the total cross section. Figure 3-9 shows this effective recoil damage energy as a function of the incident neutron energy. The data trends here are smooth and consistent with the SPKA-2020 analysis of the MF6 data. For example, at 1-MeV the cross section is almost totally due to elastic scattering and the Figure 3-9 average recoil energy is 22.6 keV – which is nearly identical to the Table 3-5 entry of 22.59 eV.

When this same comparison is conducted for the 10-MeV incident neutron energy, however, the comparison is not as good – the "full recoil" curve in Figure 3-9 is showing a significantly larger recoil energy that Table 3-5 (187 keV versus the expected 75.46 keV). However, the explanation for this difference is that Table 3-5 only represents the energy from the primary recoil atom while Figure 3-9, given the methodology used, sums the energies of **all** of the outgoing charged particles – and the large energies associated with the outgoing proton and alpha particle bias the comparison.

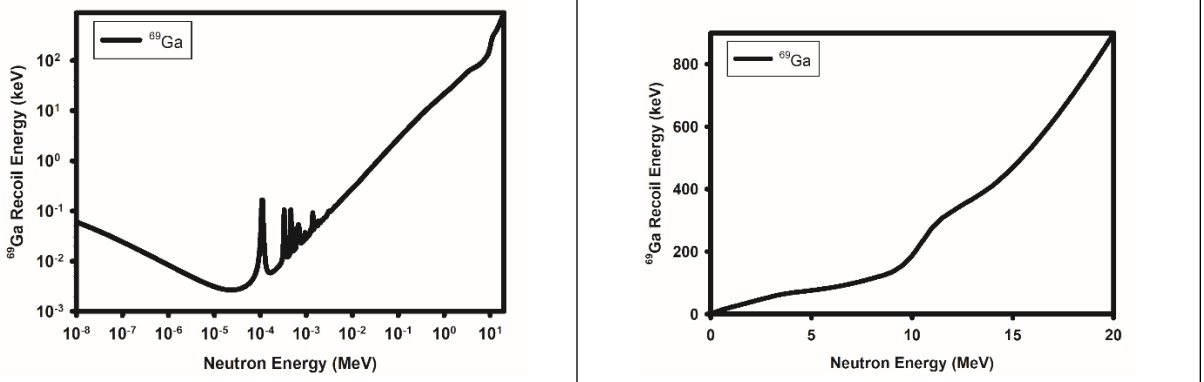

a) Logarithmic Energy Axis

b) Linear Energy Axis

Figure 3-9. Effective Recoil Energy (from all outgoing particles) for Neutrons Incident on ^{69}Ga

In order to ensure that this explanation for the difference between the results from the two analysis approaches is valid, we made further modifications to the SNL-NJOY-2016 code so that we could tally in the MT444 damage energy (over-ridden by the recoil energy) only the contributions from heavy recoil atoms, i.e., outgoing recoil atoms with a mass greater than the lattice atom minus an alpha particle, i.e., >69-4=65. Note, in this modification we only changed which recoil particles could contribute to the damage energy tally metric – we did not change the total cross section used to renormalize the damage energy metric. Thus, for the (n,α) channel, the total reaction probability was properly addressed but only the recoil from the heavy PKA recoil atom was counted in the treatment of this reaction channel.

Using this modified approach, the results of the recoil energy estimate from the SNL-NJOY-2016 analysis approach now more accurately represent an average true PKA recoil energy. These results are shown in Figure 3-10. To support the comparison with the curves shown in Figure 3-9, Figure 3-10 shows curves for both the total recoil energy (summing over all particles in the outgoing reaction channel and using a curve label of "All Recoils") as well as just the PKA atom recoil energy (when is has a mass greater than 65, using a curve label of "PKA>65"). Now, for the 10-MeV incident neutron energy, the modified SNL-NJOY-2016 recoil energy is computed to be 70.70 keV – which is in acceptable agreement with the SPKA-2020 value of 75.46 keV.

Although the recoil energy comparison between two calculational approaches for high incident neutron energies, once modified to only compare the PKA recoil energies, was deemed to be "acceptable", it is still important that we understand the source of the remaining difference. We note that the modified (i.e., modified by rejecting the proton and alpha particle recoil energy) SNL-NJOY-2016 algorithm produces a recoil energy that are slightly lower than the SPKA-2020 recoil energy. The explanation for the difference can probably be attributed to the fact that the SPKA-2020-based approach only summed the primary recoils from a specific subset of reactions. In particular, it did not account for reactions where there were three or more particles in the outgoing channels. Since the modified NJOY-2016 approach counted all the recoil atoms that had a mass > 69–4=65, reactions such as the (n,dα) channel with a threshold of 9.86 MeV, the (n,2α) channel with a threshold of 4.75 MeV, and the (n,pα) channel with a threshold of 5.9 MeV, were discounted as they produce a primary recoil atom whose mass fell below the required mass. We further note that at incident neutron energies greater than 10 MeV, the (n,n2α), an important reaction as depicted in Figure 3-3 and 3-4, may also play a role, and this reaction would have an even smaller PKA mass and would also have been rejected in the SNL-NJOY-2016 damage metric approach. Other reaction channels, such as the (n,nα) channel with a threshold of 11.4446 MeV, may have smaller contributions to the cross section but would also not have been included in the calculation. Due to the threshold energy, this reaction would not have affected this comparison at 10-MeV incident neutron energy, but it would affect the comparison at higher neutron energies.

If we use the modified SNL-NJOY-2016 approach but recalculate the recoil energy counting all recoil atoms that have a mass greater than or equal to >69-9=60, we address most of the neglected channels discussed above, i.e., we artificially remove fewer of these reaction channels from the SNL-NJOY-2016 analysis approach making it more consistent with the SPKA-2020 approach. This recoil energy curve is also depicted in Figure 3-10, labeled as PKA>60. When we use this additional modification to the SNL-NJOY-2016 calculation, we obtain, for a 10-MeV incident neutron, an average recoil energy value of 73.3 keV – which is in much better agreement with the SPKA-2020 value of 75.46 keV, but it is still slightly discrepant.

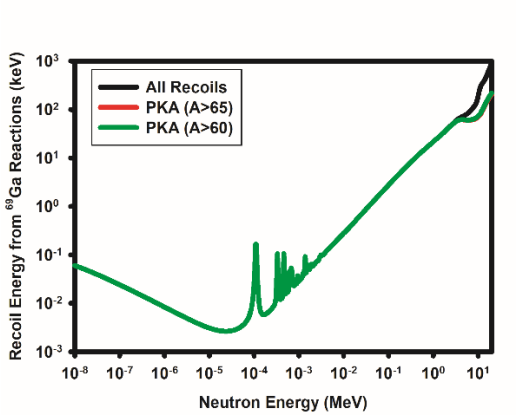

a) Logarithmic Energy Axis

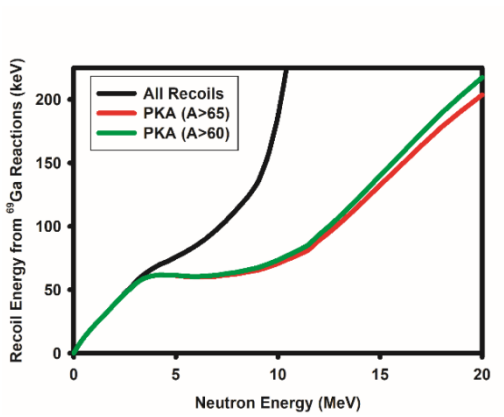

b) Linear Energy Axis

Figure 3-10. Sensitivity of the Effective ^{69}Ga Recoil Energy to the Mass of Outgoing Particles Counted

Since we have addressed the SNL-NJOY-2016 limitations by adjusting the acceptable mass for the PKA, we next looked more closely at the SPKA-2020 analysis. An inspection of the SPKA-2020 computational methodology shows that it has a limitation in that it only looked at, i.e., averaged – with the caveat that it divided by the corresponding cross section – the recoil energy for the PKA from a discrete set of reaction channels as shown in Table 3-5. This set of SPKA-2020 reaction channels did not consider the (n,2n) channel that has a threshold, in ^{69}Ga, of less than 10-MeV and this reaction channel did contribute to the SNL-NJOY-2016 PKA recoil energy estimate. The SPKA-2020 code also is not currently configured to address the significant (n,n2α) reaction channel. As another example, it is observed that, as previously indicated, the SNL-NJOY-2016 modified approach only adjusts the energy tallied in the damage energy metric and does not alter the overall cross section that is used to renormalize the output damage energy metric. Thus, in the first modified case, where we considered recoil atoms with a mass >69-4=65, the (n,dα) would have had no recoil energy at all tallied but this reaction would still have been included in the SNL-NJOY-2016 cross section normalization. In the second updated calculation, when we consider all outgoing particles with mass >69-9=60, the primary PKA from this reaction now contributes to the damage energy tally. This improves the fidelity of the average PKA recoil energy estimate in that we are still addressing just the "primary" recoil atom from a reaction channel, but are now addressing a wider range of reactions. However, we note that the SPKA-2020 approach, as shown in Table 3-5, does not include this reaction channel in its analysis. So, we still have a difference in what is being compared between the two approaches.

Thus, we can conclude that the remaining discrepancy, i.e., 73.3 keV versus 75.46 keV for an incident neutron energy of 10-MeV, can probably be attributed to the fact that the two approaches, SPKA-2020 versus SNL-NJOY-2016, are still not considering an identical set of reaction channels. While one can continue to make modifications to the codes to more closely align the output quantities for these two approaches, a better approach is to address the deficiencies in the approaches rather than merely strive to make the available metrics reflect identical assumptions. Accordingly, plans have been made to extend the SPKA-2020 code so that, in the future, it can: a) treat all reaction channels for which there is a MF6 file entry in the nuclear data file; b) supplement this analysis with the inclusion of the (n,γ) reaction, as deduced using kinematic considerations, from

the capture gamma spectrum resonance contributions described in the MF2/MT102 entry and from the emitted photon spectra in MF12/MF15.

The conclusion of this verification step is that the recoil energies generated using the TENDL-2019, and used in the computation of the various damage metrics, appear to be consistent with expectations using different approaches when analyzed in ways that provide a valid basis for comparison. For incident neutron energies below ~3-MeV, the recoil energy is insensitive to the exact approach used for summing over the outgoing charged particles. Above 3-MeV, there can be a very large sensitivity between the approaches due to the inclusion of proton and alpha particles in the outgoing channels and how these reaction channels are addressed. Further, the SNL-NJOY-2016 can also be sensitive to the details of exactly which outgoing particles are included in the summation of the recoil energy when there are more than two particles, e.g., in Figure 3-10, the approach is sensitive to whether we are counting heavy recoil particles with mass greater than 64 amu [which does not exclude (n,α) or (n,p) reactions] versus greater than 60 amu [which would also not exclude the (n,n2α) reaction].

3.3.2. ^{71}Ga

As for ^{69}Ga, the ^{71}Ga cross sections are found in recent ENDF/B-VIII.0, JEFF 3.3, JENDL 4.0, and TENDL-2019 libraries. The JEFF 3.3 evaluation, again, is based on the older TENDL-2015 evaluation. There is a draft JEFF 4T0 library [JEFF4T0] that is out for community review. The ^{71}Ga evaluation in this JEFF 4T0 library comes from the TENDL-2019 library. The ENDF/B-VIII.0 evaluation is based on an October 1998 CNDC evaluation. This ENDF/B-VIII.0 evaluation does not include any photon production MF12/14 files nor does it include MF6 recoil spectrum information. The JENDL 4.0 evaluation is based on a March 1994 KHI/JAERI evaluation. This JENDL 4.0 evaluation also fails to include either the photon production (MF13/14) or recoil spectrum (MF6) data. Based on this inspection of candidate nuclear data files, the primary recommended file is clearly the TENDL-2019 evaluation – which has both gamma production (MF14) and recoil spectra (MF6) data.

In order to evaluate the sensitivity of the damage metrics to the source of the cross section, Figure 3-11 compares the displacement kerma curves, as calculated with the SNL-NJOY-2016 code using the 770-group SAND-IV energy structure, for the ENDF/B-VIII.0, JENDL 4.0, and TENDL-2019 ^{71}Ga isotopic nuclear data evaluations. In order to more clearly depict the difference in the damage metrics in the high energy region, Figure 3-12 shows the ratio of the metrics for the ENDF/B-VIII.0 and JENDL 4.0 evaluations to the damage metric for the baseline recommended TENDL-2019 evaluation.

Since an important consideration in the cross section selection is the completeness of the treatment for all reaction channels, Table 3-6 identifies the reaction threshold energies and indicates the reaction coverage for the three most viable nuclear data evaluations. The TENDL-2019 evaluation is seen to include many reactions that are not critical to reactor dosimetry applications, e.g., have reaction thresholds above ~10 MeV or represent redundant/composite reactions. A light green shading is used in the table to highlight reaction channels that are important to the dosimetry application. Of the reactions with important threshold energies, as identified within the TENDL-2019 evaluation, the ENDF/B-VIII.0 evaluation appears to lack entries for (n,2α) [MT=108) and (n,nα) [MT=112] reaction channels. In order to put this lack of consideration of these cross sections into perspective, we consider the magnitude of these reaction channels at 10 MeV.

Figure 3-13 shows the magnitude of the important ^{71}Ga cross section channels within the TENDL-2019 evaluation. Figure 3-14 shows the fractional contribution of the various reaction channels. With respect to the total cross section at 10-MeV [2.1747 barn], the TENDL-2019 evaluation indicates that the:

- (n, nα) [MT=112 at 1.8466E-19 barn] has a fractional contribution of only 5E-18%;
- (n,2α) [MT=108 at 0.0 barn] is 0%.

So, the lack of consideration of these reaction channels in the ENDF/B-VIII.0 evaluation is not a meaningful deficiency for our application where we are only focused on fission reactor applications with meaningful neutron energies less than 10 MeV.

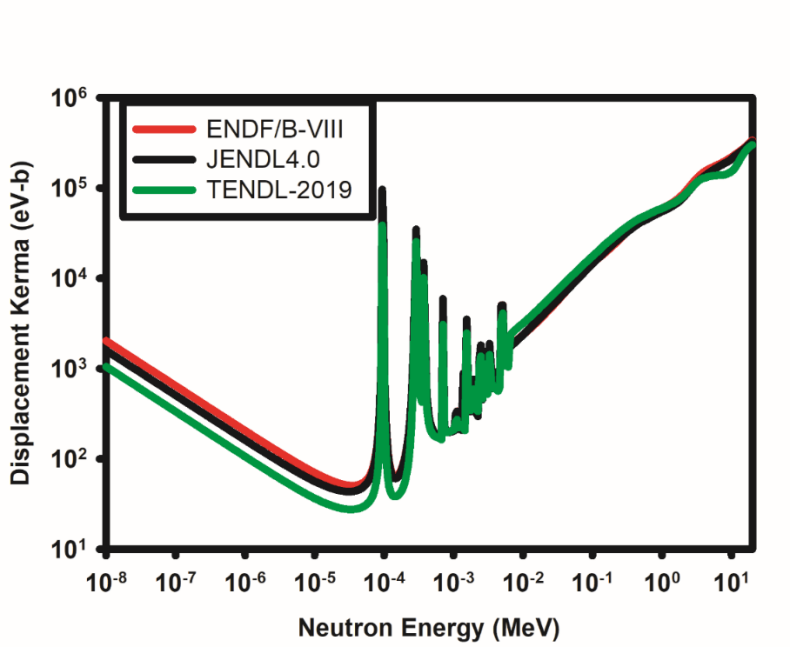

Figure 3-11. ^{71}Ga Displacement Kerma from Various Nuclear Data Evaluations

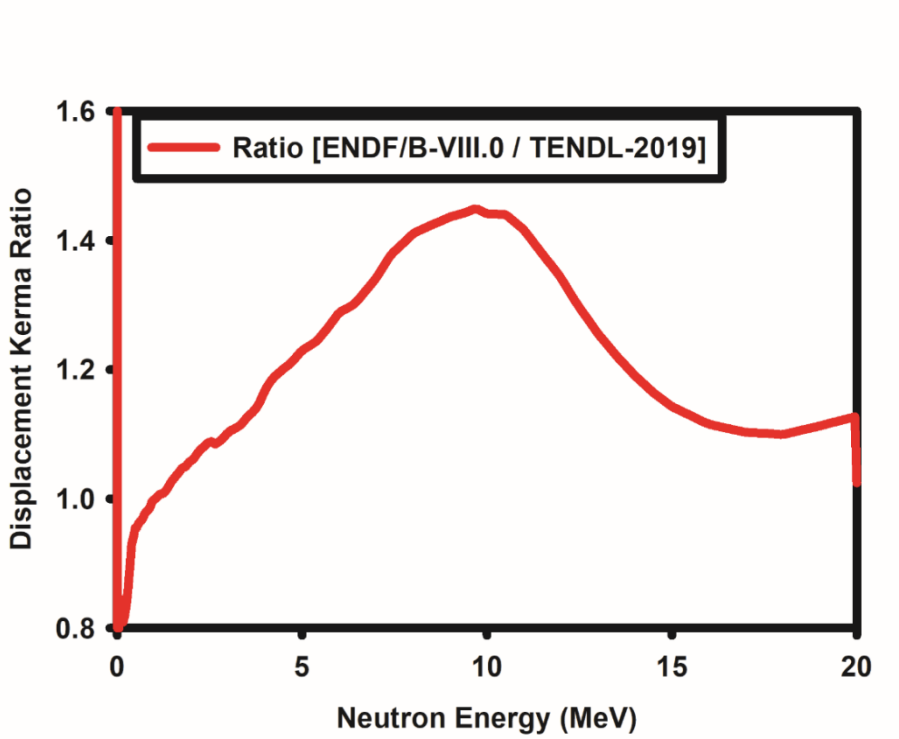

Figure 3-12. Ratio of ^{71}Ga Displacement Kerma for Various Nuclear Data Evaluations to a Baseline Reference from TENDL-2019 Evaluation

3.3.2.1. Characterization of the Completeness and Fidelity of the Reaction Channels

Table 3-6. Summary of Reactions in Various ^{71}Ga Nuclear Data Evaluations

Reaction Description	MT Identifier	Threshold Energy (MeV)	Evaluation		
			TENDL-2019	ENDF/B-VIII.0	JENDL 4.0
Total [redundant]	1	---	Yes	Yes	Yes
Elastic	2	---	Yes	Yes	Yes
Nonelastic [redundant]	3	---	Yes		
(n,n) [redundant, MT=51-91]	4	0.395496	Yes	Yes	Yes
Other (not needed)	5	>30	Yes		
(n,continuum) [redundant]	11	21.6426	Yes		
(n,2n)	16	9.43258	Yes	Yes	Yes
(n,3n)	17	17.1951	Yes	Yes	Yes
(n,na)	22	5.31912	Yes	Yes	Yes
(n,2na)	24	14.5816	Yes		
(n,3na)	25	21.748	Yes		
(n,np)	28	7.9752	Yes	Yes	Yes
(n,n2a)	29	13.3244	Yes		

Reaction	MT	Threshold	Evaluation		
(n,nd)	32	15.0683	Yes		Yes
(n,nt)	33	15.2963	Yes		
(n,n^{3}He)	34	19.7807	Yes		
(n,4n)	37	27.6549	Yes		
(n,2np)	41	17.3245	Yes		
(n,3np)	42	23.8988	Yes		
(n,n2p)	44	19.2508	Yes		
(n,npa)	45	14.0437	Yes		
Discrete inelastic	51-80	>0.395496	Yes	Yes	Yes
Continuum inelastic	91	>2.48546	Yes	Yes	Yes
(n,g)	102	---	Yes	Yes	Yes
(n,p) [can be redundant with 600-649]	103	2.05685	Yes	Yes	Yes
(n,d)	104	5.71899	Yes	Yes	Yes
(n,t)	105	8.72206	Yes	Yes	Yes
(n,^{3}He)	106	11.423	Yes	Yes	Yes
(n,a) [can be redundant with 800-849]	107	0.0	Yes	Yes	Yes
(n,2a)	108	7.22664	Yes		
(n,2p)	111	13.8638	Yes	Yes	
(n,pa)	112	8.15334	Yes		
(n,pd)	115	16.9946	Yes		
(n,pt)	116	19.006	Yes		
(n,da)	117	11.7874	Yes		
Green shading for important reaction channels, i.e., threshold <10 MeV and not redundant.					

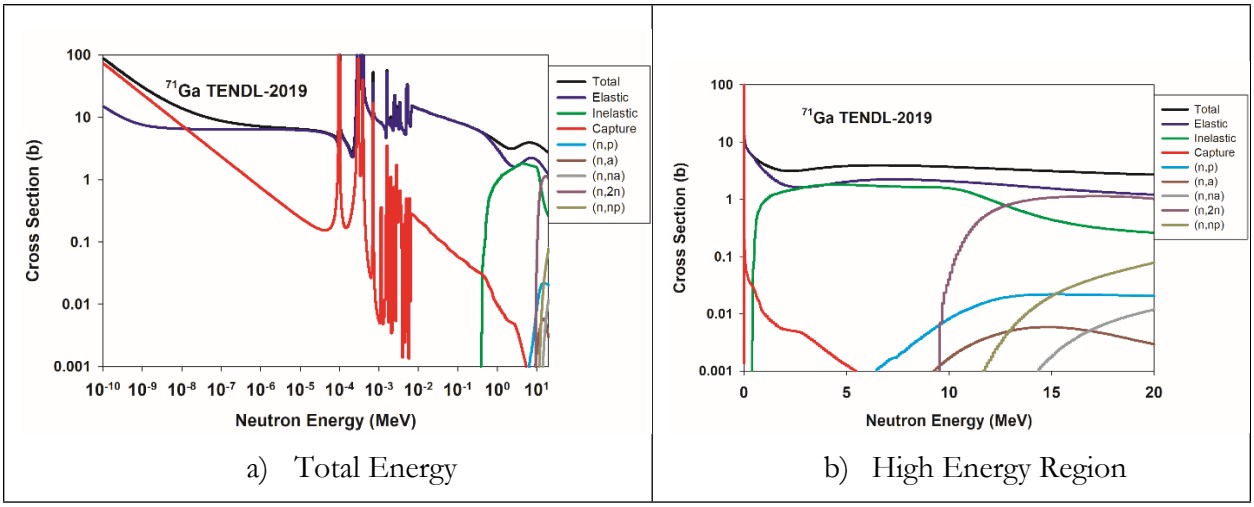

Figure 3-13. Contributions of Reaction Channels to the ^{71}Ga TENDL-2019 Cross Section

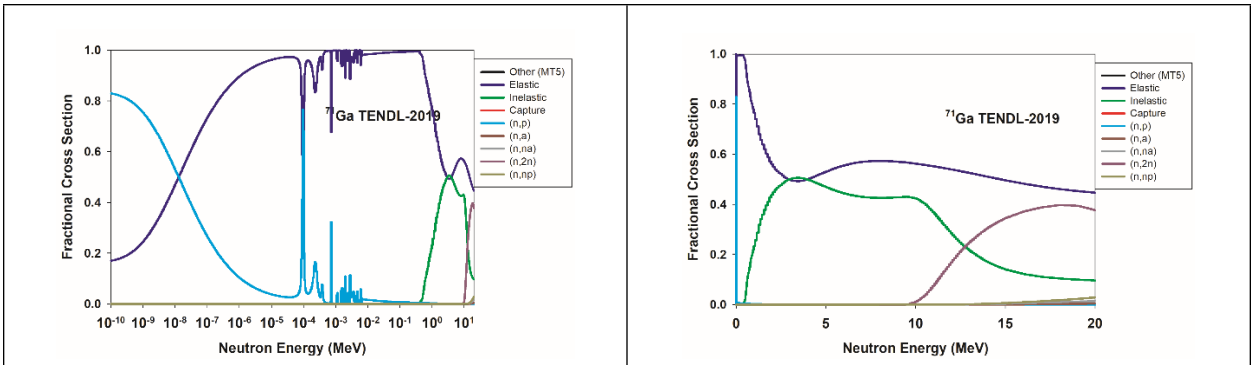

a) Total Energy b) High Energy Region

Figure 3-14. Fractional Contributions of Reaction Channels to the ^{71}Ga TENDL-2019 Cross Section

Since the TENDL-2019 and ENDF/B-VIII.0 evaluations represent the primary alternative evaluations that we can consider, it is useful to look at the amount of variation between these two evaluations as seen in the primary nuclear data. Figure 3-15 shows the variation between the TENDL-2019 and ENDF/B-VIII.0 evaluations for the angular distribution for the elastic channel. Figure 3-16 shows the ratio of the TENDL-2019 and ENDF/B-VIII.0 elastic and inelastic cross sections for ^{71}Ga.

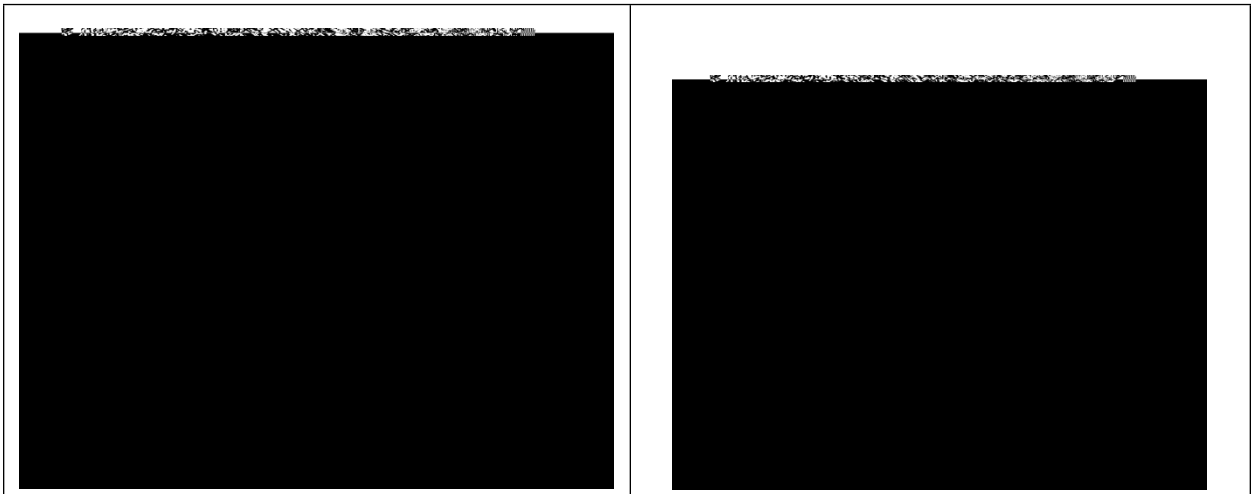

a) TENDL-2019 b) ENDF/B-VIII.0

Figure 3-15. Characterization of the Total Angular Distribution for Elastic Scattering on ^{71}Ga

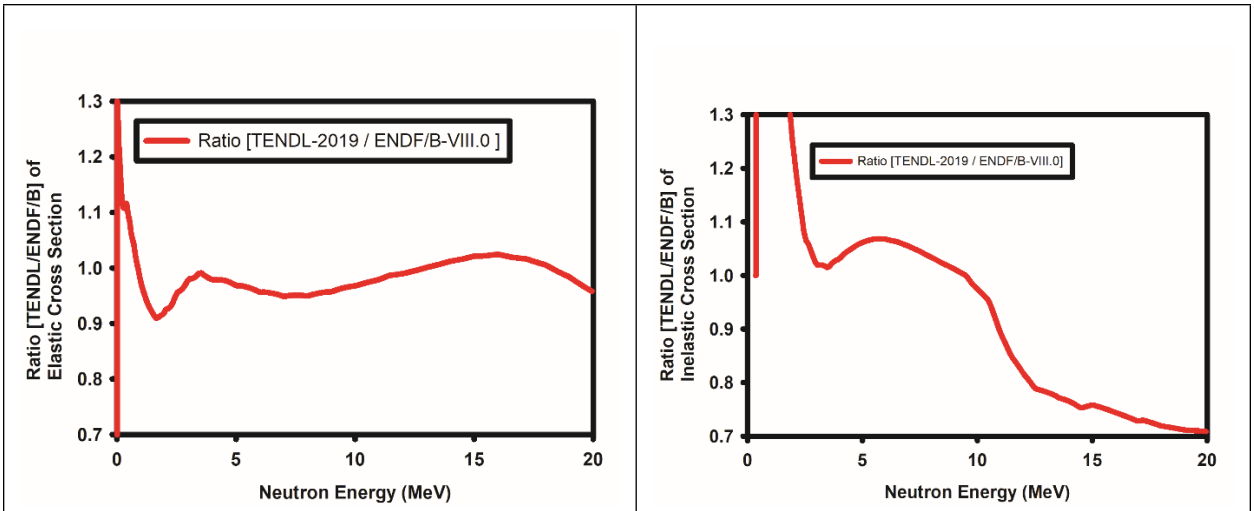

c) Elastic Reaction Channel

b) Inelastic Reaction Channel

Figure 3-16. Ratio of the TENDL-2019 and ENDF/B-VIII.0 ^{71}Ga Cross Section for the Two Major Fast Neutron Components

3.3.2.2. Characterization of the Photon Energy Emission

We next validate the consistence of the photon emission representation for the two nuclear data evaluations under consideration. Figure 3-17 compares the total kerma to the kinematic kerma limit for the two primary evaluations. Here we see that, for the TENDL-2019 evaluation, the energy emitted as gammas conserves the energy constraints at low energies where the dominant reaction is the (n,γ) capture reaction, i.e., the kerma never significantly exceeds the kinematic kerma limits at low incident neutron energies, but the TENDL-2019 does show some significant energy conservation violations in the 1 – 20 MeV region. In contrast, the ENDF/B-VIII.0 evaluation shows a total failure at the energy balance for the capture reaction and also shows significant deviations at high energy. An inspection of the NJOY-2016 output, which reports on the energy balance, confirms the poor energy balance over all of the energy range. Because of these energy conservation violations, the TENDL-2019 evaluation is clearly the better selection, but, even there, we should over-ride the total kerma with the kinematic kerma limit in our dosimetry applications.

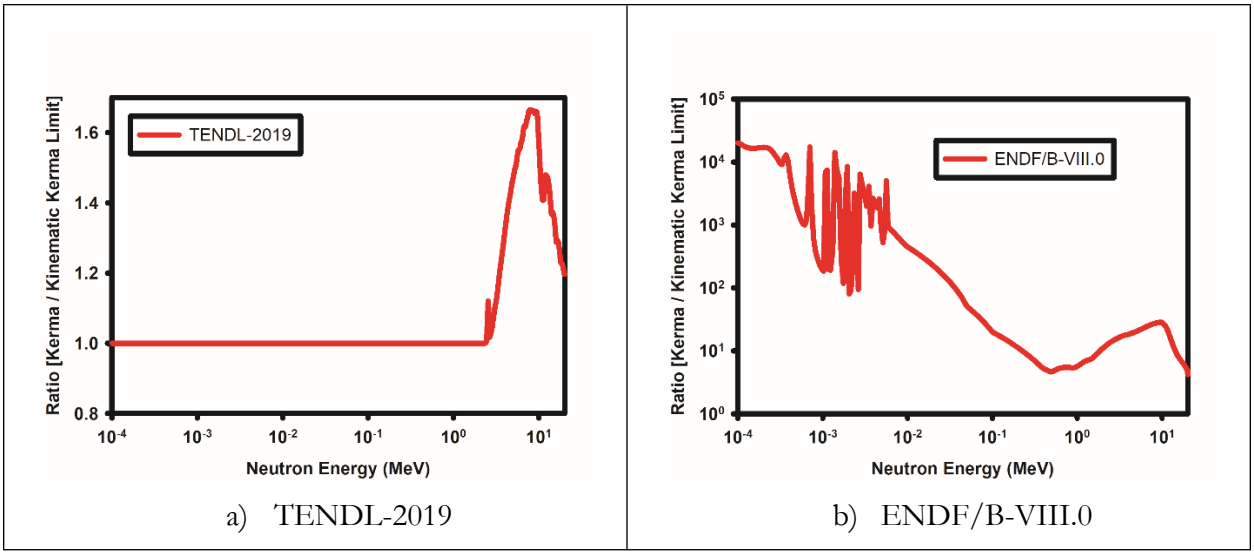

Figure 3-17. Ratio of ^{71}Ga Total kerma (MT=301) to the Kinematic Kerma Limit (MT=443) from the Two Primary Nuclear Data Evaluations

3.3.2.3. Recoil Spectrum

The first examination is a visualization of energy-dependence of the total recoil spectra. Figure 3-18 shows the ^{71}Ga recoil spectrum for several incident neutron energies. At low energies, the elastic scattering is the dominant reaction channel. However, the multiple reaction channels that open for high incident neutron energies give rise to a much more complex PKA recoil spectrum.

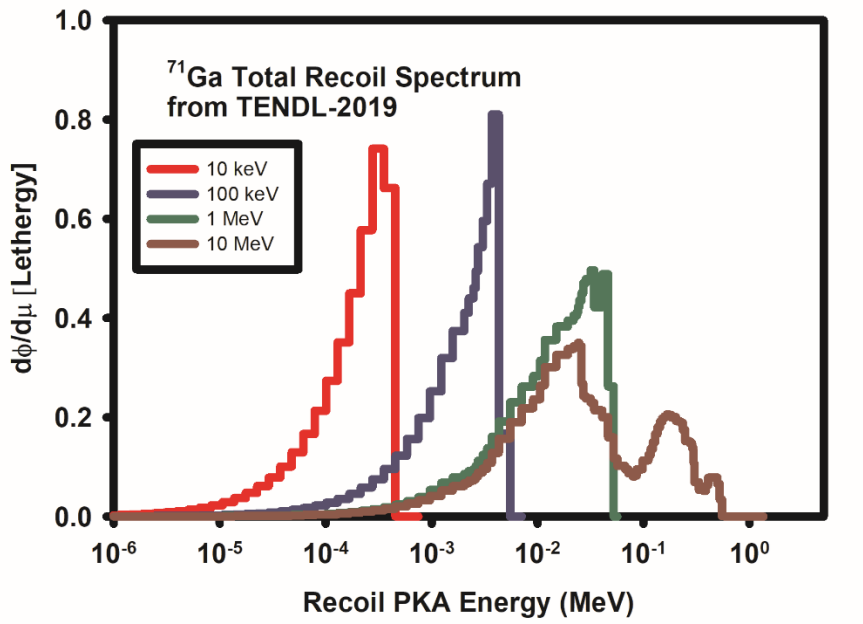

Figure 3-18. TENDL-2019 Characterization of the Total Recoil Spectrum on ^{71}Ga

Table 3-7 shows the average recoil energy, as reported by the SPKA-2020 code, for different reaction channels at selected incident neutron energies.

Table 3-7. Average Recoil Energy for Different Reaction Channels from Neutrons Incident on ^{71}Ga

Incident Neutron Energy	PKA Recoil Energy (keV)								
	Reaction Channel								
	Total (MT1)	Elastic (MT2)	Total Inelastic (MT4)	Continuum Inelastic (MT91)	(n,p) (MT103)	(n,α) (MT107)	(n,nα) (MT22)	(n,np) (MT28)	(n,d) (MT104)
10 keV	0.2748	0.2748	---	---	---	---	--	---	---
100 keV	2.8496	2.8496	---	---	---	---	--	---	---
1 MeV	20.718	21.033	19.688	---	---	---	---	---	---
10 MeV	70.775	41.591	104.15	97.049	185.79	596.15	381.01	180.47	180.31

The effective PKA recoil energy, i.e., the portion of the recoil energy that goes into the creation of Frenkel pairs, as before, can be extracted by dividing the displacement kerma, derived using a partition function that has been defaulted to unity and only considering the heavy primary PKA recoil ion, by the total cross section. Figure 3-19 shows this effective recoil energy (parametrically with a consideration of the outgoing ion masses that are considered) as a function of the incident neutron energy. As for ^{69}Ga, a big difference is seen in the effective recoil energy for high neutron recoils when the alpha particles are not counted. In this case, given the different atomic mass of the target, the first approach was to implement the algorithm by only counting outgoing recoil ions with a mass greater than 71-4=67 amu. The second approach was to only count outgoing recoil ions with a mass > 71-9=62 amu. Since reactions with multiple light ions in the outgoing channel, such as the (n,2α) channel, are not important in this isotope, there is no significant difference between counting recoil ions with a mass greater than 71-4=67 amu versus counting recoil ions with a mass greater than 71-9=62 amu. The average recoil energies in Figure 3-19 are consistent with those reported in Table 3-7.

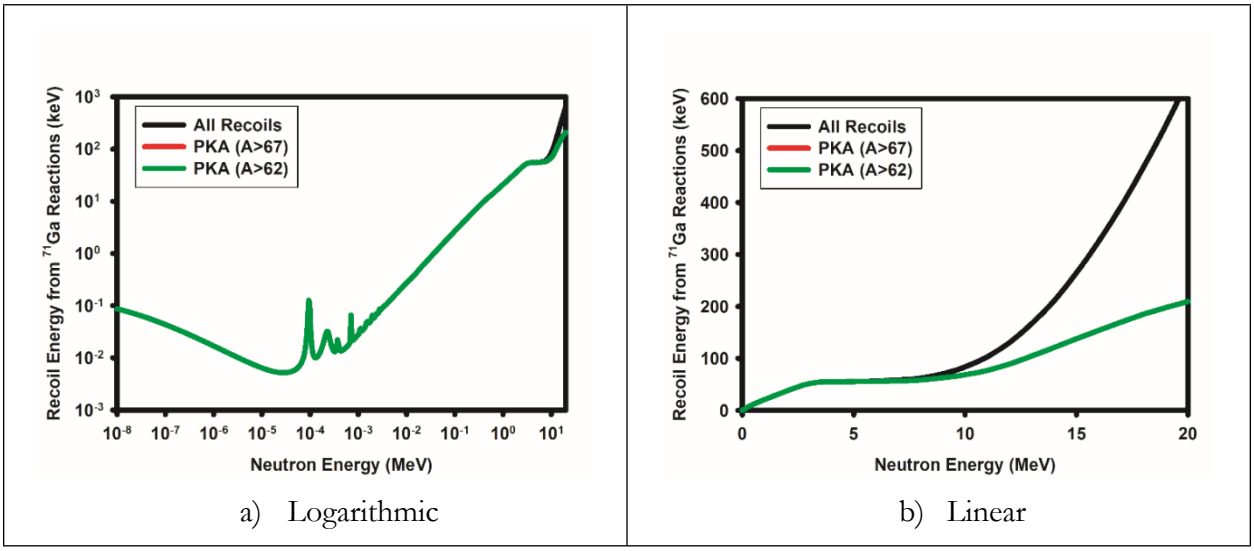

Figure 3-19. Sensitivity of the Effective ^{71}Ga Recoil Energy to the Mass of Outgoing Particles Counted

3.3.3. ^{75}As

Isotopic ^{75}As cross sections are found in recent ENDF/B-VIII.0, JEFF 3.3, JENDL 4.0, and TENDL-2019 libraries. The ENDF/B-VIII.0 uses a March 2010 evaluation by Kawano (LANL). The JENDL 4.0 evaluation uses an April 2009 evaluation by Shibata (KAEA). The JEFF 3.3 evaluation uses the TENDL-2015 evaluation. Both the ENDF/B-VIII.0 and TENDL-2019 evaluations provide MF=6 descriptions for the critical MT=102 capture gamma reaction. The ENDF/B-VIII.0 and TENDL-2019 cross sections also have MF=12 photon production information for 30 discrete inelastic channels as well as for the (n,p) and (n,α) reaction channels that leave the residual nucleus in an excited state. All of these evaluations have MF=6 energy/angle distributions that support a high-quality evaluation of the neutron kerma contributions. All of the evaluations have a MF=12 photon file, but the JENDL 4.0 evaluation only has a single MF=12 entry for a composite MT=3 entry – a composite for all non-elastic channels. This lack of a separate MT=102 capture gamma entry in the JENDL 4.0 evaluation, using either MF=6 or MF=12 files, is a major issue in calculating the kerma contributions for the various reaction channels. The TENDL-2019 evaluation, which is based primarily on calculations, has MF=3 cross section entries for 33 reaction channels (not counting the discrete inelastic, continuum inelastic, and the separate residual excitation states for some reaction channels) and MF=6 recoil distribution entries for all reaction channels. Some of these reaction channels represent very high threshold reactions that are not relevant for fission reactor environments. The ENDF/B-VIII.0 evaluation, which is a data-driven evaluation supplemented by calculations, has MF=3 discrete cross sections for 10 reaction channels and MF=6 recoil distribution entries for six reaction channels.

Based on this information, the selection of a recommended cross section for our analysis of dosimeter response functions comes down to either the ENDF/B-VIII.0 or TENDL-2019 evaluation. Considerations here included:

- Both evaluations have MF=6 energy/angle distributions and MF=12/14 photon production files;
- TENDL-2019 represents an improvement/refinement over the TENDL-2015 library, which is the basis for the JEFF 3.3 evaluation;
- The JENDL 4.0 evaluation does not have a breakout for the capture gamma spectrum in either MF=6 or MF=12;
- TENDL-2019 includes more reaction channels, but is based, primarily, upon calculations and does not give sufficient consideration to the available experimental data;
- The ENDF/B-VIII.0 evaluation represents a recent calculation and is data-driven - using Hauser-Feshbach calculations from the CoH-Ariel and EMPIRE codes as a guide. The evaluation documentation describes the process as "available experimental data were interpreted using nuclear reaction model code EMPIRE-2.19b31".
- For model support, the TENDL-2019 evaluation is based on TALYS code calculations; and the ENDF/B-VIII.0 evaluation is based on EMPIRE code calculations. Both codes represent the state-of-the-art in nuclear cross section modeling.
- The ENDF/B-VIII.0 evaluation does not have any MF=33 covariance information. The TENDL-2019 evaluation has MF=33 covariance information for all reaction channels.

In order to evaluate the sensitivity of the damage metrics to the source of the cross sections, Figure 3-20 compares the displacement kerma curves, as calculated with the SNL-NJOY-2016 code using the 770-group SAND-IV energy structure, for the ENDF/B-VIII.0, JENDL 4.0, and TENDL-2019 ^{75}As isotopic nuclear data evaluations. The TENDL-2019 and ENDF/B-VIII.0 displacement

kermas are very similar for energies less than 1 MeV. Since the logarithmic scale of the y-axis in Figure 3-20 makes it difficult to see small differences, Figure 3-21 shows the ratio [ENDF/B-VIII.0/TENDL-2019] of the displacement kerma from these two evaluations. There is a need to better understand the source of the difference in the high energy (> 1 MeV) displacement kerma between the two candidate evaluations.

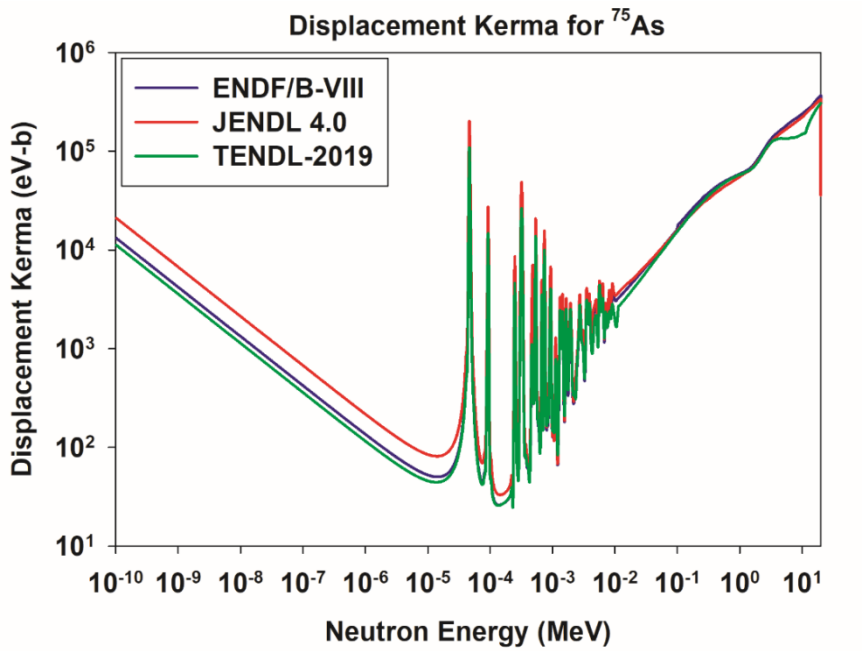

Figure 3-20. ^{75}As Displacement Kerma from Various Nuclear Data Evaluations

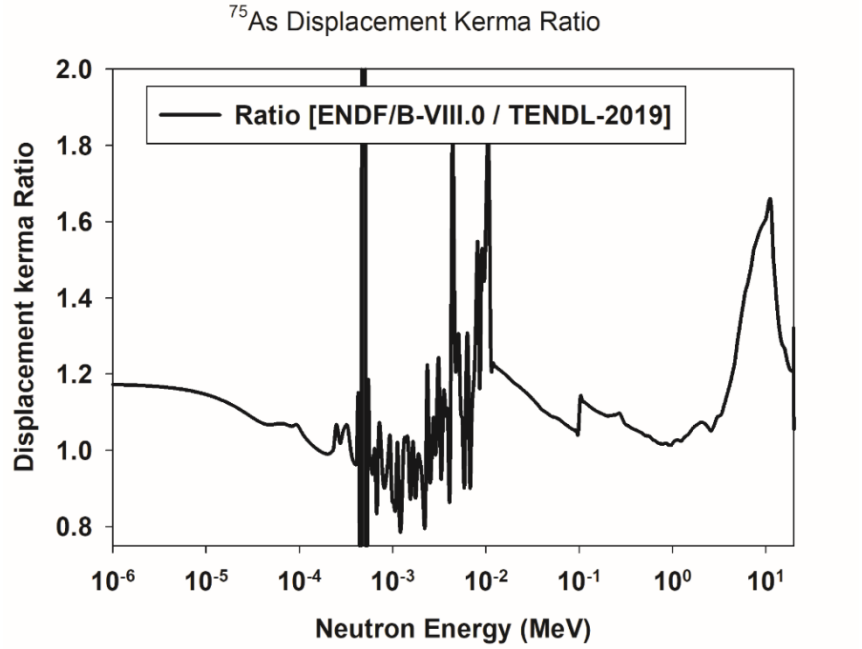

Figure 3-21. Ratio of ^{75}As Displacement Kerma for Candidate Nuclear Data Evaluations: [ENDF/B-VII.0/TENDL-2019]

Using this down-selection to two candidate evaluations for consideration as the reference cross section evaluation for the dosimetry response functions, the following subsections compare and verify some aspects of the consistency of the data in these two evaluations.

3.3.3.1. Characterization of the Completeness and Fidelity of the Reaction Channels

One element of a verification of a nuclear data evaluation is the completeness of the treatment of all of the reaction channels. Table 3-8 identifies the reaction threshold for ^{75}As and indicates the span of the reaction coverage for the two candidate evaluations. The TENDL-2019 evaluation is seen to include many reactions that are not critical to reactor dosimetry applications, e.g., have reaction thresholds above ~10 MeV or represent redundant/composite reactions. A light green shading is used in the table to highlight reaction channels that are important to the dosimetry application. Of the reactions with important threshold energies, as identified in the TENDL-2019 evaluation, the ENDF/B-VIII.0 evaluation appears to lack entries for (n,d) [MT=104), (n,t) [MT=105], (n,α) [MT=108], and (n,pα) [MT=112] reaction channels. We note that the (n,α) [MT=108] is not listed as a deficiency here since this reaction in TENDL-2019 is equivalent to the composite of the MT=801-809+849 reactions that appear in ENDF/B-VIII.0. In order to put this lack of consideration of these cross sections into perspective, we consider the magnitude of these reaction channels at 10 MeV. With respect to the total cross section at 10-MeV [3.860914 barn], the TENDL-2019 evaluation indicates that the:

- (n,d) [MT=104 at 1.12429E-4 barn] has a fraction contribution of 0.0029%;
- (n,t) [MT=105 at 7.75466E-15 barn] has a fraction contribution of 2E-13%;
- (n,2α) [MT=108 at <6.49153E-20 barn] has a fraction contribution of <1.68E-18%;
- (n,pα) [MT=112 at <1.7E-19 barn] has a fraction contribution of 4.4E-18%.

So, the lack of consideration of these reaction channels in the ENDF/B-VIII.0 evaluation is not a meaningful deficiency for our application where we are only focused on fission reactor applications with neutron energies less than 10 MeV.

Table 3-8. Summary of Reactions in Various ^{75}As Nuclear Data Evaluations

Reaction Description	MT Identifier	Threshold Energy (MeV)	Evaluation		
			TENDL-2019	ENDF/B-VIII.0	JENDL 4.0
Total [redundant]	1	---	Yes	Yes	Yes
Elastic	2	---	Yes	Yes	Yes
Nonelastic [redundant]	3	---	Yes		Yes
(n,n) [redundant, MT=51-91]	4	0.20128	Yes	Yes	Yes
Other (not needed)	5	>30	Yes		
(n,continuum) [redundant]	11	21.946	Yes		
(n,2n)	16	10.3834	Yes	Yes	Yes
(n,3n)	17	18.4694	Yes	Yes	Yes
(n,nα)	22	5.39159	Yes	Yes	Yes
(n,2nα)	24	14.817	Yes		

Reaction	MT	Threshold	Evaluation		
(n,3nα)	25	22.5738	Yes		
(n,np)	28	6.9936	Yes	Yes	Yes
(n,n2α)	29	10.7067	Yes		
(n,nd)	32	15.0726	Yes		Yes
(n,nt)	33	15.6054	Yes		
(n,n^{3}He)	34	19.638	Yes		
(n,4n)	37	29.409	Yes		
(n,2np)	41	17.327	Yes		
(n,3np)	42	24.201	Yes		
(n,n2p)	44	18.154	Yes		
(n,npα)	45	13.336	Yes		
Discrete inelastic	51-80	>0.20128	Yes	Yes	Yes
Continuum inelastic	91	>14.3932	Yes	Yes	
(n,γ)	102	---	Yes	Yes	Yes
(n,p) [redundant with 600-649]	103	0.40019	Yes	Yes	Yes
(n,d)	104	4.7391	Yes		Yes
(n,t)	105	8.73113	Yes		Yes
(n,^{3}He)	106	10.332	Yes		Yes
(n, α) [redundant with 800-849]	107	0.0	Yes		Yes
(n,2α)	108	4.30282	Yes		
(n,2p)	111	11.6459	Yes		
(n,pα)	112	7.4469	Yes		
(n,pd)	115	15.899	Yes		
(n,pt)	116	18.86	Yes		
(n,dα)	117	11.106	Yes		
(n.Xp) [redundant]	203	---			Yes
(n.Xd) [redundant]	204	---			Yes
(n.Xt) [redundant]	205	---			Yes
(n.X^{3}He) [redundant]	206	---			Yes
(n.Xα) [redundant]	207	---			Yes
(n,p_i)	600-624	>0.3984		Yes	
(n,p_c)	649	1.673346		Yes	
(n, α_i)	800-809	0.0		Yes	
(n, α_c)	849	1.3		Yes	
Green shading for important reaction channels, i.e., threshold <10 MeV and not redundant.					

Another element of a verification of the data processing is an examination of the variation between the two candidate evaluations for the contributions from the various reaction channels to the total cross section as seen in Figures 3-22, 3-23, 3-24, and 3-25. Figure 3-26 shows a comparison of the angular distribution for the elastic channel. Figure 3-27 shows the ratio between the evaluations for the elastic and inelastic cross sections.

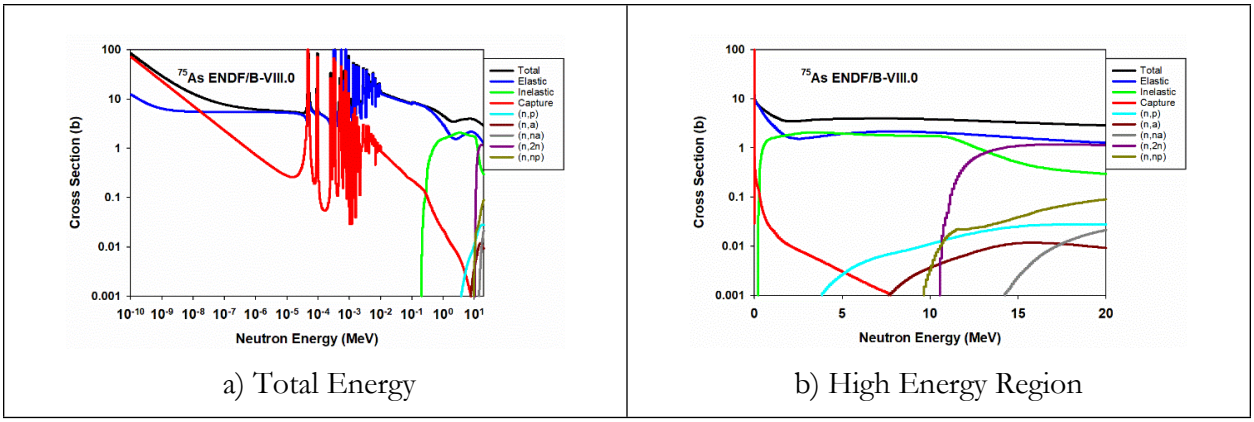

a) Total Energy b) High Energy Region

Figure 3-22. Contributions of Reaction Channels to the ^{75}As ENDF/B-VIII.0 Cross Section

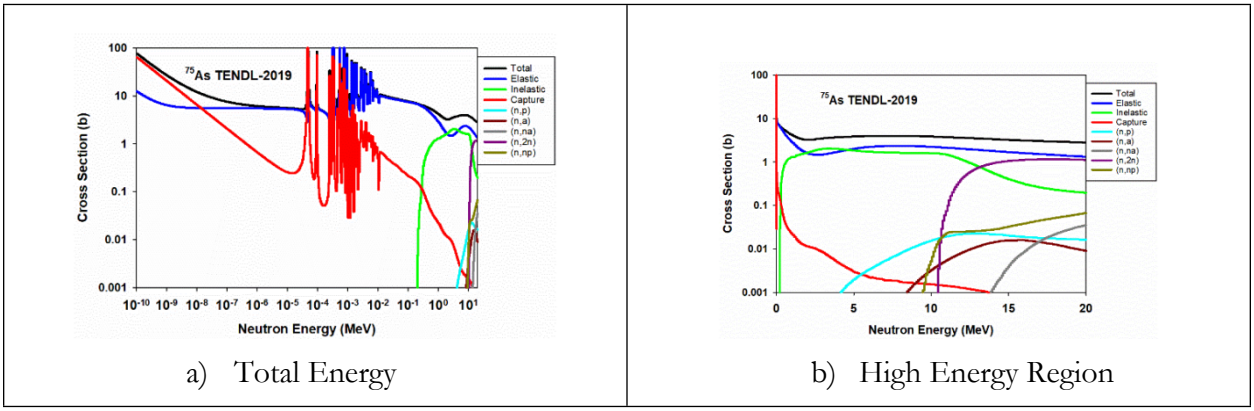

a) Total Energy b) High Energy Region

Figure 3-23. Contributions of Reaction Channels to the ^{75}As TENDL-2019 Cross Section

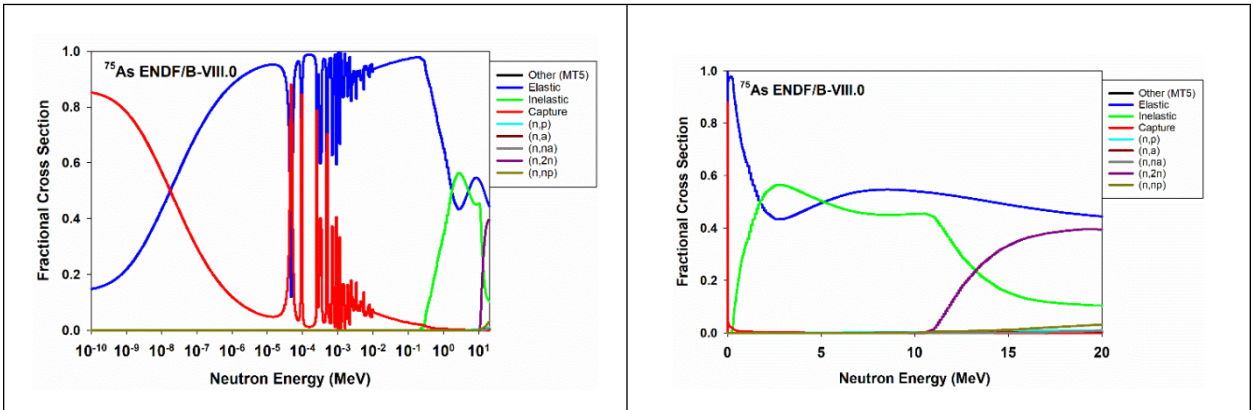

a) Total Energy b) High Energy Region

Figure 3-24. Fractional Contributions of Reaction Channels to the ^{75}As ENDF/B-VIII.0 Cross Section

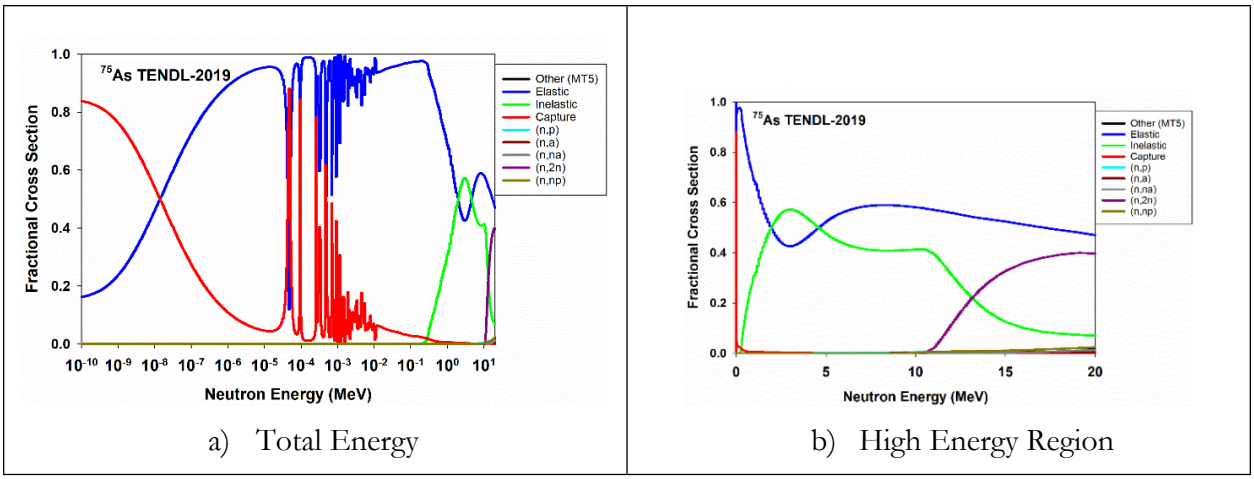

Figure 3-25. Fractional Contributions of Reaction Channels to the ^{75}As TENDL-2019 Cross Section

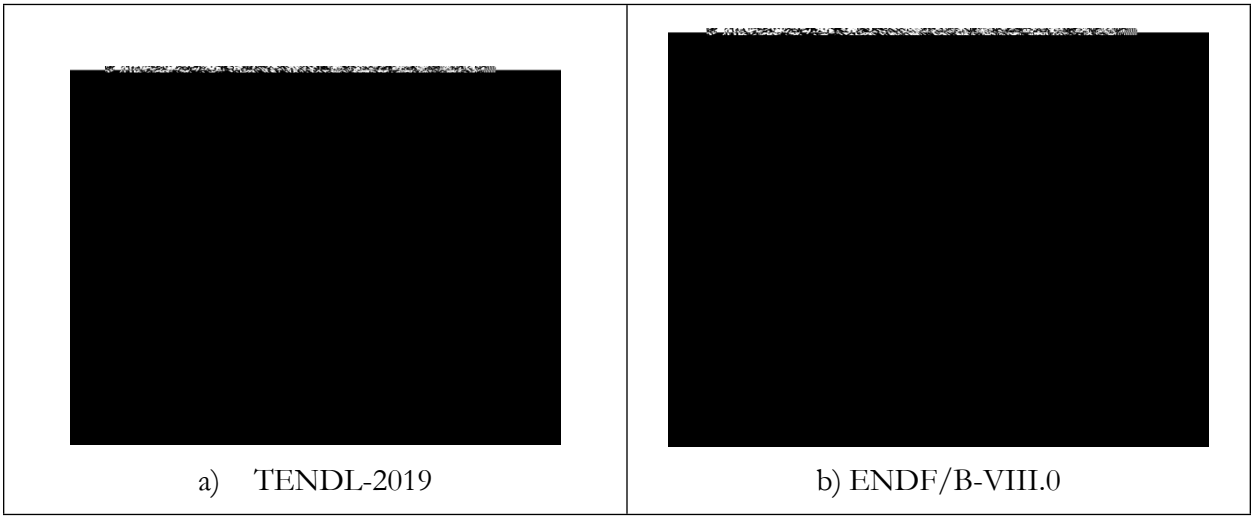

Figure 3-26. Characterization of the Total Angular Distribution for Elastic Scattering on ^{75}As

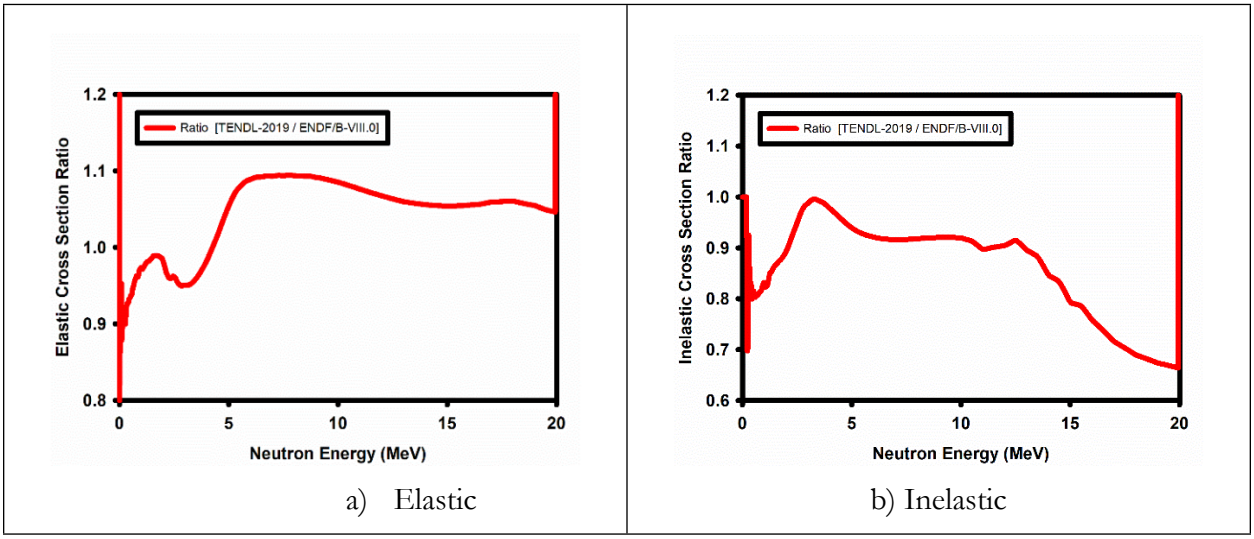

Figure 3-27. Ratio of the TENDL-2019 and ENDF/B-VIII.0 ^{75}As Cross Section for the Two Major Fast Neutron Components

3.3.3.2. Characterization of the Photon Energy Emission

We next validate the consistence of the photon emission representation for this nuclear data evaluation. Figure 3-28 compares the total kerma to the kinematic kerma limit for the two candidate evaluations. Here we see that the energy emitted as gammas conserves the energy constraints for the capture reaction, i.e., the kerma never significantly exceeds the kinematic kerma limits, but the TENDL-2019 does show some significant energy conservation violations in the 1 – 20 MeV region. The ENDF/B-VIII.0 evaluation shows a good energy balance over the total energy range. Because of these energy conservation violations, if the TENDL-2019 evaluation were used in the dosimetry metrics, we must over-ride the total kerma with the kinematic kerma limit in our dosimetry applications.

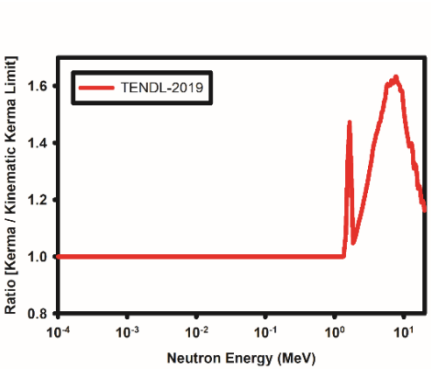

c) TENDL-2019

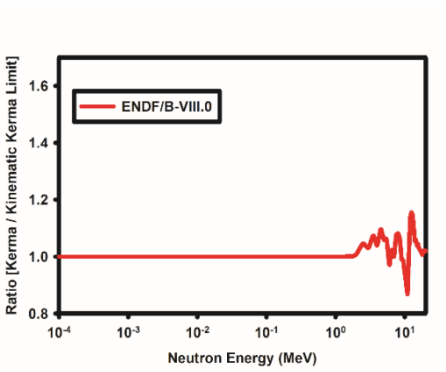

b) ENDF/B-VIII.0

Figure 3-28. Ratio of ^{75}As Total kerma (MT=301) to the Kinematic Kerma Limit (MT=443) from the Two Candidate Nuclear Data Evaluations

3.3.3.3. Total Recoil Spectrum

It is also useful to review the total recoil distribution. Figure 3-29 shows the ^{75}As recoil spectrum at several incident neutron energies. At low energies, the elastic scattering is the dominant reaction channel. However, the multiple reaction channels that open for high incident neutron energies give rise to a much more complex PKA recoil spectrum. Figure 3-29 provides a visualization of neutron energy-dependence of the total recoil spectra

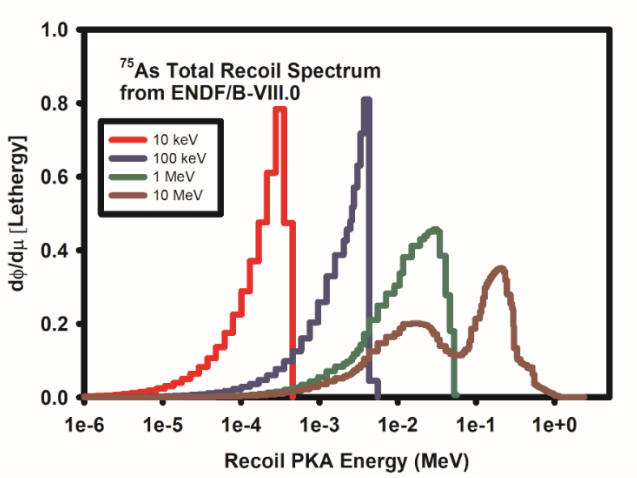

Figure 3-29. ENDF/B-VIII.0 Characterization of the Total Recoil Spectrum on ^{75}As for Various Incident Neutron Energies

3.3.3.4. Average Recoil Energy

Table 3-9 shows the average recoil energy, as calculated using the SPKA-2020 code, for different reaction channels at selected incident neutron energies.

Table 3-9. Average Recoil Energy for Different Reaction Channels from Neutrons Incident on ^{75}As

Incident Neutron Energy		PKA Recoil Energy (keV)							
		Reaction Channel							
	Total (MT1)	Elastic (MT2)	Total Inelastic (MT4)	Continuum Inelastic (MT91)	(n,p) (MT103)	(n,α) (MT107)	(n,nα) (MT22)	(n,np) (MT28)	(n,d) (MT104)
10 keV	0.261	0.261	--	--	--	---	--	--	--
100 keV	2.73	2.73	--	--	--	---	--	--	--
1 MeV	19.09	17.64	21.66	---	37.59	---	---	---	---
10 MeV	114.7	36.1	202.9	203.17	243.1	591.78	394.7	188.4	---

The PKA recoil energy, i.e., the portion of the recoil energy that goes into the creation of Frenkel pairs, can be extracted by dividing a modified damage energy tally, derived using a partition function that has been defaulted to unity and only considering the heavy primary PKA recoil ion, by the total cross section. Figure 3-30 shows this effective recoil energy (parametrically with a consideration of the outgoing ion masses) as a function of the incident neutron energy. A big difference is seen in the effective recoil energy for high energy neutron recoils when the alpha particles are not counted – implemented by only counting outgoing recoil ions with a mass greater than 75-4=71 amu. Since reactions with multiple light ions in the outgoing channel, such as the (n,2α) channel, are not important in this nucleus, there is no significant difference between counting recoil ions with a mass greater than 75-4=71 amu versus counting recoil ions with a mass greater than 75-9=66 amu.

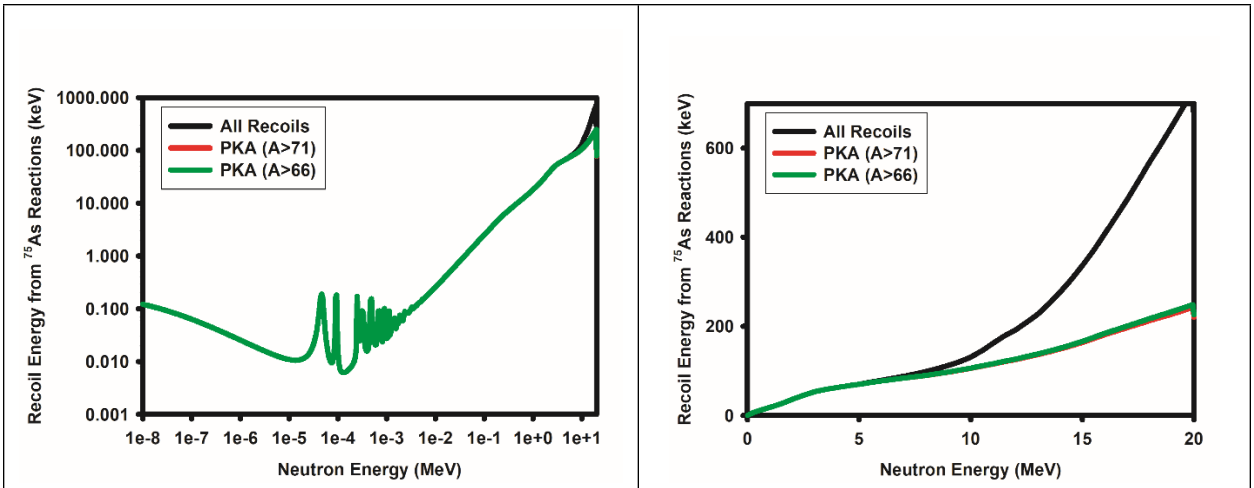

Figure 3-30. Sensitivity of the Effective ^{75}As Recoil Energy to the Mass of Outgoing Particles Counted

3.4. Stopping Power

The mass stopping power for a material is defined in ICRU 60 as "the quotient of dE by ϱdl, where dE is the energy lost by a charged particle in traversing a distance dl in the material of density ϱ." This quantity has SI units of Jm^2/kg but, in radiation damage, is typically reported in units of MeV-cm^2/mg. This mass stopping power is often partitioned into three components:

- mass electronic (or collisional) stopping power due to collisions with electrons;
- mass radiative stopping power due to the emission of bremsstrahlung in the presence of the electric fields of the nuclei and electrons in a material;
- mass nuclear stopping power due to Coulomb collisions with the atoms in a material. The nuclear stopping power can sometimes be reported separately for elastic and inelastic nuclear collisions. It must be noted that the "nuclear stopping process" does not refer to a strong or weak nuclear force, rather, it only addresses the elastic and inelastic Coulomb energy losses due to the incident ion interacting with the nucleus of the lattice atoms.

The linear stopping power is defined as the product of the material density and the mass stopping power. As seen in these definitions, the electronic stopping power goes into ionization processes while the nuclear stopping process addresses energy that goes into breaking interatomic bonds or generating lattice phonons. Damage metrics such as the linear energy transfer (LET) are proportional to the linear electronic stopping power, have SI units of J/m, and are typically reported in units of keV/μm.

Different radiation damage metrics may be based on the total stopping power, the electronic stopping power, or the nuclear stopping power. There is not a lot of experimental stopping power data for GaAs, so most damage metrics use various computational models, sometimes with semi-empirical calibration terms, to calculate the stopping power. The most common codes used to calculate the stopping power are MSTAR, SPAR, SRIM, DPASS, and CasP. The MSTAR code [MSTAR] does not include gallium or arsenic in its database. The SPAR code [SPAR] dates back to 1973. The SRIM code [Zi10] appears to have the most recent stopping power calculations. Figure 3-

31 compares the various types of stopping powers, as computed using the SRIM code, for various incident ions (proton, alpha, Ga, and As) in GaAs. The stopping powers for Ga and As are nearly identical and these curves overlap in the figure.

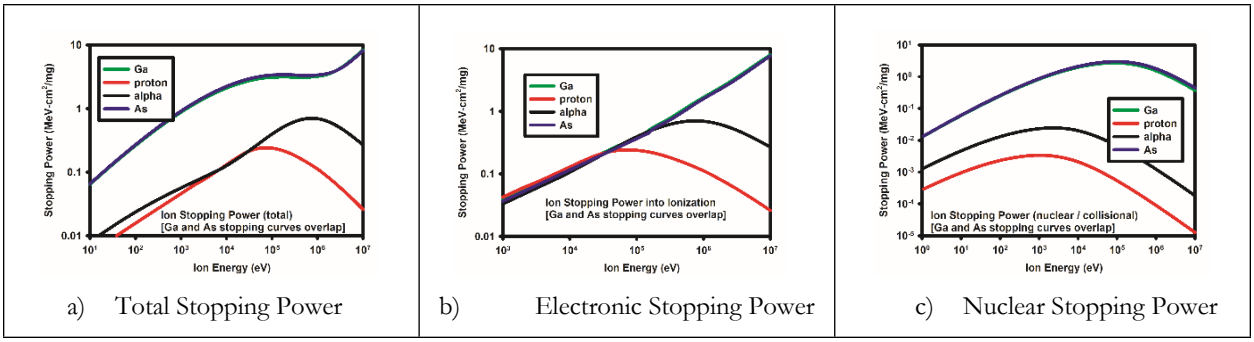

a) Total Stopping Power b) Electronic Stopping Power c) Nuclear Stopping Power

Figure 3-31. Stopping Powers for Various Ions in GaAs

Because it takes into consideration empirically corrections based on available data, the SRIM stopping power is often the most accurate model for the stopping power. In the case of GaAs, there does not appear to be a very good set of experimental stopping power data to use to either tune the empirical fitting process nor to be available for validation purposes. Unlike SRIM, the DPASS [Sig19a, Sig19b, Sig19c] and CasP [Sch12, Mat17] codes are purely based on theory without fitting of stopping power data [Sig19b]. The difference between the SRIM, DPASS, and CasP calculations for Ga on GaAs provides some guidance on the estimation of the uncertainty in the stopping power for GaAs.

3.5. 1-MeV Reference Value

Neutron-induced material damage studies are typically conducted using fission reactors where the fast neutron component of the spectrum has an average energy near 1-MeV. Because the exposure conditions in reactors are typically cited in terms of a neutron fluence on a test object, and because displacement kerma/damage-energy metrics with units of MeV-mb are not typically cited in the radiation facility characterization reports, the material damage community had adopted a practice for the radiation facilities to cite exposure conditions in terms of a 1-MeV damage equivalent fluence. They then adopted a material-specific reference displacement kerma value in order to more easily convert a displacement damage into a 1-MeV-Equivalent fluence.

This practice was started when looking at the results from displacement damage in silicon semiconductor material and trying to ensure test consistency between irradiations conducted at different reactor environments. Unfortunately, there is a complicated resonance structure in the silicon cross section near 1-MeV [Dan98, Gri03], as shown in Figure 3-32. Since one does not want a "reference value" that is subject to frequent changes as the silicon cross sections are refined and the details in the resonance cross section region refined, a fitting process was adopted in the case of silicon in order to establish the smooth reference value indicative of the response in this energy region.

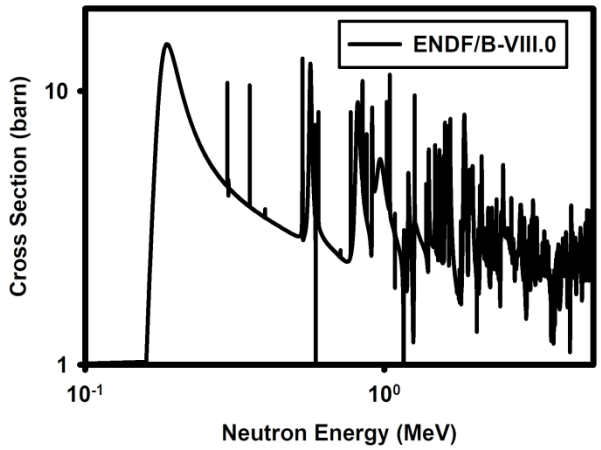

Figure 3-32. Resonance Structure in ^{28}Si Cross Section Near 1-MeV

For GaAs, Figure 3-33 shows that there is no resonance structure in the 1-MeV region for any of the three GaAs isotopes, so a fitting approach was not required in setting the value for the reference displacement kerma. Since this is a "reference" value, the exact number is not what is important. Rather, it is the universal acceptance of the value that is required. In 1993, the ASTM E722 standard adopted the round value of 70 MeV-mb for the reference GaAs displacement kerma "based on an inspection of the ENDF/B-VI microscopic displacement kerma" [ASTM722]. An inspection of the legacy work shows that the ENDF/B-VI displacement kerma at 1-MeV was ~71.33 MeV-mb (this is the average of the two energy bins near the 1-MeV point within the 640-group energy representation). This observation, using the ENDF/B-VI cross sections for both ^{nat}Ga and ^{75}As nuclei, was the basis for the adopted GaAs reference value. However, the early work also found that the displacement kerma, when computed using the mixed ENDF/B-VI/ENDL-84 cross section evaluations that were used in the NJOY-based assessment of the legacy recommended kerma response, had a value (before any damage efficiency function was applied) at 1-MeV of ~61.73 MeV-mb. These legacy values can be compared to the updated TENDL-2019/ENDF/B-VIII.0-based displacement kerma found in this work of ~60.46 MeV-mb. In the absence of a significant difference from the rationale reflected in the original work, and since most subsequent work has continued to use this 70 MeV-mb reference value, this reference value is also adopted in the updated responses reported here.

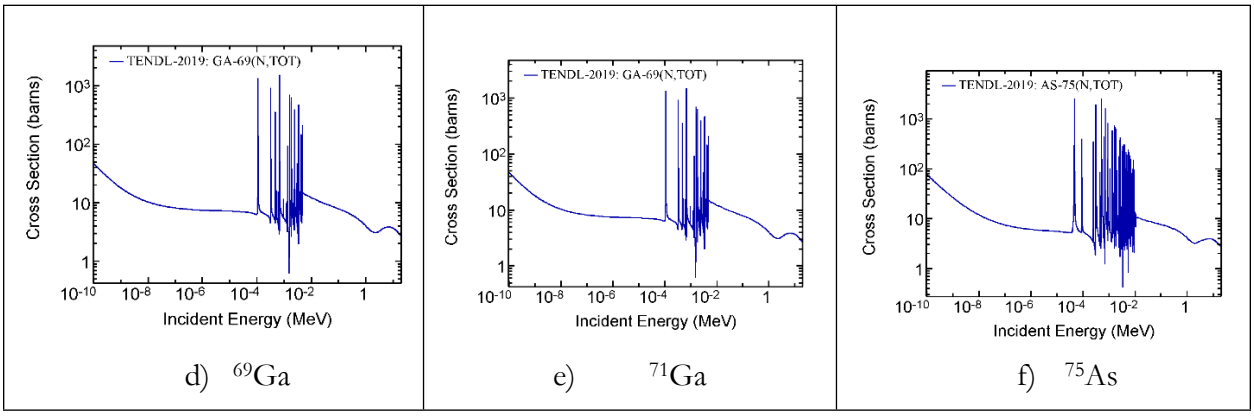

Figure 3-33. GaAs Cross Section Components

4. DAMAGE PARTITION FUNCTION

The formulation of the damage metric in Equation 2 contained the term, ${}^{type-B}\zeta\left(E_d, T_{R,j_i}, {}^{type-D}T_{dam}\right)$, which is an "effective" generation correction term. The damage partition function is the term ${}^{type-D}T_{dam}$ in this expression. This "effective" generation correction term can take different forms – that is why it has the "*type-B*" functional qualifier. The damage partition function can also take on different forms, and that is why this term has the "*type-D*" functional qualifier. The "*type-B*" qualifier must be compatible with the "*type-D*" qualifier and the "*type-D*" qualifier should, either explicitly (being part of the name) or implicitly (identified in the definition), be indicated by the form of the selected "*type-B*" qualifier.

The "effective" generation correction term isolates how much of the recoil ion energy, T_{R,j_i}, contributes to the relevant damage mode. In many cases the ${}^{type-B}\zeta\left(E_d, T_{R,j_i}, {}^{type-D}T_{dam}\right)$ term can default to be identical with the damage partition function, ${}^{type-D}T_{dam}$, multiplied by the ion energy, T_{R,j_i}. Since some other terms in the damage metric can be dependent upon this quantity, is also given a more compact notation: ${}^{ion}_{type-B/D}T_{R,j_i} = {}^{type-B}\zeta\left(E_d, T_{R,j_i}, {}^{type-D}T_{dam}\right)$. Note that this notation includes subscripts that capture both the *type-B* and *type-D* dependences.

Some damage modes can be sensitive to the energy that goes into ionization processes, i.e., changes in the electronic state. The fraction of the recoil atom energy that goes into this type of effect is often called the ionization fraction, f_{ion}. Other damage modes can be sensitive to the energy that goes into lattice atom-related phenomena, e.g., the number of lattice atoms that have been displaced from their original location, the number of vacancies and interstitials created (Frenkel pairs), or the amount of energy that goes into the crystal lattice in the form of phonons. The fraction of the recoil atom energy that goes into any of these types of effects is called the displacement fraction or the nuclear fraction, f_{nucl}. One must be very careful with the context of the word "nuclear" here. This correction term and the damage partition function have nothing to do with nuclear reactions or the strong or weak nuclear force. Rather, the term "nuclear" addresses damage modes that are related to the nuclear stopping power of the ion, i.e., energy imparted to the nuclei of lattice atoms as opposed to the electrons. As is the case for ion stopping power, which is divided into electronic and nuclear components, by convention, all of the recoil energy goes into one or the other of these two categories. So, the fractions sum to unity, i.e., $f_{ion} + f_{nucl} = 1$. The damage partition function describes the fraction of the recoil atom energy that goes into displacement/nuclear damage modes. It:

- is a function of the recoil energy, T_{R,j_i};
- is equal to the term f_{nucl} described above;
- takes on values in the interval between zero and unity, i.e., ${}^{type-D}T_{dam} \in [0,1]$.

For many damage metrics, and in particular the displacement damage-related metrics that are discussed in Sections 7.3 through 7.8, the "effective" generation correction term is directly proportional to the damage partition function – often just multiplied by the reaction-dependent recoil ion energy. Because this energy, and not just the fractional term that represents the damage partition function, appears in many formulations supporting our models, we adopt a notation for it:

$$ {}^{type-D}T^{full}_{dam}(T_{R,j_i}) = {}^{type-D}T_{dam}(T_{R,j_i}) \cdot T_{R,j_i} \tag{6}$$

Since the definition of the exact form for the damage partition function has elements of both modeling and experimental data, and since this term plays a critical role in the definition of the damage response functions, this section details some of the commonly used forms for the damage partition function. When a recoil atom slows down in a material, there are elastic interactions with the lattice atoms (i.e., nuclear interactions) and inelastic interactions with the electrons (i.e., electronic interactions). For the elastic Coulomb scattering, the interaction is modeled as the product of the Coulomb potential, $V(r) = Z_{ion} \cdot Z_{lattice} \cdot e^2 / r$, and an atomic screening function. The different variants of the damage partition function addressed below reflect differences in the modeling of the inelastic scattering and in the selection of the elastic Coulomb screening function. These different forms are differentiated by the "*type-D*" designator in the expression.

4.1. Robinson Formalism

The classical treatment of the energy partition for ions into ionization and displacement components comes from the work by Lindhard, Scharff, and Schiott [Li63] in 1963 and is referred to as the LSS energy partition [Do72]. The LSS partition of energy into the lattice from an ion with energy T_{R,j_i} and is notated as ${}^{LSS}T_{dam}\left(T_{R,j_i}\right)$. This approach is based upon the continuous slowing down treatment of the primary and secondary recoil atoms. The LSS approach uses a Thomas-Fermi screening function over the Coulomb potential to model the elastic interactions and a non-local free uniform electron gas model for the inelastic electronic scattering. The Thomas-Fermi screening radius is given by:

$$a_{T\mathrm{hom}as-Fermi} = 0.8853 \cdot a_0 \Big/ \left(Z_{ion}^{2/3} + Z_{lattice}^{2/3}\right)^{1/2} \tag{7}$$

where a_0 is the Bohr radius [a_0=0.0529 nm]. It also needs to be noted that the LSS model only addresses the Coulomb elastic scattering term and does not address nuclear elastic scattering, i.e., elastic scattering due to the strong nuclear force – which can play a role for light incident ions, such as protons or alpha particles, at high energy.

The LSS model assumes the local density approximation (LDA); that is, the material can be represented as a "structureless" solid, referred to as a "lattice gas". Thus, the LSS theory does not account for any crystal effects upon the lattice displacement nor does it account for any complications due to the cascade development [Hel93].

The Lindhard model is limited to ion energies, T_{R,j_i}, less than about $24.8 \cdot Z_{ion}^{4/3} \cdot A_{ion}$ (in keV) [Nor75, Rob71] where A_{ion} is the atomic mass of the incident ion and Z_{ion} is the atomic number of the incident ion. In gallium, this limitation translates to a maximum permissible ion energy of 168 MeV. In arsenic, the limitation translates to a maximum permissible ion energy of 197 MeV. This energy limitation is related to the LSS assumption that the stopping power is proportional to the ion velocity and, for collisions that impart more than the Bohr velocity to the lattice recoils, $e^2/\hbar =: 25\,keV/amu$, this assumption is violated [Mo12, Zi99].

Robinson and Torrens [Rob74, Rob96] have compared the LSS approach with a detailed simulation using the Firsov theory for the inelastic energy loss. Robinson [Rob71] showed that the LSS energy partition function can be approximated by a generalized functional form. This generalized functional

representation of the damage partition function is notated as ${}^{Rob}T_{dam}\left(T_{R,j_i}\right)$ and the full energy is given by the expression:

$$ {}^{Rob}T_{dam}^{full}\left(T_{R,j_i}\right)=\frac{T_{R,j_i}}{\left[1+k_L\cdot g\left(T_{R,j_i}/E_L\right)\right]} \tag{8}$$

where:

- ${}^{Rob}T_{dam}^{full}\left(T_{R,j_i}\right)$ is the full energy that is imparted to the lattice, i.e., the damage partition function multiplied by the ion energy or the non-ionizing component of the deposited energy, from an ion with energy T_{R,j_i}.
- T_{R,j_i} is the initial energy of the incident ion, in the case of a neutron interaction this is the neutron-induced primary recoil atom, in units of eV (in order to match the units of E_L).
- Z_{ion} is the atomic number of the recoil atom
- $Z_{lattice}$ is the atomic number of the lattice atom
- A_{ion} is the atomic weight of the recoil atom
- $A_{lattice}$ is the atomic weight of the lattice atom

k_L, $g(\varepsilon)$, and E_L are defined as:

$$k_L=\frac{0.0793\cdot Z_{ion}^{2/3}\cdot Z_{lattice}^{1/2}\cdot\left(A_{ion}+A_{lattice}\right)^{3/2}}{\left(Z_{ion}^{2/3}+Z_{lattice}^{2/3}\right)^{3/4}\cdot A_{ion}^{3/2}\cdot A_{lattice}^{1/2}} \tag{9}$$

$$E_L=30.724\cdot Z_{ion}\cdot Z_{lattice}\cdot\left(Z_{ion}^{2/3}+Z_{lattice}^{2/3}\right)^{1/2}\cdot\frac{\left(A_{ion}+A_{lattice}\right)}{A_{lattice}} \tag{10}$$

$$\varepsilon=T_{R,j_i}/E_L \tag{11}$$

$$g(\varepsilon)=3.4008\cdot\varepsilon^{1/6}+0.40244\cdot\varepsilon^{3/4}+\varepsilon \tag{12}$$

When this damage partition is used as the "effective" generation term, it is notated as: ${}^{ion}_{Rob/Rob}T_{R,j_i}={}^{Rob}\zeta\left(E_d,T_{R,j_i},{}^{Rob}T_{dam}\right)={}^{Rob}T_{dam}\cdot T_{R,j_i}$.

Based on the scaling rules, as captured in reference [Akk07], one can relate the E_L energy scaling term back to the Thomas-Fermi screening function used in the elastic Coulomb scattering term. If this equation is recast into the more fundamental context, and if we notate that scaling factor as E_{Rob} while using units of eV, we have:

$$E_{Rob}=\frac{Z_{ion}\cdot Z_{lattice}\cdot\left(A_{ion}+A_{lattice}\right)}{0.6944\cdot A_{lattice}\cdot a_{T\,\mathrm{hom}as-Fermi}}=\frac{30.73963\cdot Z_{ion}\cdot Z_{lattice}\cdot\left(Z_{ion}^{2/3}+Z_{lattice}^{2/3}\right)^{1/2}\cdot\left(A_{ion}+A_{lattice}\right)}{A_{lattice}} \tag{13}$$

It is expected that E_{Rob} would be equal to E_L. T`here is a close match here, but it is not exact. We can speculate that the difference may be attributed to a small round-off in some quantities used, e.g., the numbers would match exactly if the Bohr's radius used in model development were 0.05294465 rather than the current accepted value of 0.052917725. Since this value has appeared in the supporting papers as just 0.0529, this variation in the value assumed is a credible source of the difference between the fitting expressions.

If we accept the published version of the generalized fit that uses the E_L term, we can look at a simplified form of the equations for cases where the recoil atom is the same as the lattice atoms, i.e., $A=A_{ion} = A_{lattice}$ and $Z=Z_{ion} = Z_{lattice}$. In this case, the k_L and E_L terms correspond to the scaling form seen in the original Lindhard theory:

$$k_L = \frac{0.133745 \cdot Z^{2/3}}{A^{1/2}} \tag{14}$$

$$E_L = 86.931 \cdot Z^{7/3} \quad (eV) \tag{15}$$

Note that the Robinson fit to the LSS energy partition, unlike the generalized LSS formulation, is limited, by the nature of its empirical derivation, to cases where the recoil atom is close in atomic number and atomic weight to the lattice atoms. To quote from Section 5 of Reference [Nor75]:

> "Some limitations of this model must be pointed out. The Lindhard formulation of eqs (5)-(9) applies strictly only to monatomic systems (i.e., Z1=Z2) and to energies less (perhaps much less) than about 25*Z1^4/3*A1 (keV). The former limitation should not be too serious as long as the ratio Z1/Z2 does not differ too much from unity. If necessary, it could be relaxed by repeating the Lindhard calculation for other cases"

The authors are not aware that anyone has repeated the Robinson approach and derived a simple analytical expression that captures the behavior of the atomic interactions and is applicable for cases where the atomic number of the incident ion is significantly different from that of the lattice atoms. In the absence of this extension, this means that the Robinson fit to the LSS partition function should not be used to capture the displacement energy from low mass secondary particles, e.g., protons and alpha, that result from neutron-induced reactions. The damage from the low mass secondary particles should still be considered and is modeled in the general LSS approach; it is only that the Robinson fit to the energy partition may not be accurate to address these cases where the mass of the residual ion is much less than that of the lattice atoms. Despite this documented limitation, analysis tools such as the HEATR module of the NJOY-2016 code do currently use the Robinson fit to the energy partition to address the displacement kerma factor due to both the primary residual particle and the lighter secondary particles, such as protons and alpha particles. This is usually an adequate approximation to overall kerma calculations because the displacement kerma from these light secondary particles is typically very small relative to that from the heavy primary recoil ion.

When the damage partition is being used to establish a correlation with an observed level of damage, the energy from all secondary particles should be taken into consideration, as should any relevant deposited energy from the time-dependent decay of any emitted metastable secondary particles. The adequacy of the modeling of the displacement kerma from the light recoil ions and from emitted metastable particles should be considered on an application-by-application basis.

4.2. Akkerman Formulation

The previous section addressed the LSS potential and how it is the basis for the generalized expression termed the Robinson damage partition function. Several limitations in the applicable energy range for this LSS formulation were noted, e.g., for high ion energies and for dissimilar incident and lattice atomic weights. It should be noted that, while the above energy limitation applies to the Lindhard-based LSS model, codes such as MARLOWE, that can allow the user to apply the LSS model, are often augmented to also use the semi-empirical Ziegler potential to address "the transition from the Lindhard to the Bethe regime governed by Rutherford scattering" [Hou10] through the use of a "heavy ion scaling rule" to capture the stopping power of atoms with energies greater than 25 keV per amu. In MARLOWE, this has been implemented in different ways by several different people and is typically accomplished by augmenting the MARLOWE code with new interaction potentials based on the Ziegler-Biersack-Littmark (ZBL) potential [ZBL85, Hou10].

Other deviations between the LSS potential and experimental data have been evidenced at low energies [Akk06]. In addition to the improvements at high energy, the ZBL potential also addresses some of the low energy issues associated with use of the LSS formulation and the Thomas-Fermi screening function. The ZBL screening radius differs from that in the LSS formulation and is given in Reference [Akk06] as:

$$a_{ZBL} = {0.8853 \cdot a_0} \Big/ {\left(Z_{ion}^{0.23} + Z_{lattice}^{0.23} \right)} \tag{16}$$

When this formulation is used, the damage partition function is noted as ${}^{ZBL}T_{dam}\left(T_{R,j_i}\right)$.

One often used implementation of the ZBL potential is reflected in the work by Akkerman [Akk06]. Akkerman has used these updated ZBL potentials for the elastic Coulomb scattering and a combination of a local (impact parameter dependent) model and a non-local model for the inelastic ion-atom scattering to derive a new energy partition in silicon that is valid for ion energies < 500 keV and for a wide range of incident ions (atomic weights and atomic masses).

The Akkerman damage partition is notated as: ${}^{Akk}T_{dam}\left(T_{R,j_i}\right)$. These terms use the same functional representation as was adopted by the Robinson methodology, but they defined a different form for the *g*-function, partly to address the different scaling of the screening function. The form of the Akkerman *g*-function for silicon is:

$$g_{Akk}^{Si}(\varepsilon_{Akk}) = 0.74422 \cdot \varepsilon_{Akk} + 1.6812 \cdot \varepsilon_{Akk}^{3/4} + 0.90565 \cdot \varepsilon_{Akk}^{1/6} \tag{17}$$

where the dimensionless parameter, ε_{Akk}, can be expressed as:

$$\varepsilon_{Akk} = {T_{R,j_i}} \Big/ {E_{Akk}} \tag{18}$$

where,

$$E_{Akk} = \frac{Z_{ion} \cdot Z_{lattice} \cdot \left(A_{ion} + A_{lattice}\right)}{0.6944 \cdot A_{lattice} \cdot a_{ZBL}} = \frac{Z_{ion} \cdot Z_{lattice} \cdot \left(Z_{ion}^{0.23} + Z_{lattice}^{0.23}\right) \cdot \left(A_{ion} + A_{lattice}\right)}{11.62102684 \cdot A_{lattice}} \tag{19}$$

Note, in this expression, E_{Akk}, as given by Akkerman [Akk07] has units of keV, but here, in order to preserve the same form as was given above for Robinson, it has been modified to have units of eV.

The Akkerman damage partition is then given by:

$$ {}^{Akk}T_{dam}^{full}\left(T_{R,j_i}\right) = \frac{T_{R,j_i}}{\left[1 + k_L \cdot g_{Akk}^{matl.}\left(\varepsilon_{Akk}\right)\right]} \tag{20} $$

Here the "matl." superscript on the $g_{Akk}^{matl.}$ indicates an apparent material-dependence in the functional form. In some formulations of the Akkerman damage partition for silicon [Akk20], the k_L expression is also modified to reflect the use of the ZBL potential screening radius rather than the Robinson use of the screening radius corresponding to the Thomas-Moliere potential.

When this damage partition is used as the "effective" generation term, it is notated as:

$$ {}^{ion}_{Akk/Akk}T_{R,j_i} = {}^{Akk}\zeta\left(E_d, T_{R,j_i}, {}^{Akk}T_{dam}\right) = {}^{Akk}T_{dam} \cdot T_{R,j_i} . $$

The major issue with the Akkerman generalized expression is that it appears to have been developed/published only for silicon and germanium. It has a generalized expression – but only in the phase space spanned by the incident ion and the recoil energy – not with respect to an arbitrary target lattice material. While the methodology and functional form can be used for GaAs, the exact parameters in the published expressions do not appear to be applicable to materials other than silicon. To support this observation, we quote from [Akk06]:

> "The aim of this paper is to present new calculations of Q(T) for different ions with energies up to 500 keV in silicon using our Monte Carlo code."
> …"
> "Note that the new partition factor was calculated for silicon. Modifications of the model parameters are required for the electronic stopping power in targets with heavier atoms to account for the Z_2-oscillatory dependence."

While first part of this quote supports that the original work was only derived from an investigation of silicon damage, the second part of this quote only addresses the deficiency in modeling for targets that are heavier than silicon.

One also finds in [Akk07]:

> "Our calculations of f_n for different ions with charges $Z_1 \leq 15$ in silicon, use the partition factor of (3) with (5) for the ejected Si recoils".
> …
> "We have developed a model for the energy partitioning to nuclear (f_n) and electronic (f_e) parts ($f_n+f_e=1$) for low energy ions ($E_o < 200$ keV) when slowing down in silicon."

So, even though some parties are using the Akkerman functional expression for non-silicon target materials, we have to conclude that, while the approach using the ZBL potential appears to be superior to the use of the interaction terms found in the Robinson/LSS generalized functional form, one must do the BCA calculations using the ZBL potential and find relevant fitting coefficients before this form of the damage partition function is used for GaAs. This observation is also supported by the fact that in Reference [Akk20], the Akkerman $g_{Akk}\left(\varepsilon_{Akk}\right)$ expression for germanium uses different coefficients, i.e.,

$$ g_{Akk}^{Ge}(\varepsilon_{Akk}) = -3.8123 \cdot \varepsilon_{Akk} + 6.48302 \cdot \varepsilon_{Akk}^{3/4} + 2.23097 \cdot \varepsilon_{Akk}^{1/6} $$

4.3. Coulter and Parkin Variant

Coulter and Parkin [Cou80, Par83] fit the "effective" generation term and the damage partition function using the expression:

$$ {}^{CP}T_{dam}^{full}\left(T_{R,j_i}\right) = \frac{T_{R,j_i}}{\left[1 + C_1 \cdot T_{R,j}^{0.15} + C_2 \cdot T_{R,j}^{0.75} + C_3 \cdot T_{R,j}\right]} \tag{21} $$

This form is similar to the functional form of the Robinson $g(\varepsilon)$ function, but in the C_1 term it uses the energy to the power of 0.15 rather than the 1/6, or ~0.1666, which is used in the Robinson form. Coulter and Parkin's work and publications [Par81, Par83, Par89, Cou80] provided different sets of coefficients for various materials – where their emphasis was on describing the behavior of polyatomic materials where there was a significant difference in the atomic masses of the constituent atoms.

When this damage partition is used as the "effective" generation term, it is notated as:
${}^{ion}_{CP/CP}T_{R,j_i} = {}^{CP}\zeta\left(E_d, T_{R,j_i}, {}^{CP}T_{dam}\right) = {}^{CP}T_{dam} \cdot T_{R,j_i}$.

The issue with applying the Coulter and Parkin expression to GaAs is that GaAs has lattice atoms that are very similar in atomic mass, and, since their emphasis was on the treatment of polyatomic materials where there was a big difference in the atomic masses of the constituent atoms, they never published coefficients that were directly applicable to GaAs. In their work they used the DON code to calculate the energy dependence and then extracted the functional fit. This process could be repeated for GaAs using currently available codes to describe the energy dependence and then performing a fit using their expression. However, since Coulter and Parkin used the Lindhard potentials, their energy dependence for monoatomic lattice materials is expected to be very similar to the data representation in the Robinson fit. In their publications they note that, because of the difference in the power of the C_1 term, when their expression is used for monoatomic materials their damage partition function yields values about ~6% lower than that of the Robinson expression [Par89].

4.3.1. Treatment of a Polyatomic Lattice

Since the Robinson work, and the underlying Lindhard work, did not explicitly address how to define an effective lattice mass for polyatomic materials, we look to the work by Parkin and Coulter for guidance in handling polyatomic lattice materials. Parkin [Par89], in "The Displacement Cascade in Solids", noting work by Coulter and Parkin [Cou80], concludes that:

> "In summary, the damage energy calculations produced two important findings. First, in rough general terms, combining different atom types in a polyatomic material reduces damage efficiencies relative to monoatomic materials. Second, deviation from stoichiometric behavior in the damage energies casts serious doubt on procedures in which the material is represented by average *Z* and *A*. In fact, CP found that as a general rule, damage energies in polyatomic materials are better represented by monatomic "self-atom" values than for average *Z*- and A-values."

The basis for this conclusion is seen in Figure 4-1. Thus, in our analysis we have used the self-atom formulation for the lattice atomic mass and atomic number when we use the Robinson damage partition function rather than utilizing the average lattice atom's atomic number and atomic weight.

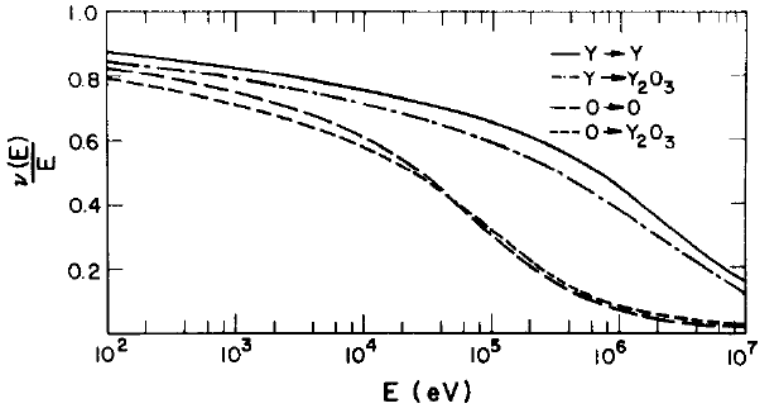

Figure 4-1. Damage Efficiencies in Y_2O_3, extracted from [Cou80]

4.4. Computed Damage Partition Models

Where the above examples of damage partition functions were the results of generalized fits, spanning a range of lattice atoms or incident ions, to analytic forms, computational models can also be used to produce damage partition functions for specific combinations of incident ions and lattice atoms. When using a computed partition model, the notation must clearly define the code. In addition, one must also consider that the partition function will clearly depend upon the set of input parameters that were used in the calculation. The most important input quantity for a calculation is the description of the interatomic Coulomb potential and Coulomb screening function that were used. The following sections provides a general description of some of the computational codes that are used to support this type of modeling.

4.4.1. SRIM

SRIM is a very popular and easy-to-run binary collision approximation (BCA) code [Zi10]. This Monte Carlo code uses the ZBL potentials to calculate the vacancy production and has an easy interface to extract the ion stopping powers. The SRIM code provides spatial profiles for the various energy deposition processes and also provides integrated summary tables that divide the deposited energy into:

- Electronic/ionization
  - from source ions
  - from recoil ions
- Phonons (includes all energies less than the displacement threshold energy)
  - from source ion
  - from recoil ions
- Vacancies, i.e., binding energy (loss to the target through creation of vacancies or replacement collisions)
  - from source ions
  - from recoil ions

There are multiply ways to determine the energy/damage partition and the vacancy profile in an SRIM calculation [Sto20, OECD, Sto13] – however, care must be taken because these different modes can yield different results. Reference [Sto20] notes:

> "Users who wish to use SRIM to compute ion-induced cascade damage, may employ either of two basic options: (1) "Ion Distribution and Quick Calculation of Damage," and (2) "Detailed Calculation with full Damage Cascades." The user must designate the nature and energy of the incident ion, the nature of the target, and both the displacement threshold energy and the lattice binding energy. One advantage of the latter option is that it provides a complete listing of the energy for all the knock-on atoms produced by the incident ions. The lattice binding energy should be set to zero for consistency with the NRT model, and …"

As further noted in this reference:

- "a number of researchers using SRIM began to observe discrepancies between results obtained with the two calculation options."
- "this difference was generally more than a factor of two"
- "results such as these led to the recommendation that the results of the vacancy.txt file should not be used, particularly from the full cascade calculation. Because the source of the anomaly in the vacancy.txt results could not be determined, it seems prudent to avoid its use even for the quick calculation. In order to use SRIM calculations to compute dpa, particularly for the purpose of comparing ion and neutron irradiation, the damage energy should be computed using the approach described in Ref. 47 [Aga21]."

Reference [Aga21] explains the difference between the calculational modes and notes:

> "we show that the SRIM F-C vacancy text file method should not be used for vacancy production calculations. This error appears to be due to mischaracterization within the SRIM F-C option of some near-threshold replacement events as vacancies instead of replacements.
>
> Use of the latest SRIM stopping powers in the SRIM F-C approach provides a better calculation of electronic and nuclear stopping compared to the Lindhard stopping power analytical approximation used to calculate the damage energy of recoil atoms in the SRIM Q-C option, and therefore SRIM F-C approach is deemed to provide the best accuracy for vacancy production (within the binary collision approximation) as long as the damage energy method is used. Alternately, the SRIM Q-C option using either the vacancy.txt or damage energy method provides relatively fast calculation speeds with moderate quantitative differences from the F-C damage energy results (~0 to ~ 30% for the investigated ion-target cases)."
>
> "Although in principle the Full Cascades vacancy.txt method should be the most appealing approach due to its simplicity, the use of relatively accurate SRIM stopping powers and detailed 3D collision information, the large overestimate of vacancy production (apparently associated with mischaracterization of some near-threshold replacements as vacancies) that varies strongly with projectile and target mass impels us to conclude that this method cannot be recommended for defect production calculations for any ion-target combination."
>
> "We recommend vacancy production calculations using the SRIM Full Cascades damage energy method (either "energy to recoils" minus recoil ionization, Eq. (2) or phonon energy, Eq. (4)). This option generally provides the highest accuracy for vacancy production due to

the use of SRIM stopping powers for both the incident ions and all recoils and detailed tracking of all ion collisions within the binary collision approximation limitations."

In Reference [Che20], in addressing the SRIM behavior, we see:

> "In general, the number of atomic displacements is proportional to the damage energy for incident ion energy above keV and about 2 times the value deduced from the modified Kinchin-Pease formula."

Because of this variation in how SRIM can be used, [Sto13] made the recommendation (for iron and iron-based alloys):

> "The following recommendations should be complied with:
>
> - (1) run SRIM using the "Quick" Kinchin and Pease option,
> - (2) choose the recommended displacement threshold energy from Ref. [ASTM521], which is 40 eV for iron or iron-based alloys,
> - (3) set the lattice binding energy to zero,
> - (4) compute the damage energy according to Eq. (5b), and
> - (5) use the computed value of T_{dam} to calculate the number of displacements according to Eq. (1)."

If we use the SRIM Q-C method with an integrated damage energy approach (based on the SRIM summary energy distribution tables), the resulting "effective" generation correction term and the damage partition function are notated as: ${}^{SRIM-QC-DE}T_{dam}\left(T_{R,j_i}\right)$. The SRIM F-C method is notated as: ${}^{SRIM-FC-DE}T_{dam}\left(T_{R,j_i}\right)$. When these damage partition functions are used as the "effective" generation term, they are notated as: ${}^{ion}_{SRIM-QC/SRIM-QC}T_{R,j_i} = {}^{SRIM-QC}\zeta\left(E_d, T_{R,j_i}, {}^{SRIM-QC}T_{dam}\right) = {}^{SRIM-QC}T_{dam} \cdot T_{R,j_i}$ and ${}^{ion}_{SRIM-FC/SRIM-FC}T_{R,j_i} = {}^{SRIM-FC}\zeta\left(E_d, T_{R,j_i}, {}^{SRIM-FC}T_{dam}\right) = {}^{SRIM-FC}T_{dam} \cdot T_{R,j_i}$.

Table 4-1 and Figure 4-2 compare the damage partition metrics between the SRIM calculation modes and the conventional Robinson formula for GaAs. If one examines the energy partition, the table and Figure 4-2a show that both the SRIM-QC and SRIM-FC energy partitions are seen to be very similar to the Robinson energy partition.

We can also compare the vacancy production rates in SRIM with those from the traditional Robinson approach, however, caution must be used in interpreting the variation that can be seen in the vacancy production rate. As noted in reference [Sto13] in addressing the use of the NRT predicted number of vacancies, "It is not the 'right' number of displacements in any absolute sense; its importance lies in its broad adoption as a standard reference value". Also, since the Robinson empirical fitting for the energy partitioning into ionization and displacement does not directly address vacancy production, in order to obtain estimates of the vacancy creation from the energy going into displacements, we apply the Kinchin-Pease treatment and identify an energy of $(2gE_d)/\beta$ going into the creation of every Frenkel pair. When we performed the SRIM calculations referenced later in this section, we used the default E_d value in SRIM for GaAs, which is 25 eV, rather than the recommended value of 10 eV cited in Section 3.2.3. The SRIM default value of 25 eV is close to the 23 eV value used in Reference [Aga21] for GaAs. So, to be consistent in the

comparison of the vacancy production between Robinson and SRIM, we decided to use a consistent value for E_d.

If one examines the vacancy production, then Table 4-1 and Figure 4-2b confirm the results cited in the literature, i.e., that the SRIM Q-C method gives results vacancy production rates roughly consistent with the Robinson formula when one takes into consideration that the improved ZBL potentials are used in SRIM whereas the Robinson formula is based on the LSS potential which uses the Thomas-Fermi Coulomb screening function. And, the SRIM F-C method is found to give vacancy production levels that are about 2X larger.

Table 4-1. Comparison of Damage Partition Metrics Between Robinson and SRIM Modes

Energy (keV)	Robinson with Kinchin-Pease		SRIM-QC*		SRIM-FC*	
	Percent Energy into Displacements (%)	Vacancies / Incident-Ion&	Percent Energy into Displacements (%)	Vacancies / Incident-Ion	Percent Energy into Displacements (%)	Vacancies / Incident-Ion
1.00	82.4113	13.18581	83.75	12.8	81.31	25.2
5.00	77.9248	62.33986	79.72	62.7	80.72	114.7
10.00	75.618	120.9889	77.74	123	79.7	221.2
25.00	72.0378	288.1512	74.75	296.8	77.65	529.7
50.00	68.7304	549.8432	72.02	572.9	75.5	1025.6
75.00	66.4491	797.3894	70.16	837	73.95	1505.2
100.00	64.63	1034.079	68.71	1094.2	72.76	1971.6
200.00	59.3746	1899.987	64.2	2046.3	68.62	3722.5
250.00	57.369	2294.761	62.41	2487.	66.83	4539.3
300.00	55.6016	2668.875	60.8	2908.1	65.27	5321.8
400.00	52.5651	3364.17	57.96	3696.6	62.44	6790.7
500.00	49.99969	3999.751	55.44	4418.7	59.89	8145.2
750.00	44.8709	5384.51	50.17	5997	54.43	11103.4
1000.00	40.9206	6547.296	45.97	7325.1	50.05	13618.3
2000.00	30.8208	9862.661	34.94	11129.8	38.22	20794.8
5000.00	18.3198	14655.87	20.59	16379.1	22.65	30716.2
10000.00	11.1554	17848.67	12.36	19627.1	13.58	36773.1

*** SRIM Monte Carlo calculation used 100,000 histories**

& Vacancies calculated using the displacement damage energy divided by the Kinchin-Pease formula $2 \cdot E_d / \beta$ for energy required to create a Frenkel pair with SRIM default for GaAs of E_d=25 eV and β=0.8.

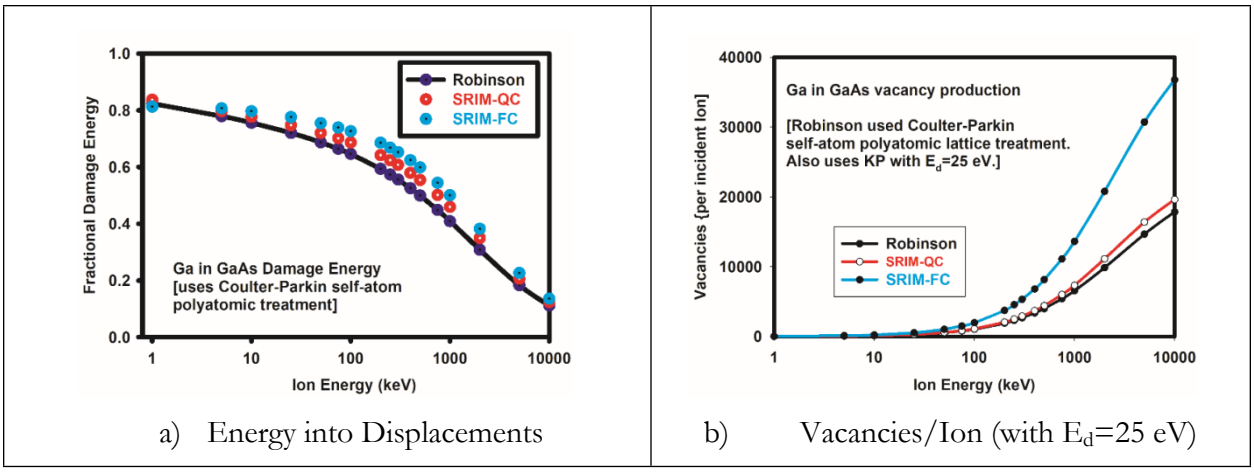

a) Energy into Displacements b) Vacancies/Ion (with E_d=25 eV)

Figure 4-2. Comparison of SRIM "Full" and "Quick" Simulation Modes and Robinson Damage Partition Function

4.4.2. MARLOWE

MARLOWE is another popular binary collision approximation code [MARLOWE, Ort14, Dem16]. With respect to the implementation of "damage energy" in the MARLOWE code, Robinson notes [Rob83]:

> "The damage energy appears in MARLOWE as the sum of three terms.
>
> a) The kinetic energy transferred in quasi-elastic collisions to target atoms which are not displaced (each contribution < E_d).
>
> b) The energy expended by displaced particles in overcoming binding (each contribution = E_b).
>
> c) The final kinetic energy of each recoil which stops within the target (each contribution < E_c)."

Thus, MARLOWE includes the energy less than E_d in its definition of the "damage energy" from ion cascades. In the above quote, E_b is the binding energy and E_c is the cut-off energy below which the ion is not tracked in the calculation [Rob92]. As a consequence, MARLOWE does not directly use a displacement damage threshold energy. The proper way to determine the numerical quantities related to the partition of the low damage events is addressed in reference [Viz15]. The treatment used for the cut-off energy needs to be consistent with the treatment for the displacement threshold that is addressed in Section 5. This implies that auxiliary documentation should define how the partition function addresses subthreshold events, e.g., in the Robinson formalism there is no explicit lower bound and in the MARLOWE formalism the user can use input parameters to define a binding energy and use a vacancy/interstitial recombination radius to control the number of resulting vacancies/interstitials.

The MARLOWE code supports a more complex division of energy. Here, the energy loss is partitioned into:

- Inelastic energy loss
- Binding loss (displacements)
- Binding loss (replacement)
- Binding loss (non-lattice)

- Sub-threshold loss (lattice)
- Sub-threshold Loss (non-lattice)
- Remaining kinetic energy
- Available for damage
- In replacement sequences
- Carried by focusons
- Replacement threshold
- Focuson threshold
- Carried through front surface
- Binding loss (front surface)
- Remaining kinetic (front adatoms)

The MARLOWE binary collision approximation code [MARLOWE] can be used to calculate the ion energy-dependent partition function using a range of interaction models that have been developed. There are two types of interactions in MARLOWE: those that describe the inelastic energy loss (e.g., Firsov or Lindhard electronic interactions) and those that describe the interatomic potentials (e.g., Moliere or Lenz-Jensen potential) that affect the ion interactions with the lattice atoms. The former is called the electronic potential and is typically described by the LSS or ZBL potential. The latter is called the nuclear potential - even though it has nothing to do with nuclear interactions.

It must be noted that, while the previously mentioned energy limitation applies to the LSS model, codes such as MARLOWE that incorporate the LSS model often are augmented to also use the semi-empirical Ziegler potential to address "the transition from the Lindhard to the Bethe regime governed by Rutherford scattering" [Hou10] through the use of this "heavy ion scaling rule" to capture the stopping power of atoms with energies greater than 25 keV per amu. In MARLOWE, this has been implemented by several different people and is typically accomplished by augmenting the MARLOWE code with new interaction potentials based on the ZBL potential [ZBL85, Hou10]. Because of the dependence upon the selected potential, an "effective" generation term and a damage partition function calculated with MARLOWE should be notated as: ${}^{MARLOWE(potential)}T_{dam}\left(T_{R,j_i}\right)$.

When these damage partition functions are used as the "effective" generation term, they are notated as: ${}^{ion}_{MARLOWE/MARLOWE}T_{R,j_i} = {}^{MALROWE(potential)}\zeta\left(E_d, T_{R,j_i}, {}^{MARLOWE(potential)}T_{dam}\right) = {}^{MARLOWE(potential)}T_{dam} \cdot T_{R,j_i}$.

It should be noted that, while some analysis/codes only treat the damage energy from the primary residual atom, the formal definition of damage energy requires that the damage from all emitted particles be considered. Thus, the definition requires that the damage energy be summed over all of the particles in the outgoing reaction channel. In some of the formulations found in the literature, this is not explicitly taken into account.

In cases where a neutron-induced residual reaction product is emitted in an excited state that subsequently decays with the emission of a different ion, the damage energy from the subsequent decay products should also be included in the neutron damage energy. The SPECTER code [Gre85] includes this consideration for some cases of interest to the pressure vessel embrittlement community, e.g., beta decay of ^{28}Al.

4.4.3. Molecular Dynamics

Molecular Dynamics (MD) codes are another class codes that can model the atomic interactions and describe the time-dependent evolution of the system and, in principle, be used to derive the energy partition. MD codes are more accurate than BCA codes, but they also require longer computational times. The improved accuracy of the MD codes can be important in modeling lower energy atomic interactions. Thus, many approaches marry a BCA code for modeling high energy atom-lattice interaction with an MD treatment at lower energy.

One critical limitation of MD codes for deducing the energy partitioning between ionization and displacement is that MD codes do not typically model the electronic interactions. As seen in reference [Hem20]:

> "Electronic stopping (ES) of energetic atoms is not taken care of by the interatomic potentials used in molecular dynamics (MD) simulations when simulating collision cascades."
> "The Lindhard-Scharff (LS) formula for electronic stopping is therefore included as a drag term for energetic atoms in the open-source large scale atomic molecular massively parallel simulator (LAMMPS) code."
>
> "This does not include the inelastic collisions between a fast particle and electrons in the system – i.e., electronic stopping. Therefore, ES has to be accounted for separately in MD simulations of collision cascades."
>
> "The easiest way to include the effect of ES in a molecular dynamics (MD) code is by damping the velocity of an atom by a viscous force"
>
> "A different approach is taken by Duffy et al., wherein the energy is transferred from an energetic ion to a background electron gas by frictional forces. This heats up the electron gas and subsequently raises the local temperature by thermal energy transfer between the electron gas and the ambient nuclei [13, 14]. This local hot-spot formation can have implications on the final number of defects produced and on in-cascade defect clustering."

Another issue that arises when one compares results between MD codes and the traditional NRT approach, is that, as stated in reference [Sto20],:

> "stable defect production from the MD simulations are about one-third of the NRT value …"

And, as reported in reference [Cro16]:

> "It has long been acknowledged, both experimentally (e.g., Ref. [4]) and from Molecular Dynamics (MD) simulations that the NRT formula overestimates the amount of created defects. MD simulations have shown that this overestimation comes from the partial recrystallization that takes place during the heat spike of the cascade."

So, MD codes can produce a more accurate metric for the number of vacancies produced, as well as a metric for more complex types of defects, but they have the limitation of needing to have an external model applied to address the electronic interactions and the challenge of having this external model not break down in the Bethe region for high energy recoils, such as for alpha particles..

The "effective" generation correction term and the damage partition function for a MD code are noted in our formalism as: ${}^{MD(code,potential)}T_{dam}\left(T_{R,j_i}\right)$. When these damage partition functions are used as the "effective" generation term, they are notated as:
${}^{ion}_{MD/MD}T_{R,j_i} = {}^{MD(code,potential)}\zeta\left(E_d, T_{R,j_i}, {}^{MD(code,potential)}T_{dam}\right) = {}^{MD(code,potential)}T_{dam} \cdot T_{R,j_i}$.

5. THRESHOLD TREATMENT OF DISPLACEMENTS

The formulation of the damage metric in Equation 2 contained the term, ${}^{type-A}\Lambda\left(E_d, {}^{ion}_{type-B/D}T_{R,j_i}\right)$, which is a term that treats the efficiency of the damage near the displacement threshold energy. This threshold treatment term can take different forms – that is why it has the "*type-A*" functional qualifier, and it is a function of the displacement threshold energy, E_d. Some common forms for this term, with their associated "*type-A*" qualifier, are addressed in the following subsections. As noted earlier, ${}^{ion}_{type-B/D}T_{R,j_i}$ is a shorthand notation for the functional expression, ${}^{type-B}\zeta\left(E_d, T_{R,j_i}, {}^{type-D}T_{dam}\right)$, that was addressed in Section 4. As was the case in the Section 4 discussion of the damage partition function, the "*type-A*" qualifier often dictates the allowed forms for the "*type-B*" and "*type-D*" qualifiers.

5.1. Kinchin-Pease

The original Kinchin-Pease model [Rob68, Kin55, Si69, Od76, Rob75] relates the number of defects, ${}^{orig\_K\&P}v_d\left(E_d, E_I, {}^{ion}_{LSS/LSS}T_{R,j_i}\right)$, to the primary recoil atom energy:

$$ {}^{orig\_K\&P}v_d\left(E_d, E_I, {}^{ion}_{LSS/LSS}T_{R,j_i}\right) = \begin{pmatrix} 0 & 0 \le {}^{ion}_{LSS/LSS}T_{R,j_i} < E_d \\ 1 & E_d \le {}^{ion}_{LSS/LSS}T_{R,j_i} < 2\gamma E_d \\ T_R/(2\gamma E_d) & 2\gamma E_d \le {}^{ion}_{LSS/LSS}T_{R,j_i} < E_I \\ E_I/(2\gamma E_d) & E_I \le {}^{ion}_{LSS/LSS}T_{R,j_i} < \infty \end{pmatrix} \tag{22} $$

where ${}^{ion}_{LSS/LSS}T_{R,j_i}$ is the damage energy from the recoil ion based on use of the Lindhard partition function and E_I is the damage energy above which ions lose their energy only through ionization and below which energy loss could be modeled with an elastic hard sphere scattering model. When this model was coupled with the LSS model for the energy partition function, then there was no longer a need to introduce the E_I energy and the equation could be rewritten as a function of the non-ionizing portion of the ion energy, ${}^{ion}_{LSS/LSS}T_{R,j_i}$.

The commonly seen version of the Kinchin-Pease model uses this LSS energy partition function and has the number of defects, ${}^{K\&P}v_d\left(E_d, {}^{ion}_{LSS/LSS}T_{R,j_i}\right)$, given by the expression:

$$ {}^{K\&P}v_d\left(E_d, {}^{ion}_{LSS/LSS}T_{R,j_i}\right) = \begin{pmatrix} 0 & 0 \le {}^{ion}_{LSS/LSS}T_{R,j_i} < E_d \\ 1 & E_d \le {}^{ion}_{LSS/LSS}T_{R,j_i} < 2\gamma E_d \\ {}^{ion}_{LSS/LSS}T_{R,j_i} \Big/ (2\cdot E_d) & 2\gamma E_d \le {}^{ion}_{LSS/LSS}T_{R,j_i} < \infty \end{pmatrix} \tag{23} $$

In order to support a later discussion of damage energy, we also define the term that represents the baseline energy required to create the Frenkel pairs within the context of the Kinchin-Pease threshold treatment:

$$ {}^{K\&P}\varsigma_d\left(E_d, {}^{ion}_{LSS/LSS}T_{R,j_i}\right) = {}^{ion}_{LSS/LSS}T_{R,j_i} / (2\gamma E_d) \tag{24} $$

Then, equation (23) can be re-written as:

$$ {}^{K\&P}\nu_d\left(E_d, {}^{ion}_{LSS/LSS}T_{R,j_i}\right) = {}^{K\&P}\Lambda(E_d, {}^{ion}_{LSS/LSS}T_{R,j_i})\, g^{ion}_{LSS/LSS}T_{R,j_i} / (2\gamma E_d) \tag{25} $$

where:

$$ {}^{K\&P}\Lambda\left(E_d, {}^{ion}_{LSS/LSS}T_{R,j_i}\right) = \begin{pmatrix} 0 & 0 \le {}^{ion}_{LSS/LSS}T_{R,j_i} < E_d \\ (2\cdot E_d)\Big/ {}^{ion}_{LSS/LSS}T_{R,j_i} & E_d \le {}^{ion}_{LSS/LSS}T_{R,j_i} < 2\gamma E_d \\ 1 & 2\gamma E_d \le {}^{ion}_{LSS/LSS}T_{R,j_i} < \infty \end{pmatrix} \tag{26} $$

This formulation extracts the efficiency of the damage near the displacement threshold energy.

5.2. Sharp Threshold Kinchin-Pease

The Kinchin-Pease model is sometimes quoted as using a sharp transition, the transition being modeled as occurring at E_d. The sharp-threshold Kinchin-Pease model typically builds the threshold treatment upon the Robinson formulation of the damage partition function. Here the number of Frenkel pairs created is given by:

$$ {}^{sp\_K\&P}\nu_d\left(E_d, {}^{ion}_{Rob/Rob}T_{R,j_i}\right) = \begin{pmatrix} 0 & 0 \le {}^{ion}_{Rob/Rob}T_{R,j_i} < E_d \\ {}^{ion}_{Rob/Rob}T_{R,j_i}\Big/(2\cdot E_d) & E_d \le {}^{ion}_{Rob/Rob}T_{R,j_i} < \infty \end{pmatrix} \tag{27} $$

In order to support a later discussion of damage energy, we also define the term:

$$ {}^{sp\_K\&P}\varsigma_d\left(E_d, {}^{ion}_{Rob/Rob}T_{R,j_i}\right) = {}^{K\&P}\varsigma_d\left(E_d, {}^{ion}_{Rob/Rob}T_{R,j_i}\right) = {}^{ion}_{LSS/LSS}T_{R,j_i} / (2\gamma E_d) \tag{28} $$

Then, Equation (27) is equation can be re-written as:

$$ {}^{sp\_K\&P}\nu_d\left(E_d, {}^{ion}_{Rob/Rob}T_{R,j_i}\right) = {}^{sp\_K\&P}\Lambda(E_d, {}^{ion}_{Rob/Rob}T_{R,j_i})\, g^{ion}_{LSS/LSS}T_{R,j_i} / (2\gamma E_d) \tag{29} $$

where,

$$ {}^{sp\_K\&P}\Lambda\left(E_d, {}^{ion}_{Rob/Rob}T_{R,j_i}\right) = \begin{pmatrix} 0 & 0 \le {}^{ion}_{Rob/Rob}T_{R,j_i} < E_d \\ 1 & E_d \le {}^{ion}_{Rob/Rob}T_{R,j_i} < \infty \end{pmatrix} \tag{30} $$

Equation 30 then expresses the efficiency of the damage near the displacement threshold energy. Above the threshold region, the slope of the defect creation with respect to energy, ${}^{sp\_K\&P}\eta$, is:

$$ {}^{sp\_K\&P}\eta = dv[{}^{ion}_{Rob/Rob}T_{R,j_i}]/d[{}^{ion}_{Rob/Rob}T_{R,j_i}] = [1/(2gE_d)] \tag{31} $$

The reference energy (note, this is a reference energy and not a minimum energy) required to create a single Frenkel pair, ${}^{sp\_K\&P}\alpha$, is then given by:

$$ {}^{sp\_K\&P}\alpha = (2gE_d) \tag{32} $$

The sharp threshold Kinchin-Pease form of the equation described above is what is built into codes such as NJOY [NJOY2016] and used to compute the quantity identified in their code output as the "damage energy".

5.3. NRT

After the original Kinchin-Pease formulation, the radiation damage community did additional theoretical work and computer simulations. A group of experts at an IAEA Specialist's meeting on radiation damage units adopted a modified formulation for the number of displacements. This approach used the Robinson-Sigmund modification of the hard-sphere scattering energy loss model. The NRT model typically builds the threshold treatment upon the Robinson formulation of the damage partition function, so ${}^{ion}_{NRT/NRT}T_{R,j_i} = {}^{ion}_{Rob/Rob}T_{R,j_i}$. This model is called the Norgett, Robinson, and Torrens (NRT) Frenkel pair model, or the modified Kinchin-Pease, and is given by:

$$ {}^{NRT}v_d\left(E_d, {}^{ion}_{NRT/NRT}T_{R,j_i}\right) = \begin{pmatrix} 0 & 0 \le {}^{ion}_{NRT/NRT}T_{R,j_i} < E_d \\ 1 & E_d \le {}^{ion}_{NRT/NRT}T_{R,j_i} < 2\cdot E_d / \beta \\ \beta \cdot {}^{ion}_{NRT/NRT}T_{R,j_i} / (2\cdot E_d) & 2\cdot E_d / \beta \le {}^{ion}_{NRT/NRT}T_{R,j_i} < \infty \end{pmatrix} \tag{33} $$

where β is an atomic scattering correction and is taken to be 0.8. This adopted value of 0.8 is close to the $\zeta(m=1)$ value used in the Robinson-Sigmund analysis.

Figure 5-1 shows the defect creation rate as a function of the non-ionizing damage delivered to GaAs.

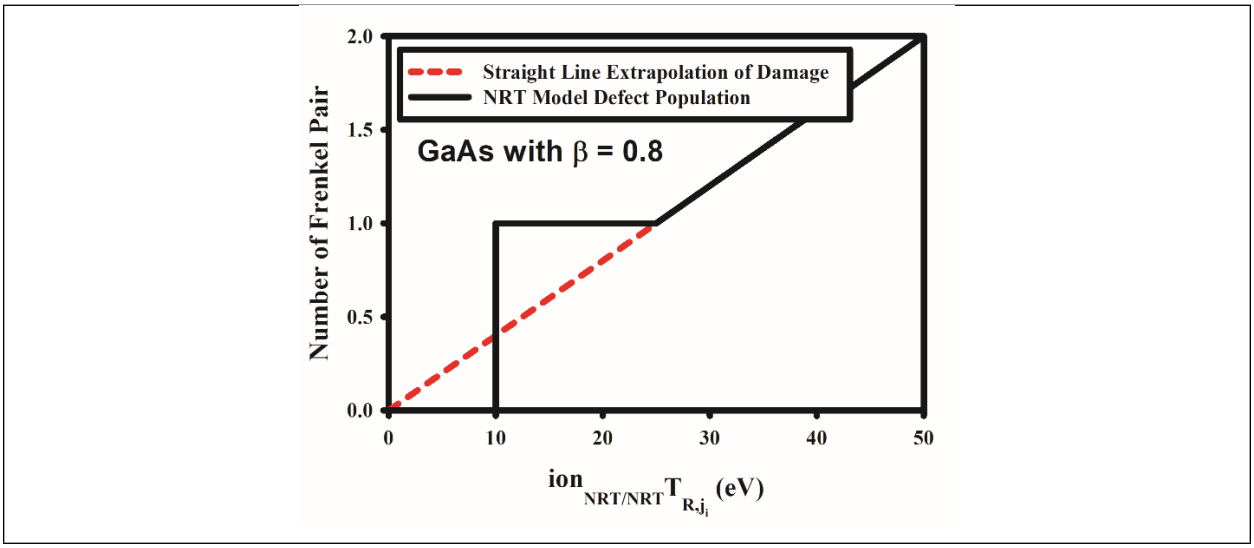

Figure 5-1. Non-ionizing Ion Energy Dependence of NRT Frenkel Pair Creation in GaAs

To support placing this into the context of the damage energy, we define the term:

$$ {}^{NRT}\varsigma_d\left(E_d, {}^{ion}_{NRT/NRT}T_{R,j_i}\right) = (\beta g^{ion}_{NRT/NRT}T_{R,j_i}) / (2gE_d) \tag{34} $$

This equation can be re-written as:

$$ {}^{NRT}v_d\left(E_d, {}^{ion}_{NRT/NRT}T_{R,j_i}\right) = {}^{NRT}\Lambda(E_d, {}^{ion}_{NRT/NRT}T_{R,j_i})g(\beta g^{ion}_{NRT/NRT}T_{R,j_i}) / (2gE_d) \tag{35} $$

where,

$$ {}^{NRT}\Lambda\left(E_d, {}^{ion}_{NRT/NRT}T_{R,j_i}\right) = \begin{pmatrix} 0 & 0 \le {}^{ion}_{NRT/NRT}T_{R,j_i} < E_d \\ (2\cdot E_d) \Big/ (\beta g^{ion}_{NRT/NRT}T_{R,j_i}) & E_d \le {}^{ion}_{NRT/NRT}T_{R,j_i} < (2gE_d/\beta) \\ 1 & (2gE_d/\beta) \le {}^{ion}_{NRT/NRT}T_{R,j_i} < \infty \end{pmatrix} \tag{36} $$

Equation 36 then expresses the efficiency of the damage near the displacement threshold energy.

The reference energy required to create a Frenkel pair, ${}^{NRT}\alpha$, is then given by:

$$ {}^{NRT}\alpha = (2gE_d)/\beta \tag{37} $$

Note from Equation 36 that the energy required to create the first defect is only E_d, whereas at high recoil energies the non-ionizing energy associated with the creation of each defect is ${}^{NRT}\alpha$, more than twice value at the displacement threshold. Figure 5-2 shows that, because of this treatment of displacements near the threshold energy, the NRT threshold function, ${}^{NRT}\Lambda\left(E_d, {}^{ion}_{Rob/Rob}T_{R,j_i}\right)$, shows an enhancement for energies between E_d and ${}^{NRT}\alpha$. As seen in Figure 5-2, the sharp transition Kinchin-Pease threshold function does not exhibit this enhancement.

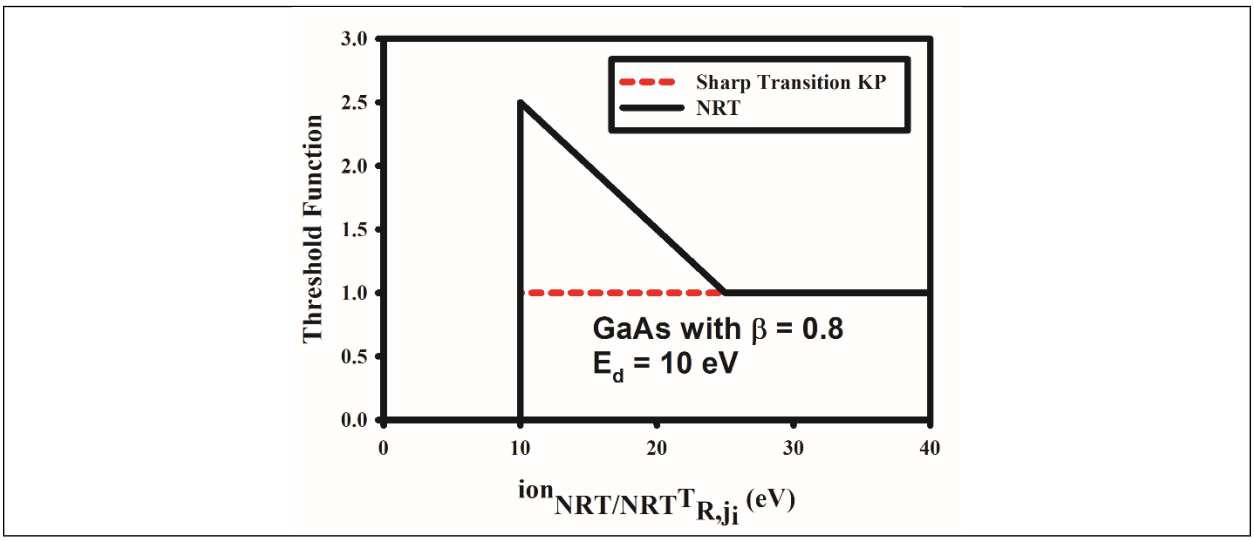

Figure 5-2. Energy-dependence of the Sharp-transition Kinchin-Pease and NRT Threshold Functions in GaAs

5.4. Other Variants

A variety of other variants for the threshold treatment have appeared in the literature. These other variants are not commonly used in current material damage studies, but, for completeness, some of the published variants are described in the following subsections.

5.4.1. Robinson-Sigmund Modification

The community has examined various forms for the number of Frenkel pairs resulting from different analytic forms of the differential elastic scattering cross section between atoms, *K(E,T),* represented by a screened Coulomb interaction with the form:

$$K(E,T) = E^{-m} * T^{(-1-m)} \text{ where } -1 \le m \le 1. \tag{38}$$

Here *K(E,T)* is the probability that a particle of initial kinetic energy E will transfer energy T to another particle in a single collision.

While imposing a consistency condition on the average number of Frenkel pairs produced in a random collision cascade, Robinson calculated an asymptotic solution for $E > 2E_d$ of:

$$N(E) = \zeta(m) * E / (2 * E_d) \tag{39}$$

For m = -1 the equation represents hard sphere scattering and $\zeta(m=-1) = 1$, the Kinchin-Pease initial expression. When m = 1, the Rutherford collision region, the expression became

$$\zeta(m=1) = (12/pi\text{^}2)/ln(2) \approx 0.84 \tag{40}$$

While Robinson derived these initial results, Sigmund showed that, if "m" is permitted to vary with energy, a nonlinearity was introduced into the Frenkel pair production term.

In the Robinson-Sigmund variation, the threshold treatment is similar to that for the NRT treatment in Equation 23, but the β term is replaced by *ζ(m)*.

5.4.2. Snyder-Neufeld

Snyder-Neufeld introduced a model using a slightly different formulation for the Frenkel pair generation efficiency term. The model historically was applied using the Robinson damage partition function. Their formulation is described by:

$$^{SN}\nu_d\left(E_d, {}^{ion}_{Rob/Rob}T_{R,j_i}\right) = {}^{K\&P}\Lambda(E_d, {}^{ion}_{Rob/Rob}T_{R,j_i})\,g\,{}^{SN}\varsigma_d[E_d, {}^{ion}_{Rob/Rob}T_{R,j_i}] \tag{41}$$

$$^{SN}\varsigma_d\left(E_d, {}^{ion}_{Rob/Rob}T_{R,j_i}\right) = ({}^{ion}_{Rob/Rob}T_{R,j_i} + E_d)/(2gE_d) \tag{42}$$

5.4.3. Neufeld-Snyder

Another variation in the Frenkel pair generation efficiency term is found in the Neufeld-Snyder formulation, also based upon the Robinson damage partition function, given by:

$$^{NS}\nu_d\,{}^{ion}_{Rob/Rob}T_{R,j_i} = {}^{K\&P}\Lambda(E_d, {}^{ion}_{Rob/Rob}T_{R,j_i})\,g\,{}^{NS}\varsigma_d[E_d, {}^{ion}_{Rob/Rob}T_{R,j_i}] \tag{43}$$

$$^{NS}\varsigma_d\left(E_d, {}^{ion}_{Rob/Rob}T_{R,j_i}\right) = ({}^{ion}_{Rob/Rob}T_{R,j_i} + E_d)/(3gE_d) \tag{44}$$

5.4.4. Bacon

Work by Bacon [Ba95, Ga01] used MD calculations, with the Robinson treatment of the energy loss due to ionization before the MD calculation was performed, that modeled the many-body effects of the thermal spike phase in the cascade development and found that the results could be fit with an equation of the form:

$$\nu_d^{Bacon}\left(E_d, T_{R,j_i}^{ion}, m\right) = \Lambda^{K\&P}(E_d, T_{R,j_i}^{ion})\,\xi_d^{Bacon}(E_d, T_{R,j_i}^{ion}, m) \quad (45)$$

$$\xi_d^{Bacon}\left(E_d, T_{R,j_i}^{ion}, m\right) = A\left(T_{MD/Rob,R,j_i}^{ion}\right)^m \quad (46)$$

This form corresponds to the NRT model (for $\beta = 0.8$) when $m = 1$ and $A = 0.8/(2*E_d)$. Bacon fit the MD results for various metals and observed a trend of decreased Frenkel pair production efficiency with increasing recoil ion energy. The fit for the coefficient "m" yielded a value of 0.76 for Titanium and as 0.787 for Zirconium.

6. DAMAGE EFFICIENCY FUNCTION

The formulation of the damage metric in Equation 2 contained the term ${}^{type-C}\xi\left(T_{R,j_i}, {}^{ion}_{type-B/D}T_{R,j_i}\right)$, which is a residual damage efficiency correction or defect survival term. This threshold treatment term can take different forms – that is why it has the "*type-C*" functional qualifier, and it can be a function of either the recoil ion energy, T_{R,j_i}, or the damage energy, ${}^{ion}_{type-B/D}T_{R,j_i}$. Some common forms for this term, with their associated "*type-C*" qualifier, are addressed in the following subsections. As was the case in the Section 4 discussion of the damage partition function, the "*type-C*" qualifier is often correlated with the forms for the "*type-B*" and "*type-D*" qualifiers.

6.1. ASTM E722

Figure 6-1 shows a plot of the efficiency curve, with highlighted datapoints, that corresponds exactly to what was used in the current ASTM E722 1-MeV(GaAs) damage function [ASTM722]. Table 6-1 shows the tabular data. This efficiency curve, as implemented in the NJOY code calculation used to define the energy-dependent response, used an empirical fit to the GaAs recombination lifetime data as the basis for the response function, and is defined by a log-log interpolation between the recoil atom energy points. This efficiency is notated as ${}^{ASTM-E722}\xi\left(T_{R,j_i}, {}^{ion}_{Rob/Rob}T_{R,j_i}\right)$. Although this functional form permits a dependence on both the recoil atom energy and the "effective" damage energy, this efficiency function, with *type-C*=ASTM-E722, is only a function of the recoil atom energy, T_{R,j_i}. In light of the discussion in Section 6.3, physics considerations suggest that this should probably have been formulated as a function of ${}^{ion}_{Rob/Rob}T_{R,j_i}$ rather than T_{R,j_i}. However, since this application of this damage efficiency function is restricted to neutrons incident on GaAs, the change of the dependent parameter from T_{R,j_i} to ${}^{ion}_{Rob/Rob}T_{R,j_i}$ would not significantly affect the application – it would just affect the appearance of the curve and any analytic fits that are extracted to smooth out the data interpolation. Figure 6-2 shows how this damage efficiency curve would appear when plotted against ${}^{ion}_{Rob/Rob}T_{R,j_i}$. Note, because of plotting limitations, the smooth curve in Fig. 6-2 reflects a spline fit, but the accepted values are the result of log-log interpolation between the depicted datapoints.

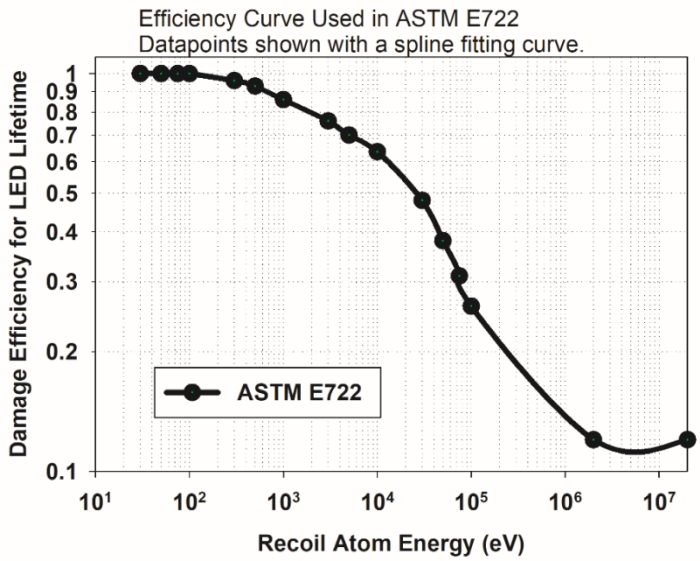

Figure 6-1. Damage Efficiency Curve Adopted in ASTM E722

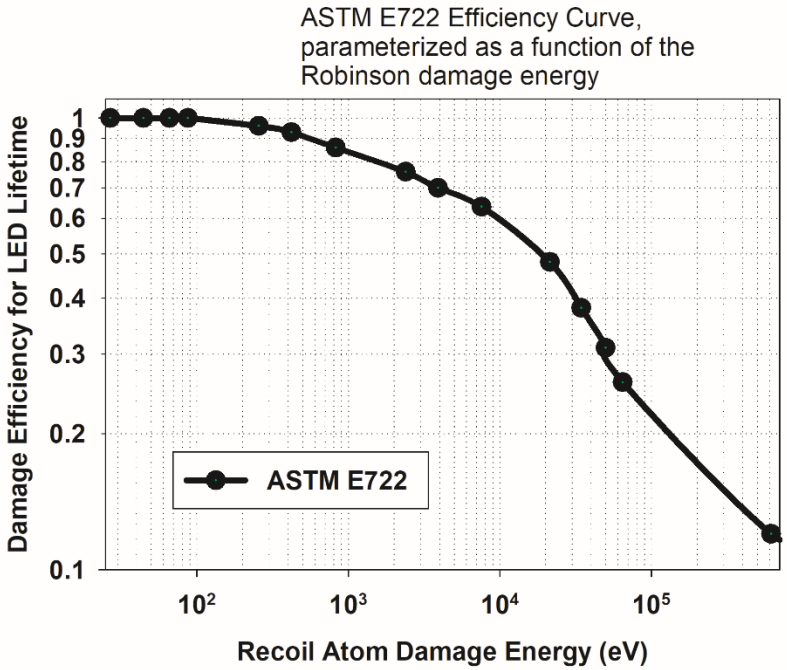

Figure 6-2. ASTM E722 Damage Efficiency Curve, Plotted as a Function of the Ion Damage Energy

Table 6-1. Tabulated ASTM E722 GaAs Damage Efficiency

Recoil Atom Energy (eV)	Recoil Atom Damage Energy (eV)[&]	ASTM Damage Efficiency
3.000000E+01	2.682930E+01	1.000
5.000000E+01	4.429800E+01	1.000
7.500000E+01	6.591890E+01	1.000
1.000000E+02	8.736930E+01	1.000
3.000000E+02	2.555562E+02	0.960
5.000000E+02	4.203030E+02	0.930
1.000000E+03	8.241128E+02	0.860
3.000000E+03	2.383901E+03	0.760
5.000000E+03	3.896241E+03	0.700
1.000000E+04	7.561803E+03	0.636
3.000000E+04	2.136851E+04	0.480
5.000000E+04	3.436520E+04	0.380
7.500000E+04	4.983684E+04	0.310
1.000000E+05	6.462996E+04	0.260
2.000000E+06	6.164163E+05	0.120
2.000000E+07	1.269360E+06	0.120

[&] Damage energy computed using Robinson partition function.

An issue in the application of the damage efficiency function is how this efficiency function is applied to light recoil ions in the outgoing reaction channel. Section 4.1 discussed the fact that the Robinson formulation of the damage partition function is not applicable to cases where the recoil atom has a much smaller atomic mass than the lattice atoms. Here it was noted that, despite this limitation, most approaches, e.g., modeling implemented in the NJOY code, still apply the Robinson damage partition function to outgoing protons and alpha particles because there is no other readily available option. It was also noted in Section 4.1 that this is not a significant issue since, for most applications, the contribution to the (displacement) damage energy from the lighter ions in the outgoing reaction channel, i.e., the protons, deuterons, tritons, and alpha particles, is very small relative to that from the heavy PKA. The standard application of the ASTM E722 damage efficiency function is through the use of a modified version of the NJOY-2016 code. In this implementation, this same damage efficiency function, expressed as a function of the recoil atom energy, is applied to both the PKA and to lighter outgoing ions. This represents a case where the distinction between a parameterization in terms of the recoil ion energy versus the damage energy can be significant. However, as was the case for the application of the baseline Robinson formula as part of the NRT treatment, the contribution from the lighter recoil ions to the damage metrics is usually small enough that this does not affect the application. Thus, this represents an area where the modeling, and its implementation in the codes, should be improved, but it will not have any effect on most previous applications.

6.2. Athermal Recombination-Corrected Damage Energy (ARC-DE)

The NRT-dpa model has the number of defects being, essentially, proportional to the radiation energy deposited per volume. This model, as discussed in Section 4.4.3, is based on the use of MD codes and is known to over-estimate the production of Frenkel pairs in metals under energetic ion displacement cascade conditions [OECD].

To address short-comings in the NRT-dpa model, an athermal recombination-corrected (arc) dpa equation was developed [OECD, Nor18a, Nor18b]. This form corresponds to the NRT Frenkel pair generation term where an efficiency function is applied to the creation of displacements above the threshold region. The arc-dpa model is given by:

$$ {}^{arc-dpa}\nu_d\left(E_d, {}^{ion}_{Rob/Rob}T_{R,j_i}\right) = \begin{cases} 0 & 0 \le {}^{ion}_{Rob/Rob}T_{R,j_i} < E_d \\ 1 & E_d \le {}^{ion}_{Rob/Rob}T_{R,j_i} < 2\cdot E_d/\beta \\ \beta \cdot {}^{ion}_{Rob/Rob}T_{R,j_i} \cdot {}^{arc-dpa}\xi\left(T_{R,j_i}, {}^{ion}_{Rob/Rob}T_{R,j_i}\right)/\left(2\cdot E_d\right) & 2\cdot E_d/\beta \le {}^{ion}_{Rob/Rob}T_{R,j_i} < \infty \end{cases} \quad (47) $$

where ${}^{arc-dpa}\xi\left(T_{R,j_i}, {}^{ion}_{Rob/Rob}T_{R,j_i}\right)$ is an efficiency factor, applied only above the threshold region, intended to represent the ratio of the number of true defects divided by the number of defects as defined by the NRT formalism in Equation 33.

In the above threshold region, this equation can also be written as:

$$ {}^{arc-dpa}\nu_d\left(E_d, {}^{ion}_{Rob/Rob}T_{R,j_i}\right) = {}^{NRT}\Lambda(E_d, {}^{ion}_{Rob/Rob}T_{R,j_i}) \cdot {}^{arc-dpa}\varsigma_d\left(E_d, {}^{ion}_{Rob/Rob}T_{R,j_i}\right) \quad (48) $$

In order to support a later discussion of damage energy, we define the term:

$$ {}^{arc-dpa}\varsigma_d\left(E_d, T_{R,j_i}, {}^{ion}_{Rob/Rob}T_{R,j_i}\right) = \beta \cdot {}^{ion}_{Rob/Rob}T_{R,j_i} \cdot {}^{arc-dpa}\xi({}^{ion}_{Rob/Rob}T_{R,j_i}) / (2 \cdot E_d) \quad (49) $$

The efficiency factor should, based on the underlying physics: a) be close to the NRT value at the threshold displacement energy; b) have a power law form at low displacement energies; and c) saturate at a high displacement energy. This arc-dpa efficiency factor has the form:

$$ {}^{arc-dpa}\xi\left(T_{R,j_i}, {}^{ion}_{Rob/Rob}T_{R,j_i}\right) = \frac{1 - c_{arc-dpa}}{\left(2 \cdot E_d / 0.8\right)^b} \cdot {}^{ion}_{Rob/Rob}T_{R,j_i}^{b_{arc-dpa}} + c_{arc-dpa} \quad (50) $$

where ${}^{ion}_{Rob/Rob}T_{R,j_i}$ is the NRT/Robinson damage energy, E_d is the displacement threshold energy, and $b_{arc\text{-}dpa}$ and $c_{arc\text{-}dpa}$ are two unitless fitting parameters designed to match experimentally derived data with a physical meaning that is discussed in Reference [OECD]. The parameter "$b_{arc\text{-}dpa}$" has the physical interpretation that it gives the point where there is a transition from a power law behavior into a linear behavior that corresponds to where high energy cascades split into equivalent lower energy sub-cascades with a constant damage efficiency. $c_{arc\text{-}dpa}$ can be physically interpreted as related to how efficiently interstitials are transported to the outer periphery of the displacement cascade where recombination is less likely. Also, it corresponds to the saturation level at high energy.

Unlike for the ASTM E722 efficiency, this formulation has an expression for the efficiency that is only a function of the "effective" damage energy, and not, explicitly, the recoil atom energy.

6.3. Replacement-per-atom (rpa)

In many materials, atom mixing is an important phenomenon and damage metrics can depend upon the number of atom replacements in a collision cascade. A major component in atom mixing comes from the heat spike in a collisional cascade [Gad95, Nor98a, Nor98b]. In this replacement atom model, the actual number of atoms that are displaced from the initial lattice site and end up in another site can significantly exceed the number of residual Frenkel pairs predicted in BCA models. This rpa model is presented in reference [OECD]. The rpa model is given by:

$$ {}^{rpa}\nu_d\left(E_d, {}^{ion}_{Rob/Rob}T_{R,j_i}\right) = \begin{pmatrix} 0 & 0 \le {}^{ion}_{Rob/Rob}T_{R,j_i} < E_d \\ 1 & E_d \le {}^{ion}_{Rob/Rob}T_{R,j_i} < 2 \cdot E_d / \beta \\ \beta \cdot {}^{ion}T_{dam} \cdot {}^{rpa}\xi\left({}^{ion}_{Rob/Rob}T_{R,j_i}\right) / \left(2 \cdot E_d\right) & 2 \cdot E_d / \beta \le {}^{ion}_{Rob/Rob}T_{R,j_i} < \infty \end{pmatrix} \quad (51) $$

where $\xi_{rpa}\left({}^{ion}T_{dam}\right)$ is an efficiency factor given by the functional form:

$$ {}^{rpa}\xi({}^{ion}_{Rob/Rob}T_{R,j_i}) = \left[\frac{b_{rpa}^{c_{rpa}}}{\left(2 \cdot E_d / 0.8\right)^{c_{rpa}}} + 1\right] \cdot \frac{{}^{ion}_{Rob/Rob}T_{R,j_i}^{c_{rpa}}}{b_{rpa}^{c_{rpa}} + {}^{ion}_{Rob/Rob}T_{R,j_i}^{c_{rpa}}} \quad (52) $$

${}^{ion}_{Rob/Rob}T_{R,j_i}$ is the damage energy, and b_{rpa} and c_{rpa} are two unitless fitting parameters designed to match experimentally derived data with a physical meaning that is discussed in Reference [OECD].

This equation can be written as:

$$ {}^{rpa}\nu_d\left(E_d, {}^{ion}_{Rob/Rob}T_{R,j_i}\right) = {}^{NRT}\Lambda(E_d, {}^{ion}_{Rob/Rob}T_{R,j_i}) \cdot {}^{rpa}\varsigma_d[\beta \cdot {}^{ion}_{Rob/Rob}T_{R,j_i} \cdot {}^{rpa}\xi({}^{ion}_{Rob/Rob}T_{R,j_i}) / (2 \cdot E_d)] \quad (53) $$

In order to support a later discussion of damage energy, we also define the term:

$$ {}^{rpa}\varsigma_d\left(E_d, {}^{ion}_{Rob/Rob}T_{R,j_i}\right) = \beta \cdot {}^{ion}_{Rob/Rob}T_{R,j_i} \cdot {}^{rpa}\xi({}^{ion}_{Rob/Rob}T_{R,j_i}) / (2 \cdot E_d) \quad (54) $$

Figure 6-3, taken from Reference [OECD], shows representative results of the replacement-per-atom efficiency factors derived from MD calculations for ion beam mixing in metals. The results of fitting the data to the function form used in Equation 50 show that, unlike in the case for the arc-dpa efficiency factors from Equation 50, the rpa efficiency factors can be much greater than unity.

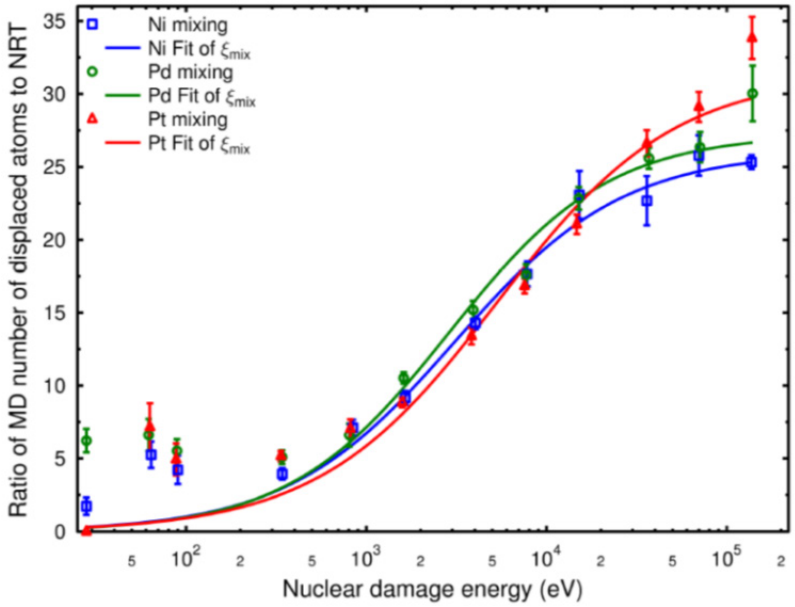

Figure 6-3. Generic Example of the RPA Correction Factor for Ion Mixing in Metals: extracted from [OECD]

7. RECOMMENDED RESPONSE FUNCTIONS FOR DAMAGE METRICS

Each of the seven calculated radiation damage metrics, and two of the derived damage metrics, are addressed in the following subsections.

7.1. Total Cross Section

For the highest quality representation of the nuclear data, isotopic evaluations were used and combined to represent the material of interest, e.g., GaAs in this case. This total cross section response function fits the formalism seen in Equation 2 when two of the correction distributions are defaulted to unity, i.e., ${}^{null}\Lambda\left(E_d, {}^{ion}_{type-B/D} T_R\right) = {}^{null}\xi\left(T_{R,j_i}\right) = 1$, and the effective generation term is also defaulted from an energy to a unit weighting of the cross section corresponding to the production of the primary outgoing heavy ion, i.e., ${}^{x\sec}\zeta\left(E_d, T_{R,j_i}, {}^{type-D} T_{dam}\right) = \delta\left[j_i, PKA\right]$. Note, the delta function is used here in order to avoid overcounting the cross section by the number of particles in the outgoing channel. Note also, in this expression the energy/angular distribution, $f\left(E, \mu, T_{R,j_i}\right)$, is properly normalized such that the integral, $\int_0^\infty dT_{R,j_i} \int_{-1}^{1} d\mu \cdot f\left(E, \mu, T_{R,j_i}\right)$, is unity.

Figure 7-1 shows the total cross section for the three naturally occurring isotopes in GaAs. This figure shows the major reaction contributors as well as depicting the total cross section. Figures are provided with the energy x-axis in both linear and logarithmic scaling so that the importance of the various channels in the different energy regions can be clearly seen.

For all three isotopes, the (n,γ) capture reaction is the dominant reaction channel for low energy ($<10^{-3}$ eV) incident neutrons. In this energy region the various damage metrics can be very sensitive to the fidelity of the modeling of the photon spectrum from the capture reaction within the nuclear data evaluation. As the neutron energy increases, the elastic channel begins to dominate. In this region, the reaction kinematics, in conjunction with the physics constraints of energy and momentum conservations, provide for the damage metrics that are driven by the recoil atoms. Above about 1-MeV, the inelastic scattering becomes important. Above about 10-MeV, the various transmutation reactions, e.g., (n,p) and (n,α) reaction channels, begin to dominate. The fidelity of the recoil spectrum for these high energy reactions can be a critical consideration in assessing the accuracy of the calculated damage metrics.

7.2. Neutron Total Kerma

The energy-dependent total, in units of rad(GaAs), is shown in Figure 7-2. This response function fits the formalism seen in Equation 2 when two of the correction distributions are defaulted to unity, i.e., ${}^{null}\Lambda\left(E_d, {}^{ion}_{type-B/D} T_R\right) = {}^{null}\xi\left(T_{R,j_i}\right) = 1$, and the effective generation term is set to the total recoil atom energy, i.e., ${}^{\ker ma}\zeta\left(E_d, T_{R,j_i}, {}^{type-D} T_{dam}\right) = T_{R,j_i}$. Note here that, as required for a kerma, and as defined in Equation 2, the summation only goes over the charged particles in the outgoing reaction channel, i.e., it does not include outgoing photons or neutrons.

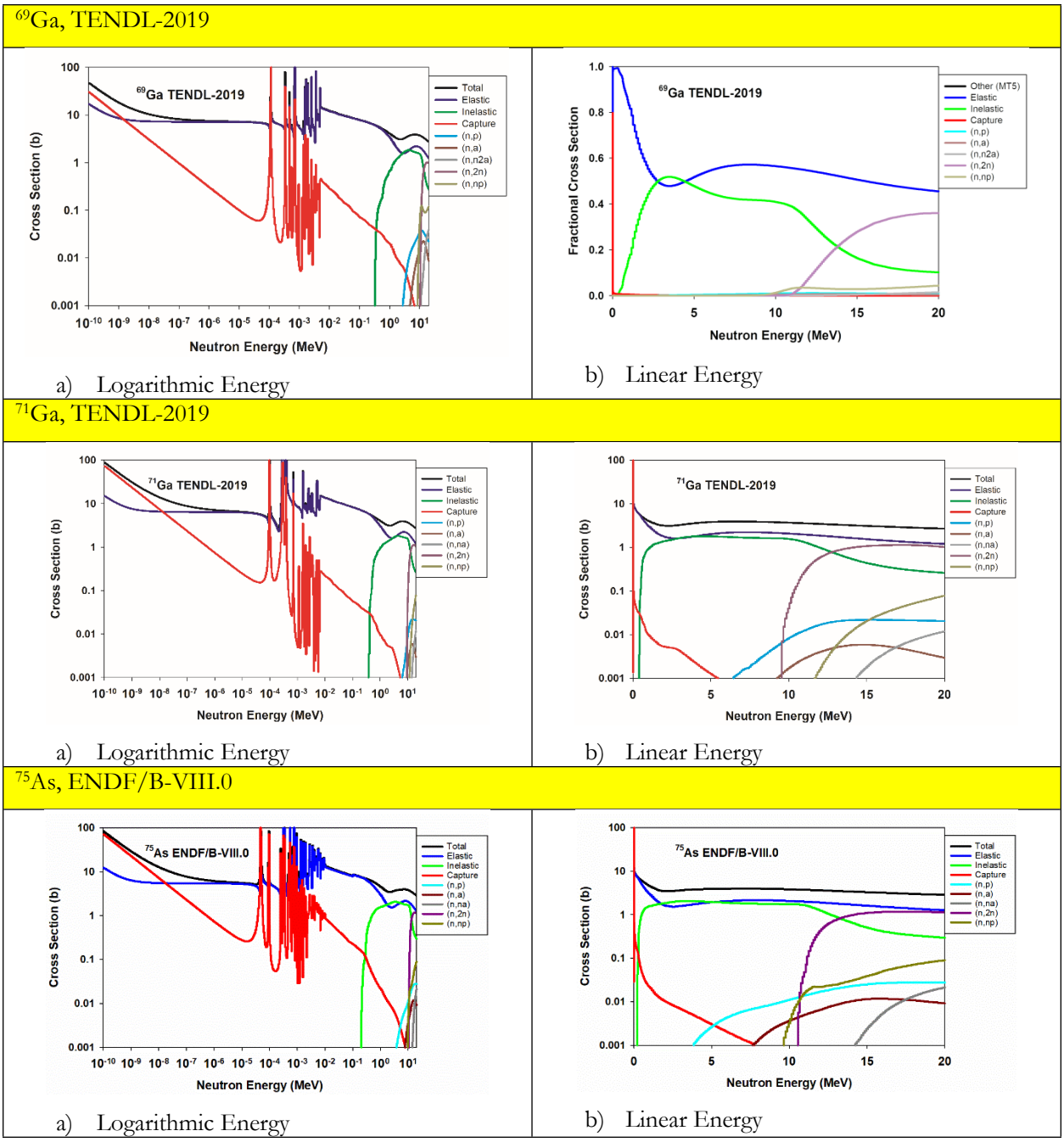

Figure 7-1. Contribution of Reaction Channels to the Total Cross Section for the Isotopes in GaAs

A critical consideration in evaluating this metric is the energy balance within the nuclear data evaluation. Older legacy evaluations frequently had poor quality representations of the emitted photon spectra that limited the capability of the processing codes, such as the NJOY-2016 code, to reconstruct the total kerma from the cross sections (MF=3), recoil particle distributions (MF=6), and photon spectra (MF=12) for the various reaction channels. The community-accepted approach is to compare the calculated kerma with the kinematic kerma maximum. Deviations here raise concerns over the quality of the nuclear data. Figure 7-3 compares the total kerma for the composite GaAs with the kinematic kerma limit. As was seen in the discussion of the isotopic cross section

selection addressed in Section 3.3, the deviations seen here are not severe. Because of this difference, even though it is relatively small, the recommended approach is to replace the calculated total kerma with the kinematic kerma limit. While this is a good fix for this total kerma metric, a similar correction has not been identified for deficiencies of the same magnitude that can be expected to appear in the displacement kerma and in the ionizing kerma response functions.

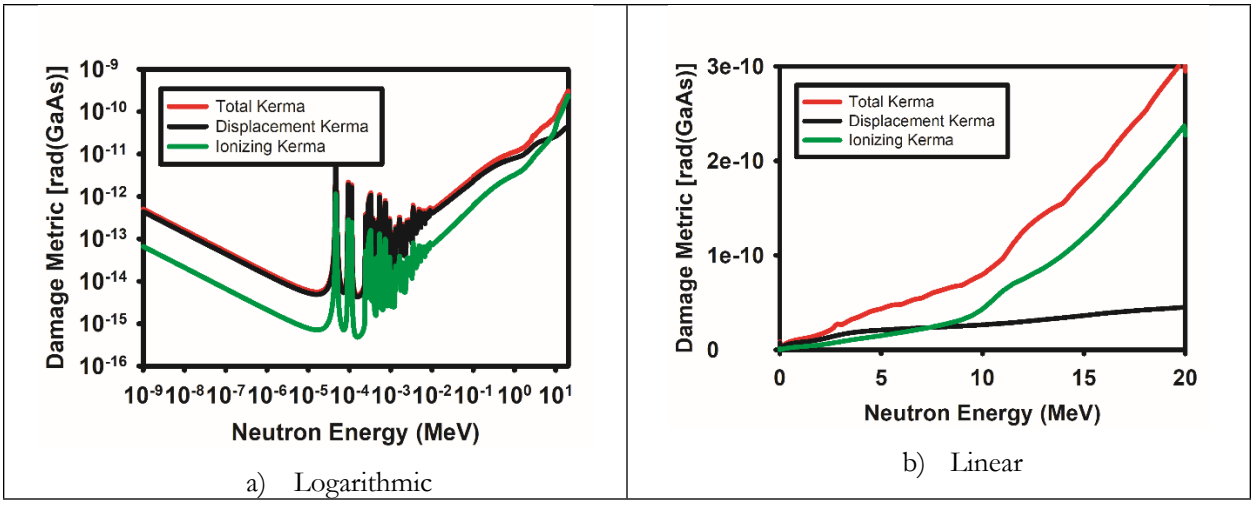

a) Logarithmic b) Linear

Figure 7-2. GaAs Neutron Kerma Metrics

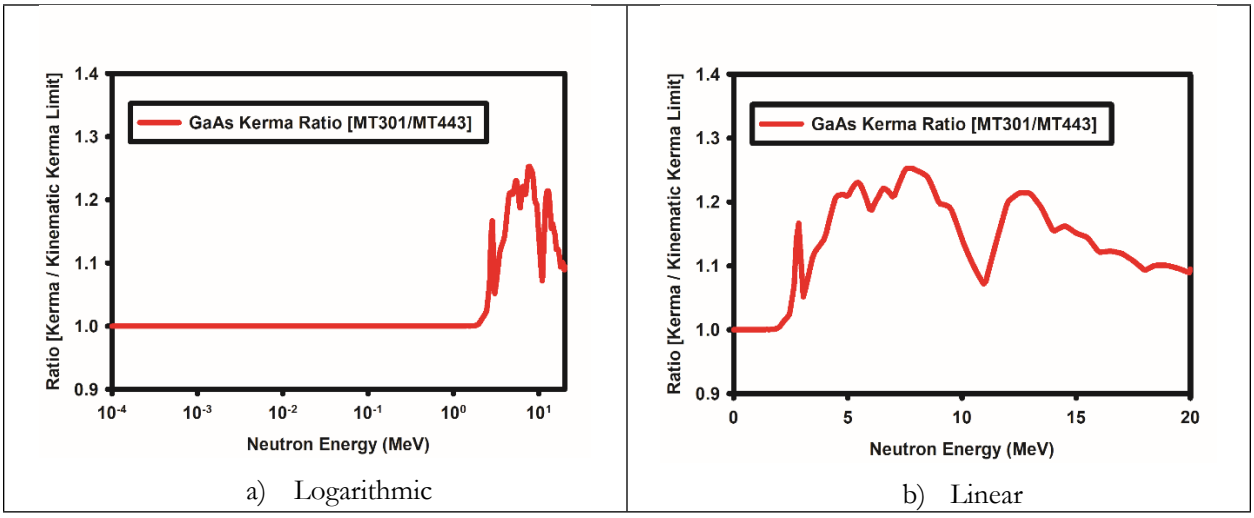

a) Logarithmic b) Linear

Figure 7-3. Ratio of GaAs Total Kerma (MT301) and Kinematic Kerma Limit (MT443)

7.3. Neutron Displacement Kerma

The energy-dependent GaAs neutron displacement kerma is also shown in Figure 7-2. This response function fits the formalism seen in Equation 2 when the efficiency correction distribution is defaulted to unity, i.e., ${}^{null}\xi\left(T_{R,j_i}\right)=1$, the displacement threshold treatment is defaulted to unity, i.e., ${}^{null}\Lambda\left(E_d,{}^{ion}_{type-B/D}T_R\right)=1$, and the effective generation term is set to the total recoil atom energy multiplied by the Robinson damage partition function, i.e., ${}^{Robinson}\zeta\left(E_d,T_{R,j_i},{}^{type-D}T_{dam}\right)=$

$^{Rob}T_{dam}(T_{R,j_i})\,g T_{R,j_i} = \dfrac{T_{R,j_i}}{\left[1+k_L\,g g(T_{R,j_i}/E_L)\right]}$. Details of the k_L, E_L, and g terms in the Robinson partition function were addressed in Section 4.1 and can be found in Reference [Nor75, Rob75].

7.4. Non-ionizing Energy Loss, NIEL

For neutrons, when charged particle equilibrium can be assumed to exist and the energy of outgoing secondary particles is below the threshold for initiating new nuclear reactions, then the non-ionizing energy loss (NIEL) is equivalent to the displacement kerma multiplied by N_o/A, where N_o is Avogadro constant and A is the atomic mass of the lattice material. For neutrons incident on representative semiconductor materials, Si and GaAs, the relationship between displacement kerma and NIEL is given by:

Si:

- 1-MeV reference displacement damage energy:

  $\kappa_{ref-DE}^{Si} = 95$ MeV-mb

- Atomic mass: $A_{Si} = 28.086$ amu

- Avogadro constant: $N_o = 6.0221367x10^{23}$ mole^{-1}

- 1-MeV reference NIEL:

  $$\kappa_{ref-NIEL}^{Si} = 95\cdot 10^{-24}\cdot\frac{6.0221367x10^{23}}{28.086} = 2.036968548 \text{ keV-cm}^2/\text{g}$$

GaAs:

- 1-MeV reference displacement damage energy:

  $\kappa_{ref-DE}^{GaAs} = 70$ MeV-mb, from Section 3.5

- Atomic mass:

  $A_{GaAs} = \frac{1}{2}\cdot(69.723+74.921595) = 72.3222975$ amu, from Section 3.1

- 1-MeV reference NIEL:

  $$\kappa_{ref-NIEL}^{GaAs} == 70\cdot 10^{-24}\cdot\frac{6.0221367x10^{23}}{72.322975} = 0.5828708913 \text{ keV-cm}^2/\text{g}$$

Thus, the displacement kerma addressed in Section 7.3 can be multiplied by the ratio of the reference NIEL and displacement energy to obtain the energy-dependent damage metric. When cast into the form of Equation 2, this is accomplished by defaulting the efficiency correction distribution to unity, i.e., $^{null}\xi\left(T_{R,j_i}\right) = 1$, defaulting the displacement threshold treatment to unity, i.e., $^{null}\Lambda\left(E_d, ^{ion}_{type-B/D}\, T_R\right) = 1$, and defining the effective generation term as the total recoil atom energy

multiplied by the Robinson damage partition function multiplied by this ratio, i.e.,

$$^{Robinson-NIEL}\zeta\left(E_d, T_{R,j_i}, {}^{type-D}T_{dam}\right) = {}^{Rob}T_{dam}(T_{R,j_i})\,\mathrm{g}\,T_{R,j_i}\,\mathrm{g}\frac{\kappa_{ref-NIEL}^{GaAs}}{\kappa_{ref}^{GaAs}} = \frac{T_{R,j_i}}{\left[1+k_L\,\mathrm{g}\,g\left(T_{R,j_i}/E_L\right)\right]}\mathrm{g}\frac{\kappa_{ref-NIEL}^{GaAs}}{\kappa_{ref}^{GaAs}}. \quad (55)$$

7.5. Neutron Ionizing Kerma

The energy-dependent GaAs neutron ionizing kerma is also shown in Figure 7-2. This response function fits the formalism seen in Equation 2 when the efficiency correction distribution is defaulted to unity, i.e., $^{null}\xi\left(T_{R,j_i}\right) = 1$, the displacement threshold treatment is defaulted to unity, i.e., $^{null}\Lambda\left(E_d, {}^{ion}_{type-B/D}T_R\right) = 1$, and the effective generation term is set to the total recoil atom energy multiplied by one minus the Robinson damage partition function, i.e., $^{ionizing\_kerma}\zeta\left(E_d, T_{R,j_i}, {}^{type-D}T_{dam}\right) = \left[1 - {}^{Rob}T_{dam}(T_{R,j_i})\right]\mathrm{g}\,T_{R,j_i}$. An easier way to generate this response function is just to subtract the displacement kerma from the total kerma. This alternate path is recommended here since we have elected to replace the total kerma with the kinematic kerma limit.

7.6. NRT-based Damage Energy

This response function fits the formalism seen in Equation 2 when the efficiency correction distribution is defaulted to unity, i.e., $^{null}\xi\left(T_{R,j_i}\right) = 1$, the displacement threshold treatment adopts the NRT correction to the sharp threshold Kinchin-Pease treatment, $^{NRT}\Lambda\left(E_d, {}^{ion}_{Rob/Rob}T_{R,j_i}\right)$, described in reference [Nor75], and the effective generation term is set to the total recoil atom energy multiplied by the Robinson damage partition function, i.e., $^{Robinson}\zeta\left(E_d, T_{R,j_i}, {}^{Rob}T_{dam}\right) = {}^{Rob}T_{dam}(T_{R,j_i})\,\mathrm{g}\,T_{R,j_i}$. Figure 7-4 shows the energy-dependent NRT-based damage energy. This curve is a scaled version, scaled to convert the rad(GaAs) units back to original NJOY damage energy units of eV-b, of the displacement kerma shown in Figure 7-2 where the NRT treatment of the displacement threshold region has also been applied. In addition to the logarithmic and linear energy axis plots, this figure also shows an expanded image of the resonance region so that the effect of the NRT threshold treatment can be seen.

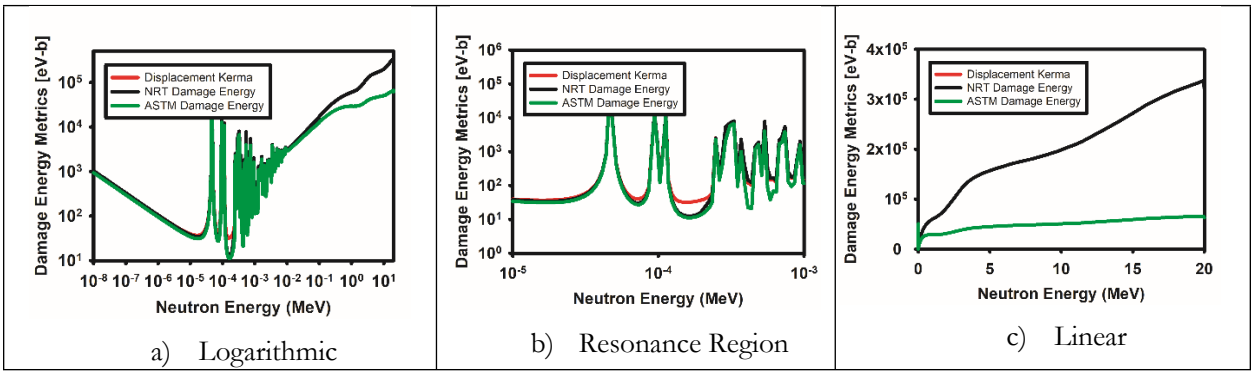

Figure 7-4. GaAs Damage Energy Metrics

7.7. 1-MeV(GaAs) Neutron Equivalent Damage Energy

The legacy work on the GaAs damage equivalence [Gri91] found that damage in carrier lifetime degradation did not scale with the NRT-based damage energy, but required the addition of a recoil atom energy-based efficiency function. The ASTM efficiency function, previously shown in Figure 6-1, was empirically unfolded from the existing database of damage to electronics gathered in a variety of neutron fields. In this formulation, the efficiency correction distribution is the ASTM recoil-energy dependent function, i.e., ${}^{ASTM-E722}\xi\left(T_{R,j_i}, {}^{ion}_{Rob/Rob}T_{R,j_i}\right)$, the displacement threshold treatment adopts the NRT correction to the sharp threshold Kinchin-Pease treatment, ${}^{NRT}\Lambda\left(E_d, {}^{ion}_{Rob/Rob}T_{R,j_i}\right)$, and the effective generation term is set to the total recoil atom energy multiplied by the Robinson damage partition function, i.e., ${}^{Robinson}\zeta\left(E_d, T_{R,j_i}, {}^{Rob}T_{dam}\right) = {}^{Rob}T_{dam}(T_{R,j_i})\,\mathbf{g}T_{R,j_i}$.

If we use this legacy effective generation term and the updated cross sections, we have a damage metric as shown in Figure 7-4 and given numerically in Appendix A. Note that this definition of the 1-MeV(GaAs) damage energy disagrees with what is found in the current ASTM E722 standard because it represents the result of using updated cross sections. The dosimetry community has not been approached to officially adopt this higher fidelity representation of the damage metric because, unfortunately, the legacy approach used to define the effective generation term involved unfolding the recoil-energy-dependent effective generation function from experimental data on the change in the carrier lifetime of GaAs electronic devices. This resulted in the definition of the effective generation term being dependent upon the cross sections used. When this work updated the cross sections, and because the new cross sections and displacement kerma are seen to vary significantly from the legacy work (as discussed in Section 8), the use of the new cross sections invalidated the derivation of the legacy efficiency function. In order to update the 1-MeV(GaAs) response function, we need to go back to the underlying experimental data and rederive a modified efficiency function that correctly reproduces the experimental observations.

7.8. 1-MeV(GaAs) Equivalent Fluence

The 1-MeV(GaAs) displacement damage energy addressed in Section 7.7 can be divided by the reference 1-MeV damage energy to derive the 1-MeV(GaAs) equivalent fluence. ratio. When cast into the form of Equation 2, this is accomplished by defining the efficiency correction distribution as the ASTM recoil-energy dependent function divided by the reference damage energy, i.e., ${}^{ASTM-1MeV(GaAs)}\xi\left(T_{R,j_i}, {}^{ion}_{Rob/Rob}T_{R,j_i}\right) = {}^{ASTM-E722}\xi\left(T_{R,j_i}, {}^{ion}_{Rob/Rob}T_{R,j_i}\right) \Big/ \kappa^{GaAs}_{ref-DE}$. As for the 1-MeV(GaAs) damage energy, this damage metric adopts the NRT correction to the sharp threshold Kinchin-Pease treatment, ${}^{NRT}\Lambda\left(E_d, {}^{ion}_{Rob/Rob}T_{R,j_i}\right)$, and the effective generation term is set to the total recoil atom energy multiplied by the Robinson damage partition function, i.e., ${}^{Robinson}\zeta\left(E_d, T_{R,j_i}, {}^{Rob}T_{dam}\right) = {}^{Rob}T_{dam}(T_{R,j_i})\,\mathbf{g}T_{R,j_i}$.

7.9. Recoil Atom Distribution

The recoil atom distributions are defined as in Equation 3. This damage metric is no longer a simple 1D function of the neutron energy, but has an energy distribution for every incident neutron energy. Figure 7-5 shows some representative recoil distributions – consistent with the discussion in Section 3.3 of the recoil distributions for the relevant isotopes.

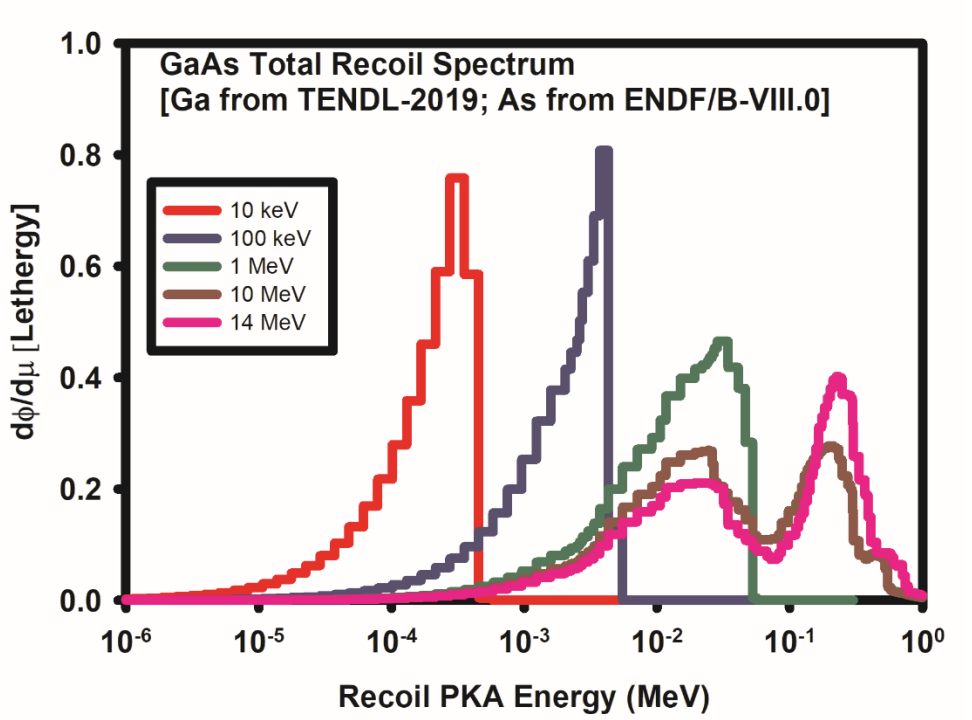

Figure 7-5. Examples of the GaAs Recoil Energy Distributions

8. COMPARISON OF RECOMMENDED DAMAGE METRICS WITH LEGACY RESPONSE FUNCTIONS

Recommended representations of the damage metrics were given in Section 7 and their numerical representations are provided in Appendix A. This section provides a summary of the change in the damage metrics between the legacy metrics used in the initial damage studies performed in 1992, response functions that are still reflected in the ASTM E722-19 standard, and the updated recommended damage metrics addressed in this report.

Figure 8-1 shows a comparison of the legacy GaAs total cross section used in the current ASTM-endorsed response function, i.e., ENDF/B-VI for the elemental ^{nat}Ga and ENDL-84 for ^{75}As, with the current recommended total cross section, i.e., TENDL-2019 for the isotopic ^{69,71}Ga and ENDF/B-VIII.0 for ^{75}As. The energy-dependent cross sections are seen to be fairly similar. There are some significant differences at low energy, but the high energy portions are very similar in magnitude.

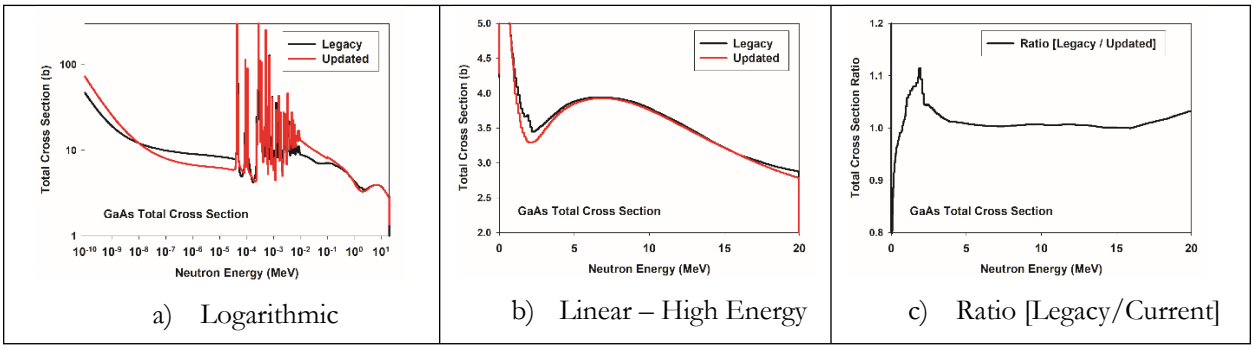

Figure 8-1. Comparison of Legacy and Current Recommendations for the GaAs Total Cross Section

Figure 8-2 shows a comparison of the GaAs total kerma. There are significant differences in the total kerma and a structure in the high energy region for the legacy response that does not appear to be physical. This difference may be the result of a poor energy balance in the legacy nuclear data evaluation due to a poor representation of the emitted gammas. Note, some of this difference would not appear in the damage metric if one were to over-ride the total kerma with the kinematic kerma limit – as was recommended in the previous discussion.

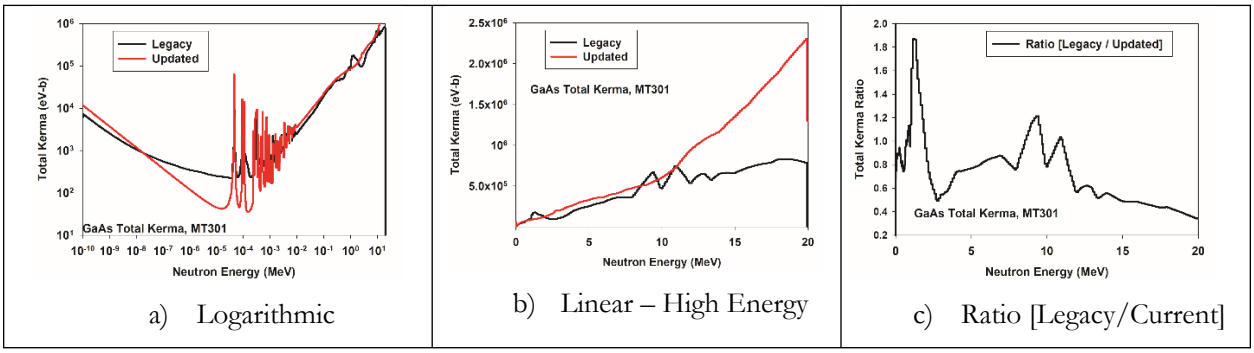

Figure 8-2. Comparison of Legacy and Current Recommendations for the GaAs Total Kerma, MT301

Figure 8-3 shows a comparison of the GaAs displacement kerma. Note, this is not the default NJOY output of the sharp threshold Kinchin-Pease damage energy, but represents the displacement kerma with no threshold treatment. Because of the model-based treatment of the displacement kerma, this damage metric does not depend upon the energy balance and, as a result, is not as sensitive to the representation of the outgoing gammas. These kermas show a smooth behavior and are not too discrepant.

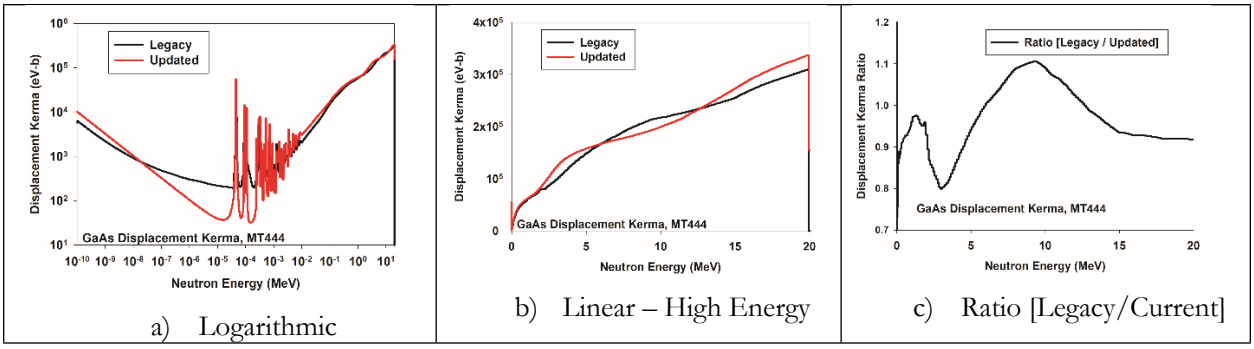

Figure 8-3. Comparison of Legacy and Current Recommendations for the GaAs Displacement Kerma, MT444 (without threshold treatment)

Figure 8-4 shows a comparison of the GaAs displacement kerma with treatment of the threshold – the sharp Kinchin-Pease, the legacy NJOY default model, for the legacy damage metric and the NRT for the updated damage metric. Some unphysical structure is seen in the legacy damage energy. This appears to be a result of the spKP threshold treatment in the legacy modeling. There is a systematic difference/offset between the legacy and updated damage energy in the fast (5 – 13 MeV) region.

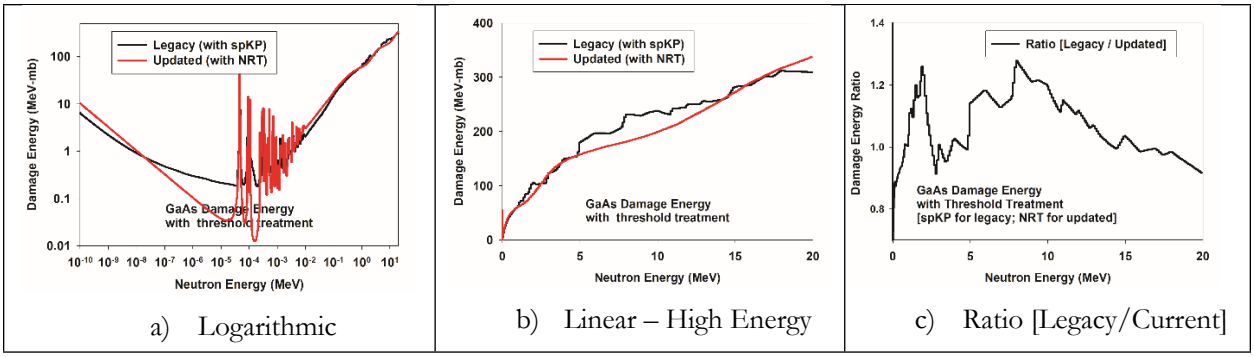

Figure 8-4. Comparison of Legacy and Current Recommendations for the GaAs Damage Energy with Threshold Treatment (spKP for legacy, NRT for updated)

Figure 8-5 shows a comparison of the GaAs ASTM-based damage energy. The use of the ASTM damage efficiency does not change the issue of the unphysical structure in the legacy energy-dependence. However, the normalization to the reference displacement 1-MeV displacement kerma removes some of the systematic high energy offset that was seen in the pure damage energy metrics.

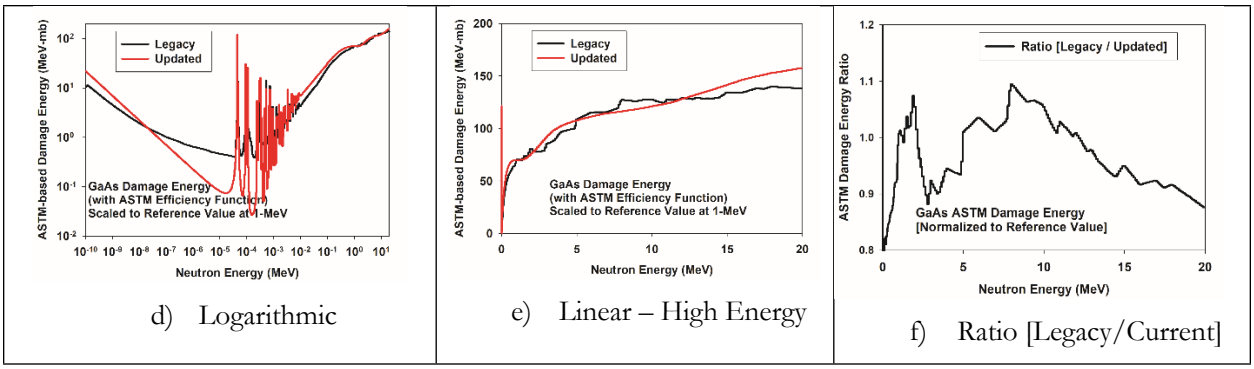

Figure 8-5. Comparison of Legacy and Current Recommendations for the GaAs Damage Energy (with Legacy ASTM Efficiency Function)

9. DERIVATION OF EFFECTIVE GENERATION TERM

The ASTM damage efficiency function, modeled as a function of the recoil atom energy, was em pirically derived using the legacy response function such that the relative damage, as measured by the minority carrier lifetime, was consistent with the observed damage as seen in various neutron spectra. Since the derivation of this efficiency function was dependent upon the relative behavior of the legacy damage metrics, in this section we examine how well this mixture of updated nuclear data but legacy efficiency function preserves the match with available experimental data.

The legacy experimental data, fluence normalized damage constants representing the carrier lifetime, are seen in Table 9-1 for seven different neutron spectra (column 4). This table also shows the damage constants when expressed as a function of the displacement kerma using the legacy and updates/recommended nuclear data (columns 5 and 6). The latest, highest fidelity, spectrum characterizations in these fields has been used to derive the average neutron energy (column 2) and the average PKA recoil energy (column 3) seen in this table.

Table 9-1. Experimental Data for GaAs LED-based Displacement Damage

Neutron Field	Avg. Neutron energy (MeV)*	Avg. PKA Recoil Energy (keV)$	Damage Constant [$ms^{-1}/(n/cm^2)$]	**Legacy** Damage Constant [ms^{-1}/DK(GaAs)]	**Current** Damage Constant [ms^{-1}/DK(GaAs)]
SNL_DT	13.99703	136.99	3.656E-7	1.41E-9	3.487E-09
CHK_DD	2.797128	49.973	1.9941E-7	1.84E-9	3.07798E-09
spr3cc	1.269636	22.1687	1.635E-7	2.53E-9	3.299E-09
LBACRR12	0.7695361	13.934	1.1695E-7	2.77E-9	3.4003E-09
SPR_120	0.6633801	11.918	1.064E-7	2.90E-9	3.517E-09
ACRR-CC	0.5971899	10.654	8.382E-8	2.63E-9	3.291E-09
POLYCA48	0.5350478	9.067	7.132E-8	2.71E-9	3.568E-09

*The average neutron energies were computed using the latest highest fidelity spectrum characterizations – typically using a least squares spectrum adjustment of an MCNP-calculated trial spectrum.
$The average recoil energies were computed using the latest spectrum characterizations and folding with the NJOY-2016 calculated effective heavy ion PKA recoil energies as discussed in Section 3.3.1.3.3 and shown in Figures 3-10, 3-19, and 3-30.

The data seen in Table 9-1 was the basis for extracting the legacy ASTM damage efficiency function. The process, described in reference [Gri91] involved unfolding the efficiency function while using the double ratio of the lifetime degradation in the neutron fields to preserve the expected Messenger-Spratt behavior, i.e., the difference in the inverse carrier lifetime should be proportional to the effective displacement damage seen in the irradiation. The consistency of the energy-dependent response metric with the data is examined by looking at the double ratios of damage between the neutron fields. The calculated-to-experimental (C/E) ratios are formed between the calculated spectrum-averaged response and the fluence-normalized experimental measurements. Then a second ratio be formed between each C/E ratio and the ratio for a selected reference field. The 14-MeV DT neutron field was selected as the reference field because it had a neutron spectrum that did not depend upon the least square spectrum adjustment approach that was used for the reactor fields. Figure 9-1 shows the double ratios for each of the reactor fields – plotted against the

average PKA recoil energy for that spectrum. The PKA recoil energy only included the recoil energy of the heavy ions. A high-quality representation of the energy-dependent response would be characterized by a flat line. Figure 9-1 shows that the response with the ASTM efficiency correction is fairly close to one over the range of neutron spectra for which data was available. Furthermore, the quality of the data fit for the updated response is seen to be similar to that for the original work. So, despite the dependence of the original derivation for the energy-dependent efficiency function, the ASTM legacy efficiency does can also be applied to the the response functions derives using the latest nuclear data evaluations.

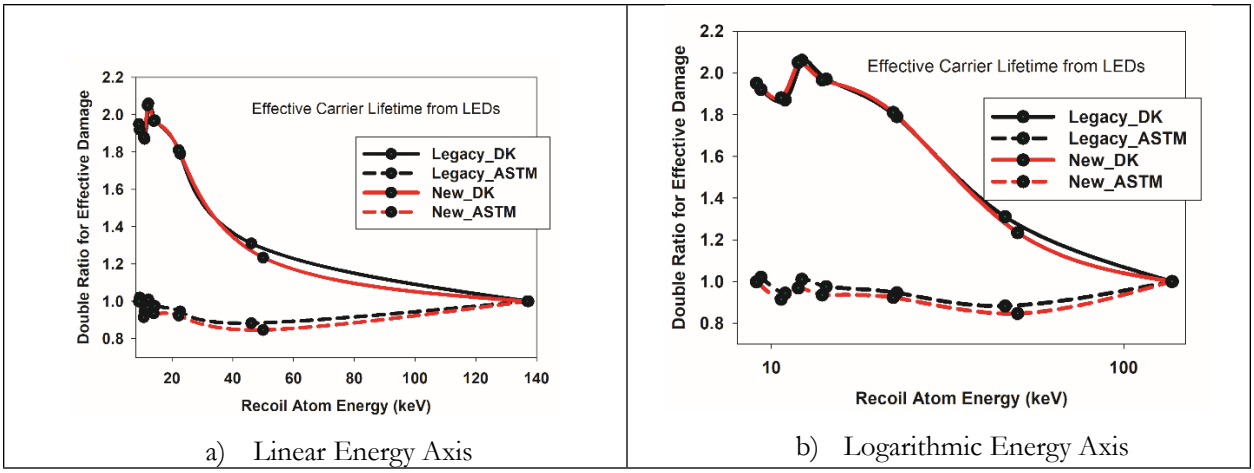

Figure 9-1. Legacy Efficiency Treatment for GaAs 1-MeV(GaAs) Damage to Electronics

Since experimental data should never be reported without also giving an indication of the estimated uncertainties in the measurements, Table 9-2 provides details on the allocation of uncertainties in the data.

Table 9-2. Approximate Uncertainties in the Damage Constants for Baseline Neutron Fields

Neutron Field	Damage Constant [$ms^{-1}/(n/cm^2)$]	Uncertainty (%) in Damage Constant*			
		Fluence	Lifetime Measurement	Other	Combined (rms)
SNL_DT	3.656E-7	3.1	2.3	3.0	4.89
CHK_DD	1.9941E-7	10.	2.0	4.0	10.95
spr3cc	1.635E-7	5.0	3.0	0.0	5.83
LBACRR12	1.1695E-7	4.3	3.5	3.5	6.56
SPR_120	1.064E-7	5.7	2.0	5.0	7.84
ACRR-CC	8.382E-8	4.6	2.0	3.5	6.12
POLYCA48	7.132E-8	5.0	1.7	3.0	6.07

*Note, uncertainty does not include contributions from the response function.
Lifetime uncertainty to be improved using a least square fit to the damage slope when multiple datapoints are available.
"Other" uncertainties include some consideration of the methodology for the spectrum characterization, e.g., variation with recent spectrum characterization data.

Additional data entries were available for the carrier removal experimental datapoints obtained from resistivity measurements in bulk material. Table 9-3 provides this double ratio data. Note, this data was compared to 14-MeV data obtained at a different accelerator-based facility. The documentation for these measurements defined that spectrum to be 14.9-MeV rather than the 14.0 MeV average energy used to characterize the LED carrier removal data.

Table 9-3. Ratio of Damage in Neutron Field to 14-MeV*

Neutron Spectrum	Legacy LED Experimental Damage Constant Ratio: 14.0 MeV / Field	Legacy Carrier Removal Experimental Damage Constant Ratio: 14.9 MeV / Field
DT	1.00	1.00
spr3cc	2.2361 ± 5.83%	3.0 ± 6.67%
LBACRR12	3.1261 ± 6.56%	3.4 ± 5.88%
The carrier removal data is ratioed to a 14.9 MeV datapoint. The LED lifetime data is ratioed to a 14 MeV spectrum.		

10. FUTURE WORK

In the process of reviewing the methodology used to generate the GaAs damage metrics, updating the nuclear data to reflect the best current recommended values, and assessing the available validation data that is used to correlate the calculated damage metrics with experimentally-observed damage modes, we identified several areas where future work is desired. These areas of future research include the topics addressed in the following bullet items.

- The legacy ASTM-endorsed recoil-energy-dependent efficiency function was derived using the legacy cross sections to match experimental data on the carrier recombination lifetime. Since this work clearly demonstrates that significant differences exist between the legacy cross sections and the current best recommended nuclear data, the process of using the experimental data to extract the shape of the recoil-energy-dependent efficiency function should be repeated using the new cross sections.
- The legacy extraction process for the efficiency function was empirical in nature, i.e., it represented a trial-and-error process to find the shape of an efficiency function that reconciled the experimental data with the calculated metric. This process, while respecting the inventory of existing experimental data, lacked a metric on the accuracy of the extracted shape as well as any uncertainty associated with the shape of the efficiency curve. The fitting process should be placed on a more rigorous foundation by using a least-squares process to determine the shape, reporting a chi-squared (χ^2) per degree-of-freedom (dof) metric to evaluate the fitting process and its consistency with the experimental data and its associated uncertainties, as well as producing an energy-dependent uncertainty for the resulting efficiency function.
- The current efficiency function for GaAs 1-MeV neutron displacement damage found in the ASTM standards is based on an empirical fitting of a correction term based on the recoil energy. However, a more physics-based approach to this type of correction exists in the arc-dpa functional form [Nor18a, OECD]. The arc-dpa form has a concave recoil energy-dependent shape rather that the convex functional form in the legacy ASTM efficiency. Investigations should be performed to see if an arc-dpa functional form can provide an equivalent fidelity fit to the available experimental data. If so, the fact that the arc-dpa has two degrees-of-freedom rather than the arbitrary shape used in the legacy approach, suggests that it would provide a more robust physics-based foundation for the correction efficiency term. It might also encourage studies with MD codes or kinetic Monte Carlo (MC) codes (kMC) to identify the underlying defect-related physics that is responsible for this correlation of the observed damage with the efficiency-correct behavior.
- The efficiency function is defined as a function of residual atom recoil energy. This correction term is typically defined as being applied on top of the Robinson partition function as modified with the NRT threshold treatment [OECD]. For many high energy transmutation reactions, this correction factor is applied to both the primary knock-on atom (PKA) as well as lighter emitted charged particles, e.g., alpha particles (at least within the current NJOY-2016 implementation). For typical fission reactor neutron spectra, the lattice atom displacements caused by direct interactions with the emitted alpha particle have a very small effect. Rather, it is the Frenkel pairs (FP) induced by the secondary lattice atoms, and their subsequent collisions, that dominates the later defect formation that is correlated with observed damage modes. Thus, using the same simple recoil energy-dependent functional form in the efficiency term for both the PKA and the emitted alpha particles may not be justified.

The systematic behavior of the stopping power, which is used to separate the recoil energy that goes into electronic modes (ionization) from that that goes into nuclear modes (displacement and lattice phonons), already addresses this issue to some degree when it parametrizes its functional form based on the ion's energy per nucleon. One could conjecture that this physics consideration is already reflected in the stopping power, and that this, in turn, is already incorporated into the functional form (and empirical fit) for the partition function (which is, effectively, an integral of the partition of the stopping power along the slowing-down path for the ion). So, consideration could be given to incorporating an energy-per-nucleon formulation into the functional form already used for the efficiency function. One drawback here is that, as noted in the Section 4.1 discussion, many of the empirical fits to the damage partition function provide explicit warnings that their fitting forms are not valid for very low mass recoil ions. This means that the Robinson fit to the LSS partition function (the traditional form associated with the application of the arc-dpa efficiency function) should not even be used to capture the displacement energy from low mass secondary particles, e.g., protons and alpha, that result from neutron-induced reactions. The damage from the low mass secondary particles must still be considered, but it should be modeled within the general damage partition formulation.

Since the damage energy, as opposed to the recoil energy, already addresses some of these physics considerations, and since the efficiency function is intended to address limitations in the ability of the commonly used partition functions to represent the actual damage, perhaps an easy approach is to parameterize the efficiency function by the damage energy rather than the recoil energy. Since most molecular dynamics (MD) approaches to determining the efficiency function already compensate for the ionization losses before the atomic collisions are simulated (although some codes do treat ionization as a friction force), these computational approaches may already be reporting results based upon the "damage energy" rather than the "recoil energy".

Work should be conducted using MD codes, such as LAMMPS, and/or binary collision approximation (BCA) codes, such as Marlowe, to identify an algorithm for relating effective Frenkel pair generation from heavy lattice recoil atoms to that from alpha particles. It is likely that a more accurate functional dependence of the general efficiency algorithm can be identified that better matches the Frenkel pair generation efficiency from the light and heavy charged particle recoil atoms.

- This work provided a set of response functions – but there was no investigation of the computational-based energy-dependent uncertainty in these response functions. An investigation, similar to that conducted for silicon [Gri91, Gri19], should be conducted for the uncertainty in the GaAs response functions.
- Efforts should be placed on gathering validation data for the various metrics presented here, in particular, cryogenic investigations of changes in the resistivity of materials can be used to validate the Frenkel pair production response function.
- The current set of data used to extract the shape of the efficiency function is based on data gathered in fast neutron fields. Efforts should be made to extend the suite of neutron benchmark fields used to gather data to thermal and epithermal neutron fields.
- A critical issue is the correlation of a computed metric with an observed damage mode. The current 1-MeV(GaAs)-equivalent fluence is based upon matching observed changes in the carrier recombination lifetime in light emitting diodes (LEDs). Investigations should be conducted on GaAs heterojunction bipolar transistors (HBTs), which are expected to also

scale with the carrier recombination lifetime, to confirm that the displacement-induced gain degradation follows the same scaling.

- Based on studies of damage in silicon semiconductors, there is reason to be cautious about: a) the fidelity of the current NJOY-2016 modeling of recoil atom energies from capture gamma reactions; b) how these low energy recoils translate into the creation of residual Frenkel pairs, i.e., the use of a displacement threshold energy to capture the probability of immediate recombination of displaced atoms; and c) the similarity of the residual defects produced from high energy recoils and those produced by low energy recoils. Investigations should be conducted into an improved treatment of the capture reaction within the NJOY-2016 modeling formalism and the extraction of the corresponding recoil spectrum. In addition, high-fidelity MD, kMC, and mean rate theory modeling [Sto08] should be used to investigate a difference in the ratio of different types of residual defects between fast and thermal neutron generated cascades.
- Most of the current experimental data has been acquired in relatively long-pulsed reactor experiments (FWHM > 8 ms). With the availability of NIF and Omega facilities to produce very fast (<10 ns) pulses of 14-MeV neutrons, studies should be conducted to establish the equivalence of this damage with that produced by steady-state accelerator DT sources, e.g., the SNL IBL or the AWE ASP facilities.

11. CONCLUSION

This report documents a set of high-fidelity model-based response functions for GaAs damage metrics that are based on the most recent recommended nuclear data. These response functions support applications by the dosimetry and radiation damage communities and provide a basis to investigate the correlation of observed damage modes with the calculated metrics. A detailed tabulation for six of the energy-dependent response functions is provided in Appendix A. Figure 7-1 depicts the total cross section, a metric that can be correlated with the number of recoil atom tracks created. Figure 7-2 depicts the total kerma, displacement kerma, and ionizing kerma in units of rad(GaAs) as used by the experimental community. Figure 7-3 depicts the NRT-based damage energy and the ASTM 1-MeV(GaAs) equivalent damage energy using units of MeV-mb. The 1-MeV(GaAs) equivalent damage energy response functions can be converted to the 1-MeV(GaAs)-equivalent fluence by dividing by the community accepted reference value of 70 MeV-mb [ASTM722].

This report also describes the methodology for describing more complex damage modes, e.g., an approach to extract a recoil atom spectrum for a given neutron spectrum and provides representative recoil spectra for several monoenergetic neutron energies as seen in Figure 7-4. If the user convolutes this recoil spectrum with the recoil energy-dependent GaAs electronic stopping power, they can generate probability distribution functions (pdf) and cumulative distribution functions (cdf) for LET spectra that can be correlated with single event effects [Gri06].

Recommendations are also provided for future work that further supports the application of the response functions here, e.g., quantification of the energy-dependent uncertainties in the calculated response functions, correlation with observed damage modes, and validation of the calculated metrics.

REFERENCES

[Abn16] J. Meija, T.B. Coplen, M. Berglund, W. A. Brand, P. De Bièvre, M. Gröning, N. E. Holden, J. Irrgeher, R. D. Loss, Thomas Walczyk, T. Prohaska, Isotopic compositions of the elements 2013 (IUPAC Technical Report), Pure Appl. Chem., Vol. 88, pp. 293-306, 2016. Published Online: 2016-02-20 | DOI: https://doi.org/10.1515/pac-2015-0503

[Aga21] S. Agarwal, Y. Lin, C. Li, R.E. Stoller, S.J. Zinkle, "On the use of SRIM for calculating vacancy production: Quick calculation and full-cascade options," Nuclear Instruments and Methods in Physics Research, Vil. B 503, pp. 11-29, 2021.

[Akk06] A. Akkerman, J. Barak, "New Partition Factor Calculations for Evaluating the Damage of Low Energy Ions in Silicon," IEEE Transactions on Nuclear Science, Vol. 53, No. 6, pp. 3667-3674, 2006. DOI:10.1109/TNS.2006.884382.

[Akk07] A. Akkerman, J, Barak, "Partitioning to elastic and inelastic processes of the energy deposited by low energy ions in silicon detectors," Nuclear Instruments and Methods in Physics Research, Vol. B 260, pp. 529-536, 2007. DOI: 10.1016/j.nimb.2007.04.164.

[Akk20] A. Akkerman, J. Barak, "A Survey of the Analytical Methods of Proton-NIEL Calculations in Silicon and Germanium,", IEEE Transactions on Nuclear Science, Vol. 67, No. 8, pp. 1813-1825, 2020. DOI:10.1109/TNS.2020.2998006.

[AME2020] M. Wang, W.J. Huang, F.G. Kondev, G. Audi, S. Naimi, "The AME2020 Atomic Mass Evaluation, (II) Tables, Graphs, and References", Chin. Phys. C45, Number 3 (2021); https://www-nds.iaea.org/amdc/.

[ASTM722] E722-14, Standard Practice for Characterizing Neutron Fluence Spectra in Terms of an Equivalent Monoenergetic Neutron Fluence for Radiation-Hardness Testing of Electronics, ASTM International, West Conshohocken, PA, 2014. https://www.astm.org/Standards/E722.htm.

[ASTM521] E521-16, Standard Practice for or Investigating the Effects of Neutron Radiation Damage Using Charged-Particle Irradiation, ASTM International, West Conshohocken, PA, 2014. https://www.astm.org/Standards/E521.htm

[Ba90] A.L. Barry, R. Maxseiner, R. Wojcik, "An improved displacement damage monitor LED", IEEE Trans. Nucl. Sci., Vol. 37, 1726, 1990.

[Ba95] D.J. Bacon, A.F. Calder, F. Gao, V.G. Kapinos, S.J. Wooding, "Computer simulation of defect production by displacement cascades in metals," Nuclear Instruments and Methods in Physics Research B, Vol. 102, pp. 37-46, 1995.

[Ch17] N. J. Chen, S. Gray, D. H. Huang, D. A. Cardimona, and F. Gao, "Computational simulation of threshold energies of GaAs," J. Mater. Res., Vol. 32, Issue 8, pp. 1555-1562, April; 2017. See DOI: https://doi.org/10.1557/jmr.2017.46

[Che20] S. Chen, D. Bernard, "On the calculation of atomic displacements using damage energy," Results in Physics, Vol. 16, 2020. See https://doi.org/10.1016/j.rinp.2019.102835.

[CIAAW] XK Zhu, J. Benefield, T.B. Coplen, Z. Gao, N. Holden, "Variation of lead isotopic composition and atomic weight in terrestrial materials" (IUPAC Technical Report), Pure Appl. Chem. 93, 155-166 (2021). https://doi.org/10.1515/pac-2018-0916.

[Cou80] C. Coulter, D.M. Parkin, "Damage Energy Functions in Polyatomic materials, Journal of Nuclear Materials, Vol.88, pp. 249-260, 1980.

[Cro16] JP Crocombette, L. Brutzel, D. Simeone, L. Luneville, "Molecular dynamics simulations of high energy cascade in ordered alloys: Defect production and subcascade division," Journal of Nuclear Materials, Vol. 474, pp. 134-142, 2016. See 10.1016/j.jnucmat.2016.03.020ff. ffhal-02429493. https://hal.archives-ouvertes.fr/hal-02429493/document

[Dan98] M. B. Danjaji, P. J. Griffin, "Uncertainty of Silicon 1-MeV Damage Function," Proceedings of the 9th International Symposium on Reactor Dosimetry held in Prague, Czech Republic, 2-6 September 1996, pp. 611-618, 1988.

[Dem16] G. Demange, E. Antoshchenkova, L. Luneville, D. Simeone, "A rational use of BCA code MARLOWE for ballistic effects of ion beam irradiation in the ion mixing formalism: comparison to Molecular Dynamics," See: arXiv:1610.08659.

[Do72] D.G. Doran, "Neutron Displacement Cross Sections for Stainless Steel and Tantalum Based on a Lindhard Model", Nucl. Sci. Eng., Vol. 49, 130, 1972.

[ENDF6] A. Trkov, M. Herman and D. A. Brown (edrs.), "ENDF-6 Formats Manual", Report BNL-90365-2009, Brookhaven National Laboratory, Upton, NY., Rev. 2 (2012).

[ENDF8] D.A. Brown, M.B. Chadwick, R. Capote et al., "ENDF/B-VIII.0: The 8th Major Release of the Nuclear Reaction Data Library with CIELO-project Cross Sections, New Standards and Thermal Scattering Data", Nuclear Data Sheets, Vol. 148, p. 1 (2018).

[ENDL84] Cullen, D.E., McLaughlin, P.K., & Lemmel, H.D., ENDL-84 The Evaluated Nuclear Data Library of the Lawrence Livermore National Laboratory in the ENDF-5 format (IAEA-NDS--11(Rev5)). International Atomic Energy Agency (IAEA), 1990. Available online at https://inis.iaea.org/collection/NCLCollectionStore/_Public/22/030/22030695.pdf?r=1.

[Ga01] F. Gaa. D.J. Bacon, L.M. Howe, C.B. So, "Temperature-dependence of defect creation and clustering by displacement cascades in α-zirconium," Jopurnal of Nuclear Materials, Vol. 294, pp. 288-298, 2001.

[Ga17] F. Gao, N. Chen, E. Hernandez-Rivera, D. Huang, P.D. LeVan, "Displacement damage and predicted non-ionizing energy loss in GaAs", Journal of Applied Physics, Vol. 121, 2017. See https://doi.org/10.1063/1.4977861

[Gad95] H. Gades, H.M. Urbassek, "Simulation of Ion-Induced Mixing in Metals," Phys. Rev. B, Vol. 51, pp 14559, 1995.

[Gh88] N.M. Ghoniem, S.P. Chou, "Binary Collision Monte Carlo Simulations of Cascades in Polyatomic Ceramics," Journal of Nuclear Materials, Vol. 155-157, pp. 1263-1267, 1988.

[Gre85] L.R. Greenwood, R.K. Smither, SPECTER: Neutron Damage Calculations for Materials Irradiation, Argonne National Laboratory, report ANL/FPP/TM-197, January 1985.

[Gri03] P. Griffin, M. Danjaji, "Sensitivity of Silicon 1-MeV Damage Function to Cross Section Evaluation," Transactions of the American Nuclear Society, Vol. 73, pp. 451-453, 1995.

[Gri06] P.J. Griffin, W.C. Cheng, "Characterization of Neutron-Induced SEE Environments in Si and GaAs Devices," presented at HEART 2006, Journal of Radiation Effects, Research and Engineering (JRERE)., 2006

[Gri19] P.J. Griffin, A.J. Koning, D. Rochman, "Impact of Nuclear Data Uncertainty in the Modeling of Neutron-Induced Recoil Atom Energy Distributions in Silicon," IEEE Transactions on Nuclear Science, Vol. 66, No. 7, pp. 1719-1729, 2019. DOI: 10.1109/TNS.2019.2894730.

[Gri91) P. Griffin, J. Kelly, et al., "Neutron Damage Equivalence in GaAs", IEEE Transactions on Nuclear Science, Vol. 38, pp. 1216-1224, Dec. 1991.

[Hel93] J. Helm, Reactor Vessel Irradiation Damage: Absorbed Dose Estimates, Electric Power Research Institute, report EP 89-21, second edition, October 18, 1993.

[Hem20] H. Hemani, A. Majalee, U. Bhardwaj, A. Arya, K. Nordlund, M. Warrier, "Inclusion and validation of electronic stopping in the open source LAMMPS code", 2020. Preprint available at arXiv: https://arxiv.org/abs/2005.11940

[Hou10] M. Hou, C.J. Ortiz, C.S. Becquart, C. Domain, U. Starkae, A. Debacker, "Microstructure evolution of irradiated tungsten: Crystal effects in He and H implantation as modelled in the Binary Collision Approximation," Journal of Nuclear Materials, Vol. 403, pp. 89-100, 2010.

[JEFF3] A. Santamarina, D. Bernard, P. Blaise, M. Coste, A. Courcelle, T.D. Huynh, C. Jouanne, P. Leconte, O. Litaize, S. Mengelle, G. Noguere, J-M. Ruggiere, O. Serot, J. Tommasi, C. Vaglio, J-F. Vidal, The JEF-3.1.1 Nuclear Data Library, JEFF Report 22, Validation Results from JEF-2.2 to JEF-3.1.1, Nuclear Energy Agency, Organization for Economic Co-operation and Development, 2009.

[JEFF4T0] Observations based on benchmarking results for JEFF-4T0, jefdoc 2094. Restricted distribution, see https://www.oecd-nea.org/dbdata/jeff/jeffdoc.html. ENDF6-format nuclear data files available at https://www.oecd-nea.org/dbdata/nds/JEFF4T0/endf6/files/.

[JENDL4] K. Shibata, O. Iwamoto, T. Nakagawa, N. Iwamoto, A. Ichihara, S. Kunieda, S. Chiba, K. Furutaka, N. Otuka, T. Ohsawa, T. Murata, H. Matsunobu, A. Zukeran, S. Kamada, and J. Katakura: "JENDL-4.0: A New Library for Nuclear Science and Engineering," *J. Nucl. Sci. Technol.* 48, pp. 1-30, 2011.

[Kha09] G. Kharashvili, V. Makarashvili, et al., "Development and Tersting of Gallium Arsenide Photoconductive Detectors for UltraFast, High Dose Rate Pulsed Electron and Bremsstrahluing Radiation Measurements", AIP Conference Proceedings, Vol. 1099, Issue 1, March 2009. DOI: 10.1063/1.3120099.

[Kin55] Kinchin, G.H., Pease, R.S., The Displacement of Atoms in Solids by Radiation, Reports on Progress in Physics, 1955. doi: 10.1088/0034-4885/18/1/301.

[Kon12] A.J. Koning and D. Rochman, "Modern Nuclear Data Evaluation With The TALYS Code System", Nuclear Data Sheets 113 (2012) 2841

[Kon19] A.J. Koning, D. Rochman, J. Sublet, N. Dzysiuk, M. Fleming and S. van der Marck, "TENDL: Complete Nuclear Data Library for Innovative Nuclear Science and Technology", Nuclear Data Sheets 155 (2019). https://doi.org/10.1016/j.nds.2019.01.002

[Li63] J. Lindhard, M. Scharff, H. Schiott, "Range Concepts and Heavy Ion Ranges," Mat. Phys. Medd. Dan. Vld. Selsk, Vol. 33, pp. 1-40, 1963.

[MARLOWE] M. T. Robinson: MARLOWE Binary Collision Cascade Simulation Program, Version 15b, A Guide for Users, December 5, 2002.

[Mat17] F. Matias, R.C. Fadanelli, et al., "Ground- and excited state scattering potentials for the stopping of protons in an electron gas", Journal of Physics B: Atomic, Molecular and Optical Physics, Vol. 50, 185201, 2017. doi.org/10.1088/1361-6455/aa843d.

[MSTAR] H. Paul, A. Schinner, "An empirical approach to the stopping power of solids and gasses for ion from 3Li to 18Ar", Nuclear Instruments and Methods in Physics Research, Vol. B195, pp. 166-174, 2001. For the source code, see https://www-nds.iaea.org/stopping/MstarWWW/MSTARInstr.html

[Mo12] F. Mota, C.J. Ortiz, R. Vila, "Primary Displacement Damage Calculation Induced by Neutron and Ion Using Binary Collision Approximation Techniques (MARLOWE code)", presentation to the First Technical Meeting on Primary Radiation Damage, IAEA Vienna, October 1-4,2012.

[NJOY2016] "Nuclear Data Processing System NJOY21 and NJOY2016", Los Alamos National Laboratory, https://github.com/njoy.

[Nor18a] K. Nordlund, SJ. Zinkle, et al., "Improving atomic displacement and replacement calculations with physically realistic damage models", Nature Communications, Vol. 9, 1084 (2018). DOI: 10.1038/s41467-018-03415-5.

[Nor18b] K. Nordlund, S.J. Zinkle, et al., "Primary radiation damage: A review of current understanding and models," Journal of Nuclear Materials, Vol. 512, pp. 450-479, 2018.

[Nor75] M. J. Norgett. M.T. Robinson, I.M. Torrens, "A Proposed Method of Calculating Displacement Dose Rates," *Nuclear Engineering and Design*, vol. 33, pp. 50-54, 1975, DOI: 10.1016/0029-5493(75)90035-7.

[Nor98] E. Normand, "Extensions of the burst generation rate method for wider application to proton/neutron-induced single event effects," in *IEEE Transactions on Nuclear Science*, vol. 45, no. 6, pp. 2904-2914, Dec. 1998, DOI: 10.1109/23.736546.

[Nor98a] K. Norlund, M. Ghaly, R.S. Averback, "Mechanisms of Ion Beam Mixing in Metals and Semiconductors," **J. Appl. Physics**, Vol. **83**, pp. 1238-1246, 1998.

[Nor98b] K. Nordlund, L. Wei, Y, Zong, R.S. Averback, "Role of Electron-phonon Coupling on Collision Cascade Development in Ni, Pd, and Pt," **Phys. Rev**. Vol. **B** (Rapid Communications), Vol. **57**, pp. 13965-13968, 1998.

[Od76] G.R. Odette, D.R. Doran, "Neutron-Energy-Dependent Defect Production Cross Sections for Fission and Fusion Applications, Nuclear Technology, Vol. 29, pp. 356-368, June 1976.

[OECD] *Primary Radiation Damage in Materials - Review of Current Understanding and Proposed New Standard Displacement Damage Model to Incorporate In-Cascade Defect Production Efficiency and Mixing Effects*, OECD/NEA Working Party on Multiscale Modeling of Fuels and Structural materials for Nuclear Systems, Expert Group on Primary Damage, NEA/NSC/DOC(2015)9, 2015. https://www.oecd-nea.org/science/docs/2015/nsc-doc2015-9.pdf.

[Ort14] C.J. Ortiz, A. Souidi, C.S. Becquart, C. Domain, M. Hou, "Recent radiation damage studies and developments of the Marlowe code", Radiation Effects and Defects in Solids, Vol. 169, No. 7, pp. 592-602, 2014.

[Otu14] Otuka, N., Dupont, E., Semkova, V., Pritychenko, B., Blokin, A. I., Aikawa, M., et al, Towards a More Complete and Accurate Experimental Nuclear Reaction Data Library (EXFOR): International Collaboration Between Nuclear Reaction Data Centres (NRDC), Nuclear Data Sheets, Vol 120, pp. 272-276, June 2014. URL for EXFOR database is: https://www-nds.iaea.org/exfor/exfor.htm.

[Par81] D.M. Parkin, C.A. Coulter, "Total and Net Displacement Functions for Polyatomic Materials," Journal of Nuclear Materials, Vol. 101, pp. 261-276, 1981.

[Par83] D.M. Parkin, C.A. Coulter, "Displacement Cascades in Polyatomic Materials," Journal of Nuclear Materials, Voo. 117, pp. 340-344, 1983.

Presentation at the TMS AIME Fall Meeting in St. Louis MO, Oct. 24-28, 1982. Available as Los Alamos National Laboratory report LA-UR-82-3126.

[Par89] Parkin D.M., The Displacement Cascade in Solids. In: McHargue C.J., Kossowsky R., Hofer W.O. (eds) Structure-Property Relationships in Surface-Modified Ceramics. NATO ASI Series (Series E: Applied Sciences), vol 170. Springer, Dordrecht, 1989, doi.org/10.1007/978-94-009-0983-0_3.

[Po81] D. Pons, J. Bourgoin, "Anisotropic-Defect Introduction in GaAs by Electron Irradiation," Phys. Rev. Lett. 47, pp. 1293-1296, November 1981. See //doi.org/10.1103/PhysRevLett.47.1293

[Rob68] M. Robinson, Phil. Mag., Vol. 12, pp. 741, 1965; Vol. 17, pp. 639, 1968.

[Rob69] M. T. Robinson, "The Energy Dependence of Neutron Radiation Damage in Solids," Nuclear Fusion Reactors, *Nuclear Fusion Reactors*, Proceedings of a conference held at UKAEA Culham Laboratory, Abingdon, 17-19 Sept. 1969, British Nuclear Energy Soc., pp. 364-378. Online: https://www.icevirtuallibrary.com/doi/abs/10.1680/nfr.44661.0025

[Rob71] M.T. Robinson, The dependence of neutron irradiation damage in solids, R.N.E.S. nuclear fusion reactor conference at Culham Laboratory, September,1969, Nuclear Fusion Reactors, pages 364-378, British Nuclear Energy Society, London,1970.

[Rob74] M.T. Robinson, O.M. Torrens, "Computer Simulation of Atomic-Displacement Cascades in Solids in the Binary-Collision Approximation," Physical Review B, Vol. **9**, pp. 5008-5024, June 1974.

[Rob75] M. Robinson, "The Theory of Radiation Induced Defect Production," in Radiation Damage in Metals, papers presented at a Seminar of the American Society for Metals November 9 and 10 1975, edited by N. L. Peterson and S. D. Hardness, pp 1-27, 1975.

[Rob82] M.T. Robinson, O.S. Oen, "On the Use of Thresholds in Damage Energy Calculations," Journal of Nuclear Materials, Vol. 110, pp. 147-149, 1982.

[Rob83] M. T. Robinson, "Computer simulation of collision cascades in monazite," Physical Review B, Vol. 27, Number 9, pp. 5347-5359, May 1983.

[Rob92] M.T. Robinson, "Computer Simulation Studies of High-Energy Collision Cascades," Nuclear Instrumentation and Methods in Physics Research B67, pp. 396-400, 1992.

[Rob96] M.T. Robinson, "Binding Energy Effects in Cascade Evolution and Sputtering," Nuclear Instrumentation and Methods in Physics Research B 115, pp. 549-553, 1996.

[Sa95] M. Sayed, J.H. Jefferson, A.B. Walker, A.G. Cullis, "Computer simulation of atomic displacements in Si, GaAs, and AlAs," Nuclear Instruments and Methods in Physics, pp. 232-235, Vol. B102, 1995.

[Sch12] G. Schiwietz, P.L. Grande, "Stopping of Protons – Improved Accuracy of the UCA Model," Nuclear Instruments and Methods in Physics, pp. 1-5, Vol. B 273, 2012.

[Si69] O. Sigmund, "A Note on Integral Equations of the Kinchin-Pease Type," Radiation Effects, Vol. 1, p. 15-18, 1969.

[Sig19a] P. Sigmund, A. Schinner, "Is electronic stopping of ions velocity-proportional in the velocity-proportional regime?", Nuclear Instruments and Methods in Physics Research B440, pp. 41-47, 2019. doi.org/10.1016/j.nimb.2018.10.031

[Sig19b] P. Sigmund, A. Schinner, "Application of the PASS Stopping Code," plenary lecture at the 24th International Conference on Ion Beam Analysis, October 14, 2019. Available at: https://findresearcher.sdu.dk:8443/ws/portalfiles/portal/155453863/IBA_2019.pdf

[Sig19c] P. Sigmund, A. Schinner, "Progress in understanding heavy-ion stopping," Nuclear Instruments and Methods in Physics Research B382, pp. 15-25, 2016. doi.org/10.1016/j.nimb.2015.12.041

[SNLNJOY2016] see GitHub code repository, https://github.com/sandialabs/NJOY2016

[Sim07] S.P. Simakov, SPKA code, FZK, 2007.

[SPAR] T.W. Armstrong, K.C. Chandler, "SPAR, a FORTRAN Program for Computing Stopping Powers and Ranges for Muons, Charged Pions, Protons, and Heavy Ions," report ORNL-4869, Oak Ridge National Laboratory, Ok Ridge, TN, May 1973.

[Sto08] R.E. Stoller, S.I. Golubov, C.S. Becquart, "Mean filed rate theory and object kinetic Monte Carlo: A comparison of kinetic models," Journal of Nuclear Materials, Vol. 384, pp. 77-90, 2008.

[Sto13] R.E. Stoller, M.B. Toloczko, G.S. Wasa, A.G. Certain, S. Dwaraknath, F.A. Garner, "On the use of SRIM for computing radiation damage exposure", Nuclear Instruments and Methods in Physics Research, Vol. B 310, pp. 75-80, 2013.

[Sto20] R.E. Stoller, "Radiation Damage Correlation," in Vol. 1 of Comprehensive Nuclear Materials (Second Edition), Chapter 1.13, pp. 456-467, Editors-in-Chief: Rudy Konings, Roger Stoller, Hardcover ISBN 9780081028650, ebook ISBN 9780081028667. July 22, 2020.

[Viz15] G. Vizkelethy, S.M. Foiles, "Determination of recombination radius in Si for binary collision approximation codes," Nuclear Instruments and Methods in Physics Research B, 2015.

[ZBL85] The Stopping and Range of Ions in Solids, J.F. Ziegler, J.P. Biersack and U. Littmark, Pergamon Press, Inc., New York, 1985.

[Zi10] J.F. Ziegler, M.D. Ziegler, J.P Biersack, SRIM – The stopping and range of ions in matter (2010), Nuclear Instruments and Methods in Physics Research Section B: Beam interactions with materials and Atoms, Vol. **268**, Issue 11-12, pp. 1818-1823, June 2010.

[Zi99] J.F. Ziegler, The Stopping of Energetic Light Ions in Elemental Matter, J. Appl. Phys. / Rev. Appl. Phys. Vol. 85, pp. 1249-1272, 1999.

APPENDIX A. TABULATED GaAs RESPONSE FUNCTIONS

Table A-1. GaAs Kerma Response Functions

Energy Bin #	Lower Energy Bound [MeV]	Upper Energy Bound [MeV]	Total Kerma [rad(GaAs)]	Displacement Kerma [rad(GaAs)]	Ionizing Kerma [rad(GaAs)]
1	1.9900E+01	2.0000E+01	3.071216E-10	4.497476E-11	2.370079E-10
2	1.9800E+01	1.9900E+01	3.045226E-10	4.482858E-11	2.343895E-10
3	1.9700E+01	1.9800E+01	3.019248E-10	4.468200E-11	2.317780E-10
4	1.9600E+01	1.9700E+01	2.993191E-10	4.453622E-11	2.291804E-10
5	1.9500E+01	1.9600E+01	2.966707E-10	4.439192E-11	2.265734E-10
6	1.9400E+01	1.9500E+01	2.940127E-10	4.424733E-11	2.239840E-10
7	1.9300E+01	1.9400E+01	2.913189E-10	4.410489E-11	2.214123E-10
8	1.9200E+01	1.9300E+01	2.885981E-10	4.396218E-11	2.188410E-10
9	1.9100E+01	1.9200E+01	2.858709E-10	4.382028E-11	2.162662E-10
10	1.9000E+01	1.9100E+01	2.831516E-10	4.367865E-11	2.137057E-10
11	1.8900E+01	1.9000E+01	2.803856E-10	4.353913E-11	2.111859E-10
12	1.8800E+01	1.8900E+01	2.776048E-10	4.340256E-11	2.087325E-10
13	1.8700E+01	1.8800E+01	2.747800E-10	4.326666E-11	2.062717E-10
14	1.8600E+01	1.8700E+01	2.719112E-10	4.312927E-11	2.038110E-10
15	1.8500E+01	1.8600E+01	2.690531E-10	4.299337E-11	2.013595E-10
16	1.8400E+01	1.8500E+01	2.661122E-10	4.285640E-11	1.989318E-10
17	1.8300E+01	1.8400E+01	2.629365E-10	4.271741E-11	1.965222E-10
18	1.8200E+01	1.8300E+01	2.597569E-10	4.257885E-11	1.941226E-10
19	1.8100E+01	1.8200E+01	2.565305E-10	4.244014E-11	1.917194E-10
20	1.8000E+01	1.8100E+01	2.532989E-10	4.230076E-11	1.893247E-10
21	1.7900E+01	1.8000E+01	2.505980E-10	4.214324E-11	1.868815E-10
22	1.7800E+01	1.7900E+01	2.484241E-10	4.196720E-11	1.843929E-10
23	1.7700E+01	1.7800E+01	2.462423E-10	4.179317E-11	1.819142E-10
24	1.7600E+01	1.7700E+01	2.439644E-10	4.161766E-11	1.794370E-10
25	1.7500E+01	1.7600E+01	2.416813E-10	4.144255E-11	1.769594E-10
26	1.7400E+01	1.7500E+01	2.393380E-10	4.126904E-11	1.745002E-10
27	1.7300E+01	1.7400E+01	2.369292E-10	4.109594E-11	1.720487E-10
28	1.7200E+01	1.7300E+01	2.344953E-10	4.092190E-11	1.695953E-10
29	1.7100E+01	1.7200E+01	2.320574E-10	4.074945E-11	1.671457E-10
30	1.7000E+01	1.7100E+01	2.296062E-10	4.057701E-11	1.647094E-10
31	1.6900E+01	1.7000E+01	2.270468E-10	4.039643E-11	1.623279E-10
32	1.6800E+01	1.6900E+01	2.244502E-10	4.020972E-11	1.600261E-10
33	1.6700E+01	1.6800E+01	2.218028E-10	4.002206E-11	1.577170E-10
34	1.6600E+01	1.6700E+01	2.191473E-10	3.983495E-11	1.554180E-10
35	1.6500E+01	1.6600E+01	2.164600E-10	3.964810E-11	1.531150E-10
36	1.6400E+01	1.6500E+01	2.136912E-10	3.946099E-11	1.508266E-10
37	1.6300E+01	1.6400E+01	2.108451E-10	3.927415E-11	1.485448E-10

Energy Bin #	Lower Energy Bound [MeV]	Upper Energy Bound [MeV]	Total Kerma [rad(GaAs)]	Displacement Kerma [rad(GaAs)]	Ionizing Kerma [rad(GaAs)]
38	1.6200E+01	1.6300E+01	2.080055E-10	3.908837E-11	1.462618E-10
39	1.6100E+01	1.6200E+01	2.051594E-10	3.890151E-11	1.439801E-10
40	1.6000E+01	1.6100E+01	2.023200E-10	3.871439E-11	1.416943E-10
41	1.5900E+01	1.6000E+01	1.999434E-10	3.850141E-11	1.394519E-10
42	1.5800E+01	1.5900E+01	1.979990E-10	3.826416E-11	1.372491E-10
43	1.5700E+01	1.5800E+01	1.960547E-10	3.802623E-11	1.350447E-10
44	1.5600E+01	1.5700E+01	1.941143E-10	3.778831E-11	1.328360E-10
45	1.5500E+01	1.5600E+01	1.921192E-10	3.755079E-11	1.306309E-10
46	1.5400E+01	1.5500E+01	1.899227E-10	3.731781E-11	1.285103E-10
47	1.5300E+01	1.5400E+01	1.875514E-10	3.708575E-11	1.264707E-10
48	1.5200E+01	1.5300E+01	1.851694E-10	3.685503E-11	1.244306E-10
49	1.5100E+01	1.5200E+01	1.827782E-10	3.662458E-11	1.223980E-10
50	1.5000E+01	1.5100E+01	1.803776E-10	3.639438E-11	1.203663E-10
51	1.4900E+01	1.5000E+01	1.781266E-10	3.616553E-11	1.183846E-10
52	1.4800E+01	1.4900E+01	1.760222E-10	3.593935E-11	1.164489E-10
53	1.4700E+01	1.4800E+01	1.739030E-10	3.571382E-11	1.145126E-10
54	1.4600E+01	1.4700E+01	1.717612E-10	3.548951E-11	1.125791E-10
55	1.4500E+01	1.4600E+01	1.695754E-10	3.526572E-11	1.106584E-10
56	1.4400E+01	1.4500E+01	1.671667E-10	3.504100E-11	1.088056E-10
57	1.4300E+01	1.4400E+01	1.645928E-10	3.481602E-11	1.070322E-10
58	1.4200E+01	1.4300E+01	1.620202E-10	3.459130E-11	1.052621E-10
59	1.4100E+01	1.4200E+01	1.594489E-10	3.436658E-11	1.034935E-10
60	1.4000E+01	1.4100E+01	1.568688E-10	3.414240E-11	1.017266E-10
61	1.3900E+01	1.4000E+01	1.550679E-10	3.392395E-11	1.000820E-10
62	1.3800E+01	1.3900E+01	1.540001E-10	3.371045E-11	9.854655E-11
63	1.3700E+01	1.3800E+01	1.529105E-10	3.349840E-11	9.701970E-11
64	1.3600E+01	1.3700E+01	1.518213E-10	3.328623E-11	9.549117E-11
65	1.3500E+01	1.3600E+01	1.507328E-10	3.307471E-11	9.396629E-11
66	1.3400E+01	1.3500E+01	1.495241E-10	3.286133E-11	9.249877E-11
67	1.3300E+01	1.3400E+01	1.482109E-10	3.264808E-11	9.108853E-11
68	1.3200E+01	1.3300E+01	1.468422E-10	3.243657E-11	8.968633E-11
69	1.3100E+01	1.3200E+01	1.454456E-10	3.222813E-11	8.828577E-11
70	1.3000E+01	1.3100E+01	1.440534E-10	3.201903E-11	8.688697E-11
71	1.2900E+01	1.3000E+01	1.425671E-10	3.180872E-11	8.563128E-11
72	1.2800E+01	1.2900E+01	1.409976E-10	3.160015E-11	8.451265E-11
73	1.2700E+01	1.2800E+01	1.393969E-10	3.139465E-11	8.339315E-11
74	1.2600E+01	1.2700E+01	1.377961E-10	3.118995E-11	8.227385E-11
75	1.2500E+01	1.2600E+01	1.361923E-10	3.098670E-11	8.116070E-11
76	1.2400E+01	1.2500E+01	1.343960E-10	3.078095E-11	8.001705E-11
77	1.2300E+01	1.2400E+01	1.324281E-10	3.057345E-11	7.884235E-11
78	1.2200E+01	1.2300E+01	1.304601E-10	3.036623E-11	7.766647E-11

Energy Bin #	Lower Energy Bound [MeV]	Upper Energy Bound [MeV]	Total Kerma [rad(GaAs)]	Displacement Kerma [rad(GaAs)]	Ionizing Kerma [rad(GaAs)]
79	1.2100E+01	1.2200E+01	1.284962E-10	3.015914E-11	7.649536E-11
80	1.2000E+01	1.2100E+01	1.265443E-10	2.995553E-11	7.531647E-11
81	1.1900E+01	1.2000E+01	1.241975E-10	2.974827E-11	7.424053E-11
82	1.1800E+01	1.1900E+01	1.214754E-10	2.953565E-11	7.326435E-11
83	1.1700E+01	1.1800E+01	1.187855E-10	2.932568E-11	7.228662E-11
84	1.1600E+01	1.1700E+01	1.161378E-10	2.911665E-11	7.131545E-11
85	1.1500E+01	1.1600E+01	1.134929E-10	2.890762E-11	7.034464E-11
86	1.1400E+01	1.1500E+01	1.105550E-10	2.871170E-11	6.909542E-11
87	1.1300E+01	1.1400E+01	1.074132E-10	2.854358E-11	6.759610E-11
88	1.1200E+01	1.1300E+01	1.043103E-10	2.838093E-11	6.611080E-11
89	1.1100E+01	1.1200E+01	1.012117E-10	2.821788E-11	6.462188E-11
90	1.1000E+01	1.1100E+01	9.810876E-11	2.805550E-11	6.313631E-11
91	1.0900E+01	1.1000E+01	9.569710E-11	2.789897E-11	6.139539E-11
92	1.0800E+01	1.0900E+01	9.391563E-11	2.775203E-11	5.940553E-11
93	1.0700E+01	1.0800E+01	9.214977E-11	2.760443E-11	5.742902E-11
94	1.0600E+01	1.0700E+01	9.041264E-11	2.746071E-11	5.547601E-11
95	1.0500E+01	1.0600E+01	8.869555E-11	2.731993E-11	5.353184E-11
96	1.0400E+01	1.0500E+01	8.702350E-11	2.717616E-11	5.161041E-11
97	1.0300E+01	1.0400E+01	8.535311E-11	2.702786E-11	4.969376E-11
98	1.0200E+01	1.0300E+01	8.367688E-11	2.687861E-11	4.780519E-11
99	1.0100E+01	1.0200E+01	8.202791E-11	2.673016E-11	4.594224E-11
100	1.0000E+01	1.0100E+01	8.039324E-11	2.658160E-11	4.408731E-11
101	9.9000E+00	1.0000E+01	7.907607E-11	2.643930E-11	4.248444E-11
102	9.8000E+00	9.9000E+00	7.804653E-11	2.630209E-11	4.112147E-11
103	9.7000E+00	9.8000E+00	7.701683E-11	2.616409E-11	3.979579E-11
104	9.6000E+00	9.7000E+00	7.596590E-11	2.603206E-11	3.848784E-11
105	9.5000E+00	9.6000E+00	7.487905E-11	2.590827E-11	3.718523E-11
106	9.4000E+00	9.5000E+00	7.375314E-11	2.578678E-11	3.607286E-11
107	9.3000E+00	9.4000E+00	7.260158E-11	2.566540E-11	3.513572E-11
108	9.2000E+00	9.3000E+00	7.144576E-11	2.554429E-11	3.421086E-11
109	9.1000E+00	9.2000E+00	7.025650E-11	2.542145E-11	3.330163E-11
110	9.0000E+00	9.1000E+00	6.905528E-11	2.529942E-11	3.239961E-11
111	8.9000E+00	9.0000E+00	6.829660E-11	2.518500E-11	3.165354E-11
112	8.8000E+00	8.9000E+00	6.796753E-11	2.507859E-11	3.105476E-11
113	8.7000E+00	8.8000E+00	6.760280E-11	2.497164E-11	3.045785E-11
114	8.6000E+00	8.7000E+00	6.720188E-11	2.486350E-11	2.986268E-11
115	8.5000E+00	8.6000E+00	6.675852E-11	2.475535E-11	2.926954E-11
116	8.4000E+00	8.5000E+00	6.622915E-11	2.464494E-11	2.872615E-11
117	8.3000E+00	8.4000E+00	6.558570E-11	2.453173E-11	2.822425E-11
118	8.2000E+00	8.3000E+00	6.493383E-11	2.441810E-11	2.772385E-11
119	8.1000E+00	8.2000E+00	6.427504E-11	2.430488E-11	2.722250E-11

Energy Bin #	Lower Energy Bound [MeV]	Upper Energy Bound [MeV]	Total Kerma [rad(GaAs)]	Displacement Kerma [rad(GaAs)]	Ionizing Kerma [rad(GaAs)]
120	8.0000E+00	8.1000E+00	6.357741E-11	2.419045E-11	2.671811E-11
121	7.9000E+00	8.0000E+00	6.292778E-11	2.408951E-11	2.623313E-11
122	7.8000E+00	7.9000E+00	6.232145E-11	2.400202E-11	2.576496E-11
123	7.7000E+00	7.8000E+00	6.168795E-11	2.391468E-11	2.531571E-11
124	7.6000E+00	7.7000E+00	6.102870E-11	2.382799E-11	2.488209E-11
125	7.5000E+00	7.6000E+00	6.029431E-11	2.374024E-11	2.441389E-11
126	7.4000E+00	7.5000E+00	5.929173E-11	2.365075E-11	2.391219E-11
127	7.3000E+00	7.4000E+00	5.824687E-11	2.356244E-11	2.348829E-11
128	7.2000E+00	7.3000E+00	5.732416E-11	2.347678E-11	2.313298E-11
129	7.1000E+00	7.2000E+00	5.631303E-11	2.339045E-11	2.274268E-11
130	7.0000E+00	7.1000E+00	5.522994E-11	2.330346E-11	2.232274E-11
131	6.9000E+00	7.0000E+00	5.454687E-11	2.321021E-11	2.192538E-11
132	6.8000E+00	6.9000E+00	5.421005E-11	2.310832E-11	2.154976E-11
133	6.7000E+00	6.8000E+00	5.380509E-11	2.300722E-11	2.117576E-11
134	6.6000E+00	6.7000E+00	5.334131E-11	2.290573E-11	2.080376E-11
135	6.5000E+00	6.6000E+00	5.278017E-11	2.280329E-11	2.041176E-11
136	6.4000E+00	6.5000E+00	5.194111E-11	2.269900E-11	2.000319E-11
137	6.3000E+00	6.4000E+00	5.103692E-11	2.258659E-11	1.963280E-11
138	6.2000E+00	6.3000E+00	5.024417E-11	2.246871E-11	1.929421E-11
139	6.1000E+00	6.2000E+00	4.938608E-11	2.235030E-11	1.893880E-11
140	6.0000E+00	6.1000E+00	4.843751E-11	2.223149E-11	1.856070E-11
141	5.9000E+00	6.0000E+00	4.794384E-11	2.211867E-11	1.820486E-11
142	5.8000E+00	5.9000E+00	4.788823E-11	2.200771E-11	1.788572E-11
143	5.7000E+00	5.8000E+00	4.777406E-11	2.189435E-11	1.756590E-11
144	5.6000E+00	5.7000E+00	4.758672E-11	2.178007E-11	1.723810E-11
145	5.5000E+00	5.6000E+00	4.732232E-11	2.166566E-11	1.688827E-11
146	5.4000E+00	5.5000E+00	4.683888E-11	2.154296E-11	1.651551E-11
147	5.3000E+00	5.4000E+00	4.620716E-11	2.141361E-11	1.617836E-11
148	5.2000E+00	5.3000E+00	4.549301E-11	2.128017E-11	1.586325E-11
149	5.1000E+00	5.2000E+00	4.468725E-11	2.114404E-11	1.551827E-11
150	5.0000E+00	5.1000E+00	4.380481E-11	2.100644E-11	1.514662E-11
151	4.9000E+00	5.0000E+00	4.316141E-11	2.087084E-11	1.482829E-11
152	4.8000E+00	4.9000E+00	4.275135E-11	2.073815E-11	1.455865E-11
153	4.7000E+00	4.8000E+00	4.224943E-11	2.060225E-11	1.425928E-11
154	4.6000E+00	4.7000E+00	4.161124E-11	2.046196E-11	1.390439E-11
155	4.5000E+00	4.6000E+00	4.109104E-11	2.032142E-11	1.362372E-11
156	4.4000E+00	4.5000E+00	4.044421E-11	2.016234E-11	1.339138E-11
157	4.3000E+00	4.4000E+00	3.944523E-11	1.998191E-11	1.307444E-11
158	4.2000E+00	4.3000E+00	3.834423E-11	1.979736E-11	1.270425E-11
159	4.1000E+00	4.2000E+00	3.731322E-11	1.960584E-11	1.240530E-11
160	4.0000E+00	4.1000E+00	3.635165E-11	1.940654E-11	1.217679E-11

Energy Bin #	Lower Energy Bound [MeV]	Upper Energy Bound [MeV]	Total Kerma [rad(GaAs)]	Displacement Kerma [rad(GaAs)]	Ionizing Kerma [rad(GaAs)]
161	3.9000E+00	4.0000E+00	3.547235E-11	1.919631E-11	1.189168E-11
162	3.8000E+00	3.9000E+00	3.460356E-11	1.897207E-11	1.148852E-11
163	3.7000E+00	3.8000E+00	3.379109E-11	1.872904E-11	1.114315E-11
164	3.6000E+00	3.7000E+00	3.311596E-11	1.846602E-11	1.093164E-11
165	3.5000E+00	3.6000E+00	3.236254E-11	1.819059E-11	1.066462E-11
166	3.4000E+00	3.5000E+00	3.124936E-11	1.787902E-11	1.021548E-11
167	3.3000E+00	3.4000E+00	2.992714E-11	1.751808E-11	9.766910E-12
168	3.2000E+00	3.3000E+00	2.881187E-11	1.713194E-11	9.538230E-12
169	3.1000E+00	3.2000E+00	2.775775E-11	1.673580E-11	9.324720E-12
170	3.0000E+00	3.1000E+00	2.647067E-11	1.633737E-11	8.837929E-12
171	2.9000E+00	3.0000E+00	2.686233E-11	1.586717E-11	8.371090E-12
172	2.8000E+00	2.9000E+00	2.735564E-11	1.534497E-11	8.098400E-12
173	2.7000E+00	2.8000E+00	2.592214E-11	1.483933E-11	7.859371E-12
174	2.6000E+00	2.7000E+00	2.324475E-11	1.434709E-11	7.386540E-12
175	2.5000E+00	2.6000E+00	2.176781E-11	1.382271E-11	6.981750E-12
176	2.4000E+00	2.5000E+00	2.044390E-11	1.331440E-11	6.642770E-12
177	2.3000E+00	2.4000E+00	1.961103E-11	1.281841E-11	6.417470E-12
178	2.2000E+00	2.3000E+00	1.866373E-11	1.232842E-11	6.049509E-12
179	2.1000E+00	2.2000E+00	1.774231E-11	1.185249E-11	5.694040E-12
180	2.0000E+00	2.1000E+00	1.695919E-11	1.138176E-11	5.470600E-12
181	1.9000E+00	2.0000E+00	1.619316E-11	1.092571E-11	5.220640E-12
182	1.8000E+00	1.9000E+00	1.544575E-11	1.049450E-11	4.927780E-12
183	1.7000E+00	1.8000E+00	1.471612E-11	1.007962E-11	4.628099E-12
184	1.6000E+00	1.7000E+00	1.421559E-11	9.716593E-12	4.489267E-12
185	1.5000E+00	1.6000E+00	1.355460E-11	9.369820E-12	4.183980E-12
186	1.4000E+00	1.5000E+00	1.313411E-11	9.075398E-12	4.051242E-12
187	1.3000E+00	1.4000E+00	1.261253E-11	8.823312E-12	3.789178E-12
188	1.2000E+00	1.3000E+00	1.230015E-11	8.592109E-12	3.708001E-12
189	1.1000E+00	1.2000E+00	1.185278E-11	8.344781E-12	3.507999E-12
190	1.0000E+00	1.1000E+00	1.146976E-11	8.139447E-12	3.330313E-12
191	9.6000E-01	1.0000E+00	1.117095E-11	7.988054E-12	3.182896E-12
192	9.2000E-01	9.6000E-01	1.103670E-11	7.888429E-12	3.148272E-12
193	8.8000E-01	9.2000E-01	1.085906E-11	7.790597E-12	3.068463E-12
194	8.4000E-01	8.8000E-01	1.072962E-11	7.681630E-12	3.047991E-12
195	8.0000E-01	8.4000E-01	1.052108E-11	7.568363E-12	2.952717E-12
196	7.6000E-01	8.0000E-01	1.028845E-11	7.444660E-12	2.843789E-12
197	7.2000E-01	7.6000E-01	1.012601E-11	7.314429E-12	2.811582E-12
198	6.9000E-01	7.2000E-01	9.921959E-12	7.199443E-12	2.722516E-12
199	6.6000E-01	6.9000E-01	9.745579E-12	7.097362E-12	2.648217E-12
200	6.3000E-01	6.6000E-01	9.593041E-12	6.989375E-12	2.603666E-12
201	6.0000E-01	6.3000E-01	9.400465E-12	6.871187E-12	2.529278E-12

Energy Bin #	Lower Energy Bound [MeV]	Upper Energy Bound [MeV]	Total Kerma [rad(GaAs)]	Displacement Kerma [rad(GaAs)]	Ionizing Kerma [rad(GaAs)]
202	5.7500E-01	6.0000E-01	9.210951E-12	6.750533E-12	2.460418E-12
203	5.5000E-01	5.7500E-01	9.056942E-12	6.641562E-12	2.415380E-12
204	5.2500E-01	5.5000E-01	8.878643E-12	6.531387E-12	2.347256E-12
205	5.0000E-01	5.2500E-01	8.679716E-12	6.413348E-12	2.266368E-12
206	4.7500E-01	5.0000E-01	8.482133E-12	6.280732E-12	2.201401E-12
207	4.5000E-01	4.7500E-01	8.290649E-12	6.139895E-12	2.150754E-12
208	4.2500E-01	4.5000E-01	8.054310E-12	5.987546E-12	2.066764E-12
209	4.0000E-01	4.2500E-01	7.815918E-12	5.829741E-12	1.986177E-12
210	3.8000E-01	4.0000E-01	7.572198E-12	5.668096E-12	1.904102E-12
211	3.6000E-01	3.8000E-01	7.356152E-12	5.512666E-12	1.843486E-12
212	3.4000E-01	3.6000E-01	7.136238E-12	5.355556E-12	1.780682E-12
213	3.2000E-01	3.4000E-01	6.891243E-12	5.186607E-12	1.704636E-12
214	3.0000E-01	3.2000E-01	6.639485E-12	5.015059E-12	1.624426E-12
215	2.8000E-01	3.0000E-01	6.382388E-12	4.839637E-12	1.542751E-12
216	2.7000E-01	2.8000E-01	6.182505E-12	4.697545E-12	1.484960E-12
217	2.5500E-01	2.7000E-01	5.995898E-12	4.566125E-12	1.429773E-12
218	2.4000E-01	2.5500E-01	5.759317E-12	4.398377E-12	1.360940E-12
219	2.3000E-01	2.4000E-01	5.551998E-12	4.249138E-12	1.302860E-12
220	2.2000E-01	2.3000E-01	5.385594E-12	4.129148E-12	1.256446E-12
221	2.1000E-01	2.2000E-01	5.219232E-12	4.009157E-12	1.210075E-12
222	2.0000E-01	2.1000E-01	5.052788E-12	3.889127E-12	1.163661E-12
223	1.9000E-01	2.0000E-01	4.874888E-12	3.759867E-12	1.115021E-12
224	1.8000E-01	1.9000E-01	4.687798E-12	3.622950E-12	1.064848E-12
225	1.7000E-01	1.8000E-01	4.500708E-12	3.486007E-12	1.014701E-12
226	1.6000E-01	1.7000E-01	4.313646E-12	3.349065E-12	9.645808E-13
227	1.5000E-01	1.6000E-01	4.126555E-12	3.212148E-12	9.144070E-13
228	1.4250E-01	1.5000E-01	3.952634E-12	3.083731E-12	8.689028E-13
229	1.3500E-01	1.4250E-01	3.791985E-12	2.964131E-12	8.278541E-13
230	1.2750E-01	1.3500E-01	3.631269E-12	2.844413E-12	7.868558E-13
231	1.2000E-01	1.2750E-01	3.467600E-12	2.722183E-12	7.454170E-13
232	1.1500E-01	1.2000E-01	3.330071E-12	2.619383E-12	7.106880E-13
233	1.1000E-01	1.1500E-01	3.220202E-12	2.537253E-12	6.829491E-13
234	1.0500E-01	1.1000E-01	3.110279E-12	2.455059E-12	6.552200E-13
235	1.0000E-01	1.0500E-01	3.000450E-12	2.372904E-12	6.275460E-13
236	9.6000E-02	1.0000E-01	2.782009E-12	2.203729E-12	5.782800E-13
237	9.2000E-02	9.6000E-02	2.693735E-12	2.137060E-12	5.566749E-13
238	8.8000E-02	9.2000E-02	2.604966E-12	2.069857E-12	5.351088E-13
239	8.4000E-02	8.8000E-02	2.513237E-12	2.000320E-12	5.129170E-13
240	8.0000E-02	8.4000E-02	2.421188E-12	1.930316E-12	4.908721E-13
241	7.6000E-02	8.0000E-02	2.327245E-12	1.858698E-12	4.685469E-13
242	7.2000E-02	7.6000E-02	2.231382E-12	1.785454E-12	4.459280E-13

Energy Bin #	Lower Energy Bound [MeV]	Upper Energy Bound [MeV]	Total Kerma [rad(GaAs)]	Displacement Kerma [rad(GaAs)]	Ionizing Kerma [rad(GaAs)]
243	6.9000E-02	7.2000E-02	2.146921E-12	1.720853E-12	4.260681E-13
244	6.6000E-02	6.9000E-02	2.072079E-12	1.663293E-12	4.087861E-13
245	6.3000E-02	6.6000E-02	1.996513E-12	1.605120E-12	3.913930E-13
246	6.0000E-02	6.3000E-02	1.920590E-12	1.546720E-12	3.738700E-13
247	5.7500E-02	6.0000E-02	1.851867E-12	1.493654E-12	3.582129E-13
248	5.5000E-02	5.7500E-02	1.790226E-12	1.446070E-12	3.441559E-13
249	5.2500E-02	5.5000E-02	1.728344E-12	1.398192E-12	3.301520E-13
250	5.0000E-02	5.2500E-02	1.666169E-12	1.350060E-12	3.161090E-13
251	4.7500E-02	5.0000E-02	1.601995E-12	1.300207E-12	3.017880E-13
252	4.5000E-02	4.7500E-02	1.535859E-12	1.248617E-12	2.872420E-13
253	4.2500E-02	4.5000E-02	1.469365E-12	1.196724E-12	2.726410E-13
254	4.0000E-02	4.2500E-02	1.402536E-12	1.144491E-12	2.580450E-13
255	3.8000E-02	4.0000E-02	1.340822E-12	1.096094E-12	2.447280E-13
256	3.6000E-02	3.8000E-02	1.284114E-12	1.051422E-12	2.326920E-13
257	3.4000E-02	3.6000E-02	1.227128E-12	1.006483E-12	2.206450E-13
258	3.2000E-02	3.4000E-02	1.169917E-12	9.613333E-13	2.085837E-13
259	3.0000E-02	3.2000E-02	1.112386E-12	9.158785E-13	1.965075E-13
260	2.8000E-02	3.0000E-02	1.054515E-12	8.699954E-13	1.845196E-13
261	2.7000E-02	2.8000E-02	1.011099E-12	8.354468E-13	1.756522E-13
262	2.5500E-02	2.7000E-02	9.744156E-13	8.062273E-13	1.681883E-13
263	2.4000E-02	2.5500E-02	9.303836E-13	7.711226E-13	1.592610E-13
264	2.3000E-02	2.4000E-02	8.937958E-13	7.419391E-13	1.518567E-13
265	2.2000E-02	2.3000E-02	8.642949E-13	7.183834E-13	1.459115E-13
266	2.1000E-02	2.2000E-02	8.346644E-13	6.947184E-13	1.399460E-13
267	2.0000E-02	2.1000E-02	8.049009E-13	6.709093E-13	1.339916E-13
268	1.9000E-02	2.0000E-02	7.743757E-13	6.463697E-13	1.280060E-13
269	1.8000E-02	1.9000E-02	7.431282E-13	6.211313E-13	1.219969E-13
270	1.7000E-02	1.8000E-02	7.116977E-13	5.957197E-13	1.159780E-13
271	1.6000E-02	1.7000E-02	6.801833E-13	5.702212E-13	1.099621E-13
272	1.5000E-02	1.6000E-02	6.485224E-13	5.445960E-13	1.039264E-13
273	1.4250E-02	1.5000E-02	6.207888E-13	5.221128E-13	9.867600E-14
274	1.3500E-02	1.4250E-02	5.969105E-13	5.027451E-13	9.416540E-14
275	1.2750E-02	1.3500E-02	5.729044E-13	4.832598E-13	8.964460E-14
276	1.2000E-02	1.2750E-02	5.487822E-13	4.636719E-13	8.511030E-14
277	1.1500E-02	1.2000E-02	5.287408E-13	4.473793E-13	8.136149E-14
278	1.1000E-02	1.1500E-02	5.125734E-13	4.342380E-13	7.833537E-14
279	1.0500E-02	1.1000E-02	4.963528E-13	4.210234E-13	7.532939E-14
280	1.0000E-02	1.0500E-02	4.800562E-13	4.077593E-13	7.229690E-14
281	9.6000E-03	1.0000E-02	4.837135E-13	4.114299E-13	7.228360E-14
282	9.2000E-03	9.6000E-03	5.196113E-13	4.424786E-13	7.713272E-14
283	8.8000E-03	9.2000E-03	5.465139E-13	4.659204E-13	8.059352E-14

Energy Bin #	Lower Energy Bound [MeV]	Upper Energy Bound [MeV]	Total Kerma [rad(GaAs)]	Displacement Kerma [rad(GaAs)]	Ionizing Kerma [rad(GaAs)]
284	8.4000E-03	8.8000E-03	3.965638E-13	3.383140E-13	5.824979E-14
285	8.0000E-03	8.4000E-03	4.929491E-13	4.211574E-13	7.179169E-14
286	7.6000E-03	8.0000E-03	3.907542E-13	3.342420E-13	5.651220E-14
287	7.2000E-03	7.6000E-03	3.479958E-13	2.979155E-13	5.008030E-14
288	6.9000E-03	7.2000E-03	3.805452E-13	3.262893E-13	5.425592E-14
289	6.6000E-03	6.9000E-03	2.693176E-13	2.309493E-13	3.836832E-14
290	6.3000E-03	6.6000E-03	4.640977E-13	3.988964E-13	6.520126E-14
291	6.0000E-03	6.3000E-03	3.578616E-13	3.078682E-13	4.999340E-14
292	5.7500E-03	6.0000E-03	3.347460E-13	2.882746E-13	4.647140E-14
293	5.5000E-03	5.7500E-03	4.642101E-13	4.002873E-13	6.392280E-14
294	5.2500E-03	5.5000E-03	2.162669E-13	1.864406E-13	2.982631E-14
295	5.0000E-03	5.2500E-03	4.058550E-13	3.505886E-13	5.526642E-14
296	4.7500E-03	5.0000E-03	5.065022E-13	4.375859E-13	6.891628E-14
297	4.5000E-03	4.7500E-03	2.253455E-13	1.952038E-13	3.014170E-14
298	4.2500E-03	4.5000E-03	1.935530E-13	1.677622E-13	2.579081E-14
299	4.0000E-03	4.2500E-03	1.576383E-13	1.367477E-13	2.089061E-14
300	3.8000E-03	4.0000E-03	2.910085E-13	2.528880E-13	3.812052E-14
301	3.6000E-03	3.8000E-03	2.217641E-13	1.928246E-13	2.893950E-14
302	3.4000E-03	3.6000E-03	6.190459E-13	5.381587E-13	8.088717E-14
303	3.2000E-03	3.4000E-03	9.109086E-14	7.936597E-14	1.172489E-14
304	3.0000E-03	3.2000E-03	1.283413E-13	1.119279E-13	1.641339E-14
305	2.8000E-03	3.0000E-03	1.333894E-13	1.165407E-13	1.684869E-14
306	2.7000E-03	2.8000E-03	2.848186E-13	2.491276E-13	3.569101E-14
307	2.5500E-03	2.7000E-03	1.443789E-13	1.262369E-13	1.814200E-14
308	2.4000E-03	2.5500E-03	2.746325E-13	2.401973E-13	3.443521E-14
309	2.3000E-03	2.4000E-03	7.190150E-14	6.296585E-14	8.935655E-15
310	2.2000E-03	2.3000E-03	4.516065E-14	3.960809E-14	5.552558E-15
311	2.1000E-03	2.2000E-03	4.585943E-14	4.029915E-14	5.560280E-15
312	2.0000E-03	2.1000E-03	7.147657E-14	6.268116E-14	8.795407E-15
313	1.9000E-03	2.0000E-03	2.238946E-13	1.968876E-13	2.700700E-14
314	1.8000E-03	1.9000E-03	1.948912E-13	1.708873E-13	2.400390E-14
315	1.7000E-03	1.8000E-03	5.161424E-14	4.550440E-14	6.109842E-15
316	1.6000E-03	1.7000E-03	3.239137E-13	2.848907E-13	3.902298E-14
317	1.5000E-03	1.6000E-03	1.837297E-13	1.618471E-13	2.188260E-14
318	1.4250E-03	1.5000E-03	1.890393E-13	1.657645E-13	2.327480E-14
319	1.3500E-03	1.4250E-03	1.113800E-13	9.761362E-14	1.376638E-14
320	1.2750E-03	1.3500E-03	1.938963E-13	1.708160E-13	2.308031E-14
321	1.2000E-03	1.2750E-03	2.261393E-14	2.003530E-14	2.578629E-15
322	1.1500E-03	1.2000E-03	2.218068E-14	1.972332E-14	2.457359E-15
323	1.1000E-03	1.1500E-03	7.550250E-14	6.604204E-14	9.460457E-15
324	1.0500E-03	1.1000E-03	2.420215E-14	2.153497E-14	2.667180E-15

Energy Bin #	Lower Energy Bound [MeV]	Upper Energy Bound [MeV]	Total Kerma [rad(GaAs)]	Displacement Kerma [rad(GaAs)]	Ionizing Kerma [rad(GaAs)]
325	1.0000E-03	1.0500E-03	2.374261E-14	2.116888E-14	2.573730E-15
326	9.6000E-04	1.0000E-03	2.600945E-14	2.319937E-14	2.810079E-15
327	9.2000E-04	9.6000E-04	3.021384E-13	2.648418E-13	3.729658E-14
328	8.8000E-04	9.2000E-04	1.046737E-13	9.133957E-14	1.333413E-14
329	8.4000E-04	8.8000E-04	2.685398E-14	2.384980E-14	3.004180E-15
330	8.0000E-04	8.4000E-04	2.475667E-14	2.212904E-14	2.627630E-15
331	7.6000E-04	8.0000E-04	3.499349E-14	3.122258E-14	3.770909E-15
332	7.2000E-04	7.6000E-04	8.007631E-13	7.023205E-13	9.844258E-14
333	6.9000E-04	7.2000E-04	3.895521E-13	3.426164E-13	4.693571E-14
334	6.6000E-04	6.9000E-04	3.197135E-13	2.789401E-13	4.077340E-14
335	6.3000E-04	6.6000E-04	1.882234E-14	1.669664E-14	2.125699E-15
336	6.0000E-04	6.3000E-04	2.326058E-14	2.066746E-14	2.593120E-15
337	5.7500E-04	6.0000E-04	2.191336E-14	1.960651E-14	2.306850E-15
338	5.5000E-04	5.7500E-04	4.116481E-14	3.666608E-14	4.498728E-15
339	5.2500E-04	5.5000E-04	1.098279E-12	9.671966E-13	1.310824E-13
340	5.0000E-04	5.2500E-04	5.195255E-14	4.568693E-14	6.265618E-15
341	4.7500E-04	5.0000E-04	2.881690E-13	2.501547E-13	3.801432E-14
342	4.5000E-04	4.7500E-04	2.159492E-13	1.880459E-13	2.790331E-14
343	4.2500E-04	4.5000E-04	1.499140E-14	1.343493E-14	1.556470E-15
344	4.0000E-04	4.2500E-04	1.776592E-14	1.596223E-14	1.803691E-15
345	3.8000E-04	4.0000E-04	5.315609E-14	4.753711E-14	5.618983E-15
346	3.6000E-04	3.8000E-04	3.126983E-13	2.782406E-13	3.445771E-14
347	3.4000E-04	3.6000E-04	3.120495E-14	2.772433E-14	3.480621E-15
348	3.2000E-04	3.4000E-04	1.218800E-12	1.060126E-12	1.586740E-13
349	3.0000E-04	3.2000E-04	1.058694E-12	9.206293E-13	1.380647E-13
350	2.8000E-04	3.0000E-04	7.683748E-13	6.864903E-13	8.188448E-14
351	2.7000E-04	2.8000E-04	1.153476E-13	1.027447E-13	1.260291E-14
352	2.5500E-04	2.7000E-04	3.480371E-14	3.076346E-14	4.040249E-15
353	2.4000E-04	2.5500E-04	3.872773E-13	3.356992E-13	5.157810E-14
354	2.3000E-04	2.4000E-04	9.237183E-15	8.203704E-15	1.033479E-15
355	2.2000E-04	2.3000E-04	7.349421E-15	6.550817E-15	7.986043E-16
356	2.1000E-04	2.2000E-04	6.400209E-15	5.719385E-15	6.808239E-16
357	2.0000E-04	2.1000E-04	5.817636E-15	5.209271E-15	6.083653E-16
358	1.9000E-04	2.0000E-04	5.422544E-15	4.863381E-15	5.591629E-16
359	1.8000E-04	1.9000E-04	5.139753E-15	4.615347E-15	5.244061E-16
360	1.7000E-04	1.8000E-04	4.935464E-15	4.435693E-15	4.997710E-16
361	1.6000E-04	1.7000E-04	4.800403E-15	4.316018E-15	4.843851E-16
362	1.5000E-04	1.6000E-04	4.750464E-15	4.270033E-15	4.804312E-16
363	1.4250E-04	1.5000E-04	4.820930E-15	4.329084E-15	4.918458E-16
364	1.3500E-04	1.4250E-04	5.072696E-15	4.546221E-15	5.264750E-16
365	1.2750E-04	1.3500E-04	5.791967E-15	5.170337E-15	6.216299E-16

Energy Bin #	Lower Energy Bound [MeV]	Upper Energy Bound [MeV]	Total Kerma [rad(GaAs)]	Displacement Kerma [rad(GaAs)]	Ionizing Kerma [rad(GaAs)]
366	1.2000E-04	1.2750E-04	8.397685E-15	7.437012E-15	9.606734E-16
367	1.1500E-04	1.2000E-04	2.075249E-14	1.818602E-14	2.566471E-15
368	1.1000E-04	1.1500E-04	1.900309E-12	1.652623E-12	2.476859E-13
369	1.0500E-04	1.1000E-04	1.627162E-13	1.415866E-13	2.112960E-14
370	1.0000E-04	1.0500E-04	2.294266E-14	2.010022E-14	2.842439E-15
371	9.6000E-05	1.0000E-04	3.621546E-13	3.174420E-13	4.471258E-14
372	9.2000E-05	9.6000E-05	2.188858E-12	1.907932E-12	2.809261E-13
373	8.8000E-05	9.2000E-05	1.946823E-13	1.687819E-13	2.590040E-14
374	8.4000E-05	8.8000E-05	1.386332E-14	1.214186E-14	1.721460E-15
375	8.0000E-05	8.4000E-05	8.340598E-15	7.342100E-15	9.984977E-16
376	7.6000E-05	8.0000E-05	6.696495E-15	5.909922E-15	7.865730E-16
377	7.2000E-05	7.6000E-05	6.131194E-15	5.414854E-15	7.163400E-16
378	6.9000E-05	7.2000E-05	6.105063E-15	5.388356E-15	7.167068E-16
379	6.6000E-05	6.9000E-05	6.420218E-15	5.658294E-15	7.619239E-16
380	6.3000E-05	6.6000E-05	7.151137E-15	6.288670E-15	8.624667E-16
381	6.0000E-05	6.3000E-05	8.607331E-15	7.547265E-15	1.060066E-15
382	5.7500E-05	6.0000E-05	1.121044E-14	9.799695E-15	1.410745E-15
383	5.5000E-05	5.7500E-05	1.614635E-14	1.407248E-14	2.073870E-15
384	5.2500E-05	5.5000E-05	2.813745E-14	2.445651E-14	3.680941E-15
385	5.0000E-05	5.2500E-05	7.117680E-14	6.173087E-14	9.445935E-15
386	4.7500E-05	5.0000E-05	8.925622E-13	7.730786E-13	1.194836E-13
387	4.5000E-05	4.7500E-05	8.535676E-12	7.391228E-12	1.144447E-12
388	4.2500E-05	4.5000E-05	1.352056E-13	1.171318E-13	1.807380E-14
389	4.0000E-05	4.2500E-05	4.181928E-14	3.627178E-14	5.547500E-15
390	3.8000E-05	4.0000E-05	2.303751E-14	2.000801E-14	3.029501E-15
391	3.6000E-05	3.8000E-05	1.611272E-14	1.401094E-14	2.101780E-15
392	3.4000E-05	3.6000E-05	1.236159E-14	1.076112E-14	1.600470E-15
393	3.2000E-05	3.4000E-05	1.009636E-14	8.798671E-15	1.297689E-15
394	3.0000E-05	3.2000E-05	8.629551E-15	7.526177E-15	1.103374E-15
395	2.8000E-05	3.0000E-05	7.633223E-15	6.661547E-15	9.716760E-16
396	2.7000E-05	2.8000E-05	7.085520E-15	6.185770E-15	8.997502E-16
397	2.5500E-05	2.7000E-05	6.727940E-15	5.874855E-15	8.530850E-16
398	2.4000E-05	2.5500E-05	6.386749E-15	5.577850E-15	8.088991E-16
399	2.3000E-05	2.4000E-05	6.162185E-15	5.382055E-15	7.801300E-16
400	2.2000E-05	2.3000E-05	6.015775E-15	5.254184E-15	7.615910E-16
401	2.1000E-05	2.2000E-05	5.892594E-15	5.146397E-15	7.461971E-16
402	2.0000E-05	2.1000E-05	5.796647E-15	5.062252E-15	7.343949E-16
403	1.9000E-05	2.0000E-05	5.720661E-15	4.995339E-15	7.253219E-16
404	1.8000E-05	1.9000E-05	5.664079E-15	4.945295E-15	7.187837E-16
405	1.7000E-05	1.8000E-05	5.627100E-15	4.912144E-15	7.149559E-16
406	1.6000E-05	1.7000E-05	5.609709E-15	4.895863E-15	7.138459E-16

Energy Bin #	Lower Energy Bound [MeV]	Upper Energy Bound [MeV]	Total Kerma [rad(GaAs)]	Displacement Kerma [rad(GaAs)]	Ionizing Kerma [rad(GaAs)]
407	1.5000E-05	1.6000E-05	5.612145E-15	4.896930E-15	7.152151E-16
408	1.4250E-05	1.5000E-05	5.628281E-15	4.909961E-15	7.183199E-16
409	1.3500E-05	1.4250E-05	5.657701E-15	4.934661E-15	7.230400E-16
410	1.2750E-05	1.3500E-05	5.699613E-15	4.970098E-15	7.295152E-16
411	1.2000E-05	1.2750E-05	5.753233E-15	5.015759E-15	7.374739E-16
412	1.1500E-05	1.2000E-05	5.810416E-15	5.064558E-15	7.458582E-16
413	1.1000E-05	1.1500E-05	5.863992E-15	5.110481E-15	7.535112E-16
414	1.0500E-05	1.1000E-05	5.926339E-15	5.164042E-15	7.622970E-16
415	1.0000E-05	1.0500E-05	5.997900E-15	5.225550E-15	7.723501E-16
416	9.6000E-06	1.0000E-05	6.070262E-15	5.287740E-15	7.825221E-16
417	9.2000E-06	9.6000E-06	6.141425E-15	5.348983E-15	7.924421E-16
418	8.8000E-06	9.2000E-06	6.221402E-15	5.417893E-15	8.035090E-16
419	8.4000E-06	8.8000E-06	6.307537E-15	5.492125E-15	8.154119E-16
420	8.0000E-06	8.4000E-06	6.404740E-15	5.576007E-15	8.287332E-16
421	7.6000E-06	8.0000E-06	6.512396E-15	5.668904E-15	8.434919E-16
422	7.2000E-06	7.6000E-06	6.631358E-15	5.771708E-15	8.596499E-16
423	6.9000E-06	7.2000E-06	6.746309E-15	5.870979E-15	8.753302E-16
424	6.6000E-06	6.9000E-06	6.853353E-15	5.963517E-15	8.898361E-16
425	6.3000E-06	6.6000E-06	6.970957E-15	6.065255E-15	9.057023E-16
426	6.0000E-06	6.3000E-06	7.096443E-15	6.173740E-15	9.227031E-16
427	5.7500E-06	6.0000E-06	7.224649E-15	6.284733E-15	9.399160E-16
428	5.5000E-06	5.7500E-06	7.345439E-15	6.389164E-15	9.562752E-16
429	5.2500E-06	5.5000E-06	7.479283E-15	6.505130E-15	9.741531E-16
430	5.0000E-06	5.2500E-06	7.625035E-15	6.631334E-15	9.937005E-16
431	4.7500E-06	5.0000E-06	7.784146E-15	6.769099E-15	1.015047E-15
432	4.5000E-06	4.7500E-06	7.955696E-15	6.917704E-15	1.037992E-15
433	4.2500E-06	4.5000E-06	8.145701E-15	7.082307E-15	1.063394E-15
434	4.0000E-06	4.2500E-06	8.353930E-15	7.262763E-15	1.091167E-15
435	3.8000E-06	4.0000E-06	8.556573E-15	7.438449E-15	1.118123E-15
436	3.6000E-06	3.8000E-06	8.759739E-15	7.614545E-15	1.145194E-15
437	3.4000E-06	3.6000E-06	8.972368E-15	7.798843E-15	1.173524E-15
438	3.2000E-06	3.4000E-06	9.209650E-15	8.004620E-15	1.205031E-15
439	3.0000E-06	3.2000E-06	9.472359E-15	8.232528E-15	1.239831E-15
440	2.8000E-06	3.0000E-06	9.763159E-15	8.484716E-15	1.278443E-15
441	2.7000E-06	2.8000E-06	9.998790E-15	8.689121E-15	1.309670E-15
442	2.5500E-06	2.7000E-06	1.021661E-14	8.878139E-15	1.338470E-15
443	2.4000E-06	2.5500E-06	1.049885E-14	9.122795E-15	1.376055E-15
444	2.3000E-06	2.4000E-06	1.075144E-14	9.342104E-15	1.409336E-15
445	2.2000E-06	2.3000E-06	1.097347E-14	9.534777E-15	1.438693E-15
446	2.1000E-06	2.2000E-06	1.120885E-14	9.738834E-15	1.470016E-15
447	2.0000E-06	2.1000E-06	1.146312E-14	9.959732E-15	1.503388E-15

Energy Bin #	Lower Energy Bound [MeV]	Upper Energy Bound [MeV]	Total Kerma [rad(GaAs)]	Displacement Kerma [rad(GaAs)]	Ionizing Kerma [rad(GaAs)]
448	1.9000E-06	2.0000E-06	1.173402E-14	1.019507E-14	1.538950E-15
449	1.8000E-06	1.9000E-06	1.202977E-14	1.045170E-14	1.578071E-15
450	1.7000E-06	1.8000E-06	1.235068E-14	1.073045E-14	1.620230E-15
451	1.6000E-06	1.7000E-06	1.270165E-14	1.103449E-14	1.667161E-15
452	1.5000E-06	1.6000E-06	1.308868E-14	1.137041E-14	1.718270E-15
453	1.4250E-06	1.5000E-06	1.345728E-14	1.169066E-14	1.766620E-15
454	1.3500E-06	1.4250E-06	1.380044E-14	1.198876E-14	1.811680E-15
455	1.2750E-06	1.3500E-06	1.418012E-14	1.231832E-14	1.861800E-15
456	1.2000E-06	1.2750E-06	1.458146E-14	1.266662E-14	1.914841E-15
457	1.1500E-06	1.2000E-06	1.494927E-14	1.298628E-14	1.962990E-15
458	1.1000E-06	1.1500E-06	1.526815E-14	1.326326E-14	2.004890E-15
459	1.0500E-06	1.1000E-06	1.560908E-14	1.355924E-14	2.049841E-15
460	1.0000E-06	1.0500E-06	1.597673E-14	1.387795E-14	2.098781E-15
461	9.6000E-07	1.0000E-06	1.632982E-14	1.418470E-14	2.145119E-15
462	9.2000E-07	9.6000E-07	1.666328E-14	1.447432E-14	2.188960E-15
463	8.8000E-07	9.2000E-07	1.702315E-14	1.478662E-14	2.236530E-15
464	8.4000E-07	8.8000E-07	1.740421E-14	1.511729E-14	2.286920E-15
465	8.0000E-07	8.4000E-07	1.781234E-14	1.547240E-14	2.339940E-15
466	7.6000E-07	8.0000E-07	1.825873E-14	1.585950E-14	2.399231E-15
467	7.2000E-07	7.6000E-07	1.873435E-14	1.627221E-14	2.462140E-15
468	6.9000E-07	7.2000E-07	1.918594E-14	1.666439E-14	2.521549E-15
469	6.6000E-07	6.9000E-07	1.959997E-14	1.702439E-14	2.575580E-15
470	6.3000E-07	6.6000E-07	2.004719E-14	1.741255E-14	2.634640E-15
471	6.0000E-07	6.3000E-07	2.051334E-14	1.781736E-14	2.695981E-15
472	5.7500E-07	6.0000E-07	2.097930E-14	1.822288E-14	2.756420E-15
473	5.5000E-07	5.7500E-07	2.143450E-14	1.861725E-14	2.817250E-15
474	5.2500E-07	5.5000E-07	2.192125E-14	1.904064E-14	2.880610E-15
475	5.0000E-07	5.2500E-07	2.244424E-14	1.949445E-14	2.949791E-15
476	4.7500E-07	5.0000E-07	2.300895E-14	1.998451E-14	3.024440E-15
477	4.5000E-07	4.7500E-07	2.360986E-14	2.050679E-14	3.103070E-15
478	4.2500E-07	4.5000E-07	2.426569E-14	2.107619E-14	3.189499E-15
479	4.0000E-07	4.2500E-07	2.498275E-14	2.169886E-14	3.283891E-15
480	3.8000E-07	4.0000E-07	2.568136E-14	2.230627E-14	3.375089E-15
481	3.6000E-07	3.8000E-07	2.636095E-14	2.289542E-14	3.465529E-15
482	3.4000E-07	3.6000E-07	2.709785E-14	2.353530E-14	3.562549E-15
483	3.2000E-07	3.4000E-07	2.790117E-14	2.423366E-14	3.667510E-15
484	3.0000E-07	3.2000E-07	2.878220E-14	2.499853E-14	3.783669E-15
485	2.8000E-07	3.0000E-07	2.975243E-14	2.584124E-14	3.911188E-15
486	2.7000E-07	2.8000E-07	3.053975E-14	2.652508E-14	4.014669E-15
487	2.5500E-07	2.7000E-07	3.125839E-14	2.714946E-14	4.108930E-15
488	2.4000E-07	2.5500E-07	3.218796E-14	2.795650E-14	4.231460E-15

Energy Bin #	Lower Energy Bound [MeV]	Upper Energy Bound [MeV]	Total Kerma [rad(GaAs)]	Displacement Kerma [rad(GaAs)]	Ionizing Kerma [rad(GaAs)]
489	2.3000E-07	2.4000E-07	3.302407E-14	2.868275E-14	4.341318E-15
490	2.2000E-07	2.3000E-07	3.374697E-14	2.931098E-14	4.435993E-15
491	2.1000E-07	2.2000E-07	3.452003E-14	2.998150E-14	4.538531E-15
492	2.0000E-07	2.1000E-07	3.534734E-14	3.070079E-14	4.646548E-15
493	1.9000E-07	2.0000E-07	3.623704E-14	3.147357E-14	4.763469E-15
494	1.8000E-07	1.9000E-07	3.719982E-14	3.230915E-14	4.890670E-15
495	1.7000E-07	1.8000E-07	3.824524E-14	3.321750E-14	5.027737E-15
496	1.6000E-07	1.7000E-07	3.938348E-14	3.420588E-14	5.177601E-15
497	1.5000E-07	1.6000E-07	4.063264E-14	3.529023E-14	5.342413E-15
498	1.4250E-07	1.5000E-07	4.182167E-14	3.632327E-14	5.498399E-15
499	1.3500E-07	1.4250E-07	4.293323E-14	3.728897E-14	5.644262E-15
500	1.2750E-07	1.3500E-07	4.413627E-14	3.833360E-14	5.802670E-15
501	1.2000E-07	1.2750E-07	4.545089E-14	3.947596E-14	5.974930E-15
502	1.1500E-07	1.2000E-07	4.663431E-14	4.050379E-14	6.130520E-15
503	1.1000E-07	1.1500E-07	4.765803E-14	4.139295E-14	6.265083E-15
504	1.0500E-07	1.1000E-07	4.875132E-14	4.234266E-14	6.408661E-15
505	1.0000E-07	1.0500E-07	4.992569E-14	4.336236E-14	6.563330E-15
506	9.6000E-08	1.0000E-07	5.106099E-14	4.434846E-14	6.712529E-15
507	9.2000E-08	9.6000E-08	5.213575E-14	4.528122E-14	6.854529E-15
508	8.8000E-08	9.2000E-08	5.327985E-14	4.627519E-14	7.004661E-15
509	8.4000E-08	8.8000E-08	5.450274E-14	4.733715E-14	7.165590E-15
510	8.0000E-08	8.4000E-08	5.581605E-14	4.847818E-14	7.337870E-15
511	7.6000E-08	8.0000E-08	5.722866E-14	4.970507E-14	7.523594E-15
512	7.2000E-08	7.6000E-08	5.875261E-14	5.102929E-14	7.723321E-15
513	6.9000E-08	7.2000E-08	6.018418E-14	5.227151E-14	7.912667E-15
514	6.6000E-08	6.9000E-08	6.149880E-14	5.341348E-14	8.085319E-15
515	6.3000E-08	6.6000E-08	6.291050E-14	5.464009E-14	8.270409E-15
516	6.0000E-08	6.3000E-08	6.442497E-14	5.595551E-14	8.469455E-15
517	5.7500E-08	6.0000E-08	6.590919E-14	5.724454E-14	8.664652E-15
518	5.5000E-08	5.7500E-08	6.735729E-14	5.850210E-14	8.855194E-15
519	5.2500E-08	5.5000E-08	6.890471E-14	5.984511E-14	9.059600E-15
520	5.0000E-08	5.2500E-08	7.056465E-14	6.128747E-14	9.277179E-15
521	4.7500E-08	5.0000E-08	7.235234E-14	6.284033E-14	9.512011E-15
522	4.5000E-08	4.7500E-08	7.428375E-14	6.451789E-14	9.765863E-15
523	4.2500E-08	4.5000E-08	7.637541E-14	6.633461E-14	1.004080E-14
524	4.0000E-08	4.2500E-08	7.864761E-14	6.830829E-14	1.033932E-14
525	3.8000E-08	4.0000E-08	8.087795E-14	7.024515E-14	1.063280E-14
526	3.6000E-08	3.8000E-08	8.303402E-14	7.211722E-14	1.091680E-14
527	3.4000E-08	3.6000E-08	8.537261E-14	7.414847E-14	1.122414E-14
528	3.2000E-08	3.4000E-08	8.792161E-14	7.636254E-14	1.155907E-14
529	3.0000E-08	3.2000E-08	9.071297E-14	7.878737E-14	1.192560E-14

Energy Bin #	Lower Energy Bound [MeV]	Upper Energy Bound [MeV]	Total Kerma [rad(GaAs)]	Displacement Kerma [rad(GaAs)]	Ionizing Kerma [rad(GaAs)]
530	2.8000E-08	3.0000E-08	9.378795E-14	8.145755E-14	1.233039E-14
531	2.7000E-08	2.8000E-08	9.629680E-14	8.363681E-14	1.265998E-14
532	2.5500E-08	2.7000E-08	9.857008E-14	8.561142E-14	1.295866E-14
533	2.4000E-08	2.5500E-08	1.015037E-13	8.815905E-14	1.334465E-14
534	2.3000E-08	2.4000E-08	1.041634E-13	9.046710E-14	1.369630E-14
535	2.2000E-08	2.3000E-08	1.064489E-13	9.245504E-14	1.399386E-14
536	2.1000E-08	2.2000E-08	1.088976E-13	9.458030E-14	1.431730E-14
537	2.0000E-08	2.1000E-08	1.115227E-13	9.685968E-14	1.466302E-14
538	1.9000E-08	2.0000E-08	1.143457E-13	9.931160E-14	1.503410E-14
539	1.8000E-08	1.9000E-08	1.173963E-13	1.019596E-13	1.543670E-14
540	1.7000E-08	1.8000E-08	1.207002E-13	1.048362E-13	1.586401E-14
541	1.6000E-08	1.7000E-08	1.243014E-13	1.079612E-13	1.634019E-14
542	1.5000E-08	1.6000E-08	1.282540E-13	1.113941E-13	1.685990E-14
543	1.4250E-08	1.5000E-08	1.320306E-13	1.146737E-13	1.735690E-14
544	1.3500E-08	1.4250E-08	1.355507E-13	1.177264E-13	1.782430E-14
545	1.2750E-08	1.3500E-08	1.393571E-13	1.210354E-13	1.832170E-14
546	1.2000E-08	1.2750E-08	1.435205E-13	1.246484E-13	1.887210E-14
547	1.1500E-08	1.2000E-08	1.472787E-13	1.279170E-13	1.936170E-14
548	1.1000E-08	1.1500E-08	1.505173E-13	1.307284E-13	1.978890E-14
549	1.0500E-08	1.1000E-08	1.539796E-13	1.337353E-13	2.024430E-14
550	1.0000E-08	1.0500E-08	1.576885E-13	1.369617E-13	2.072680E-14
551	9.6000E-09	1.0000E-08	1.612670E-13	1.400654E-13	2.120160E-14
552	9.2000E-09	9.6000E-09	1.646628E-13	1.430193E-13	2.164349E-14
553	8.8000E-09	9.2000E-09	1.682848E-13	1.461634E-13	2.212141E-14
554	8.4000E-09	8.8000E-09	1.721538E-13	1.495176E-13	2.263619E-14
555	8.0000E-09	8.4000E-09	1.763067E-13	1.531275E-13	2.317920E-14
556	7.6000E-09	8.0000E-09	1.807696E-13	1.570032E-13	2.376640E-14
557	7.2000E-09	7.6000E-09	1.855935E-13	1.611887E-13	2.440479E-14
558	6.9000E-09	7.2000E-09	1.901424E-13	1.651426E-13	2.499980E-14
559	6.6000E-09	6.9000E-09	1.943031E-13	1.687568E-13	2.554630E-14
560	6.3000E-09	6.6000E-09	1.987726E-13	1.726392E-13	2.613339E-14
561	6.0000E-09	6.3000E-09	2.035601E-13	1.768016E-13	2.675850E-14
562	5.7500E-09	6.0000E-09	2.082716E-13	1.808901E-13	2.738150E-14
563	5.5000E-09	5.7500E-09	2.128500E-13	1.848694E-13	2.798060E-14
564	5.2500E-09	5.5000E-09	2.177454E-13	1.891148E-13	2.863061E-14
565	5.0000E-09	5.2500E-09	2.229884E-13	1.936760E-13	2.931241E-14
566	4.7500E-09	5.0000E-09	2.286440E-13	1.985811E-13	3.006291E-14
567	4.5000E-09	4.7500E-09	2.347454E-13	2.038854E-13	3.086001E-14
568	4.2500E-09	4.5000E-09	2.413566E-13	2.096228E-13	3.173380E-14
569	4.0000E-09	4.2500E-09	2.485611E-13	2.158809E-13	3.268020E-14
570	3.8000E-09	4.0000E-09	2.556163E-13	2.220091E-13	3.360720E-14

Energy Bin #	Lower Energy Bound [MeV]	Upper Energy Bound [MeV]	Total Kerma [rad(GaAs)]	Displacement Kerma [rad(GaAs)]	Ionizing Kerma [rad(GaAs)]
571	3.6000E-09	3.8000E-09	2.624320E-13	2.279321E-13	3.449991E-14
572	3.4000E-09	3.6000E-09	2.698237E-13	2.343480E-13	3.547569E-14
573	3.2000E-09	3.4000E-09	2.778769E-13	2.413492E-13	3.652769E-14
574	3.0000E-09	3.2000E-09	2.867073E-13	2.490139E-13	3.769340E-14
575	2.8000E-09	3.0000E-09	2.964270E-13	2.574563E-13	3.897070E-14
576	2.7000E-09	2.8000E-09	3.044147E-13	2.643894E-13	4.002530E-14
577	2.5500E-09	2.7000E-09	3.115718E-13	2.706105E-13	4.096132E-14
578	2.4000E-09	2.5500E-09	3.208849E-13	2.786916E-13	4.219330E-14
579	2.3000E-09	2.4000E-09	3.293113E-13	2.860194E-13	4.329192E-14
580	2.2000E-09	2.3000E-09	3.365471E-13	2.923058E-13	4.424128E-14
581	2.1000E-09	2.2000E-09	3.442869E-13	2.990202E-13	4.526671E-14
582	2.0000E-09	2.1000E-09	3.525905E-13	3.062332E-13	4.635729E-14
583	1.9000E-09	2.0000E-09	3.614931E-13	3.139677E-13	4.752538E-14
584	1.8000E-09	1.9000E-09	3.711340E-13	3.223395E-13	4.879449E-14
585	1.7000E-09	1.8000E-09	3.815950E-13	3.314258E-13	5.016921E-14
586	1.6000E-09	1.7000E-09	3.929801E-13	3.413201E-13	5.166001E-14
587	1.5000E-09	1.6000E-09	4.054731E-13	3.521611E-13	5.331201E-14
588	1.4250E-09	1.5000E-09	4.174326E-13	3.625500E-13	5.488261E-14
589	1.3500E-09	1.4250E-09	4.285577E-13	3.722229E-13	5.633479E-14
590	1.2750E-09	1.3500E-09	4.406039E-13	3.826733E-13	5.793060E-14
591	1.2000E-09	1.2750E-09	4.537568E-13	3.941037E-13	5.965310E-14
592	1.1500E-09	1.2000E-09	4.656806E-13	4.044592E-13	6.122140E-14
593	1.1000E-09	1.1500E-09	4.759201E-13	4.133482E-13	6.257188E-14
594	1.0500E-09	1.1000E-09	4.868598E-13	4.228520E-13	6.400780E-14
595	1.0000E-09	1.0500E-09	4.985969E-13	4.330422E-13	6.555469E-14
596	9.6000E-10	1.0000E-09	5.099112E-13	4.428779E-13	6.703327E-14
597	9.2000E-10	9.6000E-10	5.206629E-13	4.522095E-13	6.845338E-14
598	8.8000E-10	9.2000E-10	5.321065E-13	4.621519E-13	6.995457E-14
599	8.4000E-10	8.8000E-10	5.443356E-13	4.727689E-13	7.156672E-14
600	8.0000E-10	8.4000E-10	5.574631E-13	4.841751E-13	7.328800E-14
601	7.6000E-10	8.0000E-10	5.715894E-13	4.964387E-13	7.515066E-14
602	7.2000E-10	7.6000E-10	5.868249E-13	5.096768E-13	7.714814E-14
603	6.9000E-10	7.2000E-10	6.012350E-13	5.221897E-13	7.904528E-14
604	6.6000E-10	6.9000E-10	6.143947E-13	5.336200E-13	8.077469E-14
605	6.3000E-10	6.6000E-10	6.285208E-13	5.458861E-13	8.263469E-14
606	6.0000E-10	6.3000E-10	6.436631E-13	5.590405E-13	8.462258E-14
607	5.7500E-10	6.0000E-10	6.585640E-13	5.719800E-13	8.658401E-14
608	5.5000E-10	5.7500E-10	6.730449E-13	5.845582E-13	8.848667E-14
609	5.2500E-10	5.5000E-10	6.885163E-13	5.979925E-13	9.052378E-14
610	5.0000E-10	5.2500E-10	7.051133E-13	6.124120E-13	9.270135E-14
611	4.7500E-10	5.0000E-10	7.229821E-13	6.279314E-13	9.505070E-14

Energy Bin #	Lower Energy Bound [MeV]	Upper Energy Bound [MeV]	Total Kerma [rad(GaAs)]	Displacement Kerma [rad(GaAs)]	Ionizing Kerma [rad(GaAs)]
612	4.5000E-10	4.7500E-10	7.422841E-13	6.446975E-13	9.758660E-14
613	4.2500E-10	4.5000E-10	7.631876E-13	6.628555E-13	1.003321E-13
614	4.0000E-10	4.2500E-10	7.859748E-13	6.826442E-13	1.033306E-13
615	3.8000E-10	4.0000E-10	8.082780E-13	7.020155E-13	1.062625E-13
616	3.6000E-10	3.8000E-10	8.298347E-13	7.207401E-13	1.090946E-13
617	3.4000E-10	3.6000E-10	8.532154E-13	7.410421E-13	1.121733E-13
618	3.2000E-10	3.4000E-10	8.786947E-13	7.631733E-13	1.155214E-13
619	3.0000E-10	3.2000E-10	9.065991E-13	7.874058E-13	1.191933E-13
620	2.8000E-10	3.0000E-10	9.373421E-13	8.141050E-13	1.232371E-13
621	2.7000E-10	2.8000E-10	9.626042E-13	8.360508E-13	1.265534E-13
622	2.5500E-10	2.7000E-10	9.852353E-13	8.557114E-13	1.295239E-13
623	2.4000E-10	2.5500E-10	1.014680E-12	8.812785E-13	1.333975E-13
624	2.3000E-10	2.4000E-10	1.041331E-12	9.044312E-13	1.368998E-13
625	2.2000E-10	2.3000E-10	1.064253E-12	9.243103E-13	1.399426E-13
626	2.1000E-10	2.2000E-10	1.088670E-12	9.455657E-13	1.431043E-13
627	2.0000E-10	2.1000E-10	1.114921E-12	9.683635E-13	1.465575E-13
628	1.9000E-10	2.0000E-10	1.143127E-12	9.928241E-13	1.503029E-13
629	1.8000E-10	1.9000E-10	1.173562E-12	1.019299E-12	1.542630E-13
630	1.7000E-10	1.8000E-10	1.206662E-12	1.048034E-12	1.586281E-13
631	1.6000E-10	1.7000E-10	1.242674E-12	1.079348E-12	1.633261E-13
632	1.5000E-10	1.6000E-10	1.282193E-12	1.113610E-12	1.685830E-13
633	1.4250E-10	1.5000E-10	1.319985E-12	1.146485E-12	1.735000E-13
634	1.3500E-10	1.4250E-10	1.355163E-12	1.177012E-12	1.781510E-13
635	1.2750E-10	1.3500E-10	1.393258E-12	1.210102E-12	1.831560E-13
636	1.2000E-10	1.2750E-10	1.434861E-12	1.246233E-12	1.886280E-13
637	1.1500E-10	1.2000E-10	1.472544E-12	1.279003E-12	1.935409E-13
638	1.1000E-10	1.1500E-10	1.504930E-12	1.307114E-12	1.978159E-13
639	1.0500E-10	1.1000E-10	1.539553E-12	1.337114E-12	2.024390E-13
640	1.0000E-10	1.0500E-10	1.576643E-12	1.369374E-12	2.072690E-13

Table A-2. GaAs Damage Energy Functions

Energy Bin #	Lower Energy Bound [MeV]	Upper Energy Bound [MeV]	Total Cross Section [b]	NRT Damage Energy [MeV-mb]	1-MeV(GaAs)-Eqv. Damage Energy [MeV-mb]
1	1.9900E+01	2.0000E+01	2.78813	336.1373	157.5402832
2	1.9800E+01	1.9900E+01	2.794849	335.0382	157.2740501
3	1.9700E+01	1.9800E+01	2.801491	333.9451	157.0080555
4	1.9600E+01	1.9700E+01	2.80827	332.8631	156.7446609
5	1.9500E+01	1.9600E+01	2.815091	331.7789	156.4834609
6	1.9400E+01	1.9500E+01	2.821961	330.7109	156.2250995
7	1.9300E+01	1.9400E+01	2.828852	329.6408	155.9732026
8	1.9200E+01	1.9300E+01	2.835882	328.5768	155.7222597
9	1.9100E+01	1.9200E+01	2.842893	327.5148	155.4736784
10	1.9000E+01	1.9100E+01	2.849953	326.4687	155.2236898
11	1.8900E+01	1.9000E+01	2.857313	325.4446	154.9875125
12	1.8800E+01	1.8900E+01	2.865024	324.4256	154.7646934
13	1.8700E+01	1.8800E+01	2.872915	323.3954	154.5423752
14	1.8600E+01	1.8700E+01	2.880835	322.3764	154.3205103
15	1.8500E+01	1.8600E+01	2.888705	321.3493	154.097715
16	1.8400E+01	1.8500E+01	2.896696	320.3072	153.8765657
17	1.8300E+01	1.8400E+01	2.904756	319.2682	153.6504071
18	1.8200E+01	1.8300E+01	2.912837	318.2281	153.4256797
19	1.8100E+01	1.8200E+01	2.920987	317.183	153.199521
20	1.8000E+01	1.8100E+01	2.929107	316.0019	152.9748175
21	1.7900E+01	1.8000E+01	2.937608	314.6819	152.6997584
22	1.7800E+01	1.7900E+01	2.946318	313.3769	152.377731
23	1.7700E+01	1.7800E+01	2.955059	312.0609	152.058566
24	1.7600E+01	1.7700E+01	2.96391	310.7479	151.7379937
25	1.7500E+01	1.7600E+01	2.97271	309.4469	151.4204986
26	1.7400E+01	1.7500E+01	2.98163	308.1489	151.103242
27	1.7300E+01	1.7400E+01	2.990661	306.8439	150.7902552
28	1.7200E+01	1.7300E+01	2.999651	305.5508	150.4773162
29	1.7100E+01	1.7200E+01	3.008732	304.2578	150.1648065
30	1.7000E+01	1.7100E+01	3.017872	302.9038	149.8556602
31	1.6900E+01	1.7000E+01	3.027233	301.5038	149.5221591
32	1.6800E+01	1.6900E+01	3.036683	300.0967	149.170529
33	1.6700E+01	1.6800E+01	3.046253	298.6937	148.8186843
34	1.6600E+01	1.6700E+01	3.055803	297.2926	148.4682469
35	1.6500E+01	1.6600E+01	3.065434	295.8896	148.1166407
36	1.6400E+01	1.6500E+01	3.075145	294.4886	147.767897
37	1.6300E+01	1.6400E+01	3.084924	293.0956	147.4203221
38	1.6200E+01	1.6300E+01	3.094685	291.6945	147.0722701
39	1.6100E+01	1.6200E+01	3.104516	290.2914	146.7247191
40	1.6000E+01	1.6100E+01	3.114326	288.6944	146.3766671

Energy Bin #	Lower Energy Bound [MeV]	Upper Energy Bound [MeV]	Total Cross Section [b]	NRT Damage Energy [MeV-mb]	1-MeV(GaAs)-Eqv. Damage Energy [MeV-mb]
41	1.5900E+01	1.6000E+01	3.124226	286.9154	145.9506606
42	1.5800E+01	1.5900E+01	3.134257	285.1314	145.4501824
43	1.5700E+01	1.5800E+01	3.144277	283.3474	144.9516363
44	1.5600E+01	1.5700E+01	3.154357	281.5664	144.4523745
45	1.5500E+01	1.5600E+01	3.164407	279.8194	143.9552358
46	1.5400E+01	1.5500E+01	3.174618	278.0794	143.4686166
47	1.5300E+01	1.5400E+01	3.184998	276.3494	142.9886766
48	1.5200E+01	1.5300E+01	3.195398	274.6214	142.508975
49	1.5100E+01	1.5200E+01	3.205839	272.8953	142.0304662
50	1.5000E+01	1.5100E+01	3.216259	271.1793	141.5524344
51	1.4900E+01	1.5000E+01	3.226789	269.4833	141.0796505
52	1.4800E+01	1.4900E+01	3.237349	267.7923	140.6116135
53	1.4700E+01	1.4800E+01	3.247909	266.1103	140.1476555
54	1.4600E+01	1.4700E+01	3.258449	264.4323	139.6846278
55	1.4500E+01	1.4600E+01	3.269039	262.7473	139.2264186
56	1.4400E+01	1.4500E+01	3.279869	261.0603	138.7610294
57	1.4300E+01	1.4400E+01	3.290679	259.3753	138.2901538
58	1.4200E+01	1.4300E+01	3.301409	257.6903	137.8199938
59	1.4100E+01	1.4200E+01	3.31222	256.0093	137.3507642
60	1.4000E+01	1.4100E+01	3.322999	254.3713	136.8820354
61	1.3900E+01	1.4000E+01	3.33395	252.7704	136.4316741
62	1.3800E+01	1.3900E+01	3.34492	251.1804	135.9980106
63	1.3700E+01	1.3800E+01	3.356009	249.5895	135.5674719
64	1.3600E+01	1.3700E+01	3.36703	248.0035	135.1385791
65	1.3500E+01	1.3600E+01	3.378049	246.4035	134.7089707
66	1.3400E+01	1.3500E+01	3.389159	244.8045	134.2738998
67	1.3300E+01	1.3400E+01	3.400299	243.2185	133.8362049
68	1.3200E+01	1.3300E+01	3.411559	241.6556	133.4051653
69	1.3100E+01	1.3200E+01	3.422769	240.0877	132.9815204
70	1.3000E+01	1.3100E+01	3.433979	238.5107	132.5571837
71	1.2900E+01	1.3000E+01	3.445258	236.9468	132.1161493
72	1.2800E+01	1.2900E+01	3.456538	235.4059	131.6665514
73	1.2700E+01	1.2800E+01	3.467868	233.871	131.2288565
74	1.2600E+01	1.2700E+01	3.479218	232.347	130.7933324
75	1.2500E+01	1.2600E+01	3.490537	230.8042	130.3625313
76	1.2400E+01	1.2500E+01	3.501907	229.2483	129.9193977
77	1.2300E+01	1.2400E+01	3.513247	227.6945	129.4671997
78	1.2200E+01	1.2300E+01	3.524616	226.1417	129.0145246
79	1.2100E+01	1.2200E+01	3.535956	224.615	128.5632808
80	1.2000E+01	1.2100E+01	3.547296	223.0609	128.1204096
81	1.1900E+01	1.2000E+01	3.558605	221.4666	127.6435467

Energy Bin #	Lower Energy Bound [MeV]	Upper Energy Bound [MeV]	Total Cross Section [b]	NRT Damage Energy [MeV-mb]	1-MeV(GaAs)-Eqv. Damage Energy [MeV-mb]
82	1.1800E+01	1.1900E+01	3.569834	219.8922	127.1329067
83	1.1700E+01	1.1800E+01	3.581064	218.3248	126.6253915
84	1.1600E+01	1.1700E+01	3.592294	216.7575	126.1225994
85	1.1500E+01	1.1600E+01	3.603523	215.2884	125.6221927
86	1.1400E+01	1.1500E+01	3.614603	214.0278	125.1768169
87	1.1300E+01	1.1400E+01	3.625622	212.8082	124.8430534
88	1.1200E+01	1.1300E+01	3.636511	211.5856	124.5279198
89	1.1100E+01	1.1200E+01	3.647461	210.368	124.2115935
90	1.1000E+01	1.1100E+01	3.65838	209.1943	123.896436
91	1.0900E+01	1.1000E+01	3.66907	208.0925	123.592466
92	1.0800E+01	1.0900E+01	3.679609	206.9858	123.3070782
93	1.0700E+01	1.0800E+01	3.690049	205.9081	123.022883
94	1.0600E+01	1.0700E+01	3.700498	204.8525	122.7475377
95	1.0500E+01	1.0600E+01	3.710846	203.7745	122.4853358
96	1.0400E+01	1.0500E+01	3.720855	202.6625	122.2170512
97	1.0300E+01	1.0400E+01	3.730685	201.5434	121.9401077
98	1.0200E+01	1.0300E+01	3.740484	200.4303	121.6602778
99	1.0100E+01	1.0200E+01	3.750243	199.3163	121.3811874
100	1.0000E+01	1.0100E+01	3.759982	198.2493	121.1018346
101	9.9000E+00	1.0000E+01	3.769311	197.2205	120.8182358
102	9.8000E+00	9.9000E+00	3.77834	196.1857	120.528769
103	9.7000E+00	9.8000E+00	3.787229	195.1957	120.2335295
104	9.6000E+00	9.7000E+00	3.796098	194.2675	119.9625733
105	9.5000E+00	9.6000E+00	3.804877	193.3565	119.72444
106	9.4000E+00	9.5000E+00	3.812966	192.4464	119.4896462
107	9.3000E+00	9.4000E+00	3.820866	191.5383	119.2491753
108	9.2000E+00	9.3000E+00	3.828874	190.6172	119.0082033
109	9.1000E+00	9.2000E+00	3.836673	189.7022	118.7643928
110	9.0000E+00	9.1000E+00	3.844451	188.8442	118.5196043
111	8.9000E+00	9.0000E+00	3.851619	188.0463	118.296332
112	8.8000E+00	8.9000E+00	3.858328	187.2444	118.0971759
113	8.7000E+00	8.8000E+00	3.864887	186.4335	117.8937262
114	8.6000E+00	8.7000E+00	3.871315	185.6226	117.6886067
115	8.5000E+00	8.6000E+00	3.877564	184.7947	117.4789788
116	8.4000E+00	8.5000E+00	3.883282	183.9458	117.2557064
117	8.3000E+00	8.4000E+00	3.888291	183.0938	117.0148061
118	8.2000E+00	8.3000E+00	3.89331	182.2448	116.7745975
119	8.1000E+00	8.2000E+00	3.898288	181.3868	116.5336733
120	8.0000E+00	8.1000E+00	3.903096	180.6299	116.2880022
121	7.9000E+00	8.0000E+00	3.907305	179.9739	116.0804735
122	7.8000E+00	7.9000E+00	3.910824	179.319	115.9082723

Energy Bin #	Lower Energy Bound [MeV]	Upper Energy Bound [MeV]	Total Cross Section [b]	NRT Damage Energy [MeV-mb]	1-MeV(GaAs)-Eqv. Damage Energy [MeV-mb]
123	7.7000E+00	7.8000E+00	3.914163	178.669	115.7353317
124	7.6000E+00	7.7000E+00	3.917331	178.011	115.5628681
125	7.5000E+00	7.6000E+00	3.9204	177.34	115.3868265
126	7.4000E+00	7.5000E+00	3.922769	176.6778	115.2010047
127	7.3000E+00	7.4000E+00	3.924417	176.0355	115.0129646
128	7.2000E+00	7.3000E+00	3.925915	175.3882	114.8343944
129	7.1000E+00	7.2000E+00	3.927175	174.7359	114.6524847
130	7.0000E+00	7.1000E+00	3.928253	174.0367	114.4686667
131	6.9000E+00	7.0000E+00	3.928672	173.2727	114.2374511
132	6.8000E+00	6.9000E+00	3.928361	172.5146	113.9614378
133	6.7000E+00	6.8000E+00	3.92778	171.7536	113.6825382
134	6.6000E+00	6.7000E+00	3.926979	170.9855	113.4015395
135	6.5000E+00	6.6000E+00	3.925797	170.2035	113.1159847
136	6.4000E+00	6.5000E+00	3.924026	169.3606	112.8211508
137	6.3000E+00	6.4000E+00	3.921626	168.4767	112.4989087
138	6.2000E+00	6.3000E+00	3.918815	167.5888	112.1561523
139	6.1000E+00	6.2000E+00	3.915754	166.698	111.8110582
140	6.0000E+00	6.1000E+00	3.912303	165.852	111.4616465
141	5.9000E+00	6.0000E+00	3.908222	165.02	111.1270243
142	5.8000E+00	5.9000E+00	3.903512	164.17	110.7966481
143	5.7000E+00	5.8000E+00	3.898441	163.3131	110.4560385
144	5.6000E+00	5.7000E+00	3.892901	162.4552	110.1101572
145	5.5000E+00	5.6000E+00	3.886991	161.5352	109.7581217
146	5.4000E+00	5.5000E+00	3.880411	160.5653	109.379823
147	5.3000E+00	5.4000E+00	3.87317	159.5647	108.9750942
148	5.2000E+00	5.3000E+00	3.86542	158.544	108.5580329
149	5.1000E+00	5.2000E+00	3.8571	157.5122	108.1297842
150	5.0000E+00	5.1000E+00	3.84823	156.4954	107.6922086
151	4.9000E+00	5.0000E+00	3.8385	155.5005	107.2722133
152	4.8000E+00	4.9000E+00	3.82789	154.4815	106.8705617
153	4.7000E+00	4.8000E+00	3.816711	153.4295	106.45913
154	4.6000E+00	4.7000E+00	3.804741	152.3757	106.0271362
155	4.5000E+00	4.6000E+00	3.792112	151.1829	105.5923753
156	4.4000E+00	4.5000E+00	3.778013	149.83	105.0937338
157	4.3000E+00	4.4000E+00	3.762353	148.4462	104.5153965
158	4.2000E+00	4.3000E+00	3.745984	147.0101	103.9198844
159	4.1000E+00	4.2000E+00	3.728924	145.5157	103.3075314
160	4.0000E+00	4.1000E+00	3.711055	143.9393	102.6771449
161	3.9000E+00	4.0000E+00	3.691115	142.2579	101.9883402
162	3.8000E+00	3.9000E+00	3.669146	140.4356	101.2270198
163	3.7000E+00	3.8000E+00	3.646497	138.4634	100.4058738

Energy Bin #	Lower Energy Bound [MeV]	Upper Energy Bound [MeV]	Total Cross Section [b]	NRT Damage Energy [MeV-mb]	1-MeV(GaAs)-Eqv. Damage Energy [MeV-mb]
164	3.6000E+00	3.7000E+00	3.623247	136.3982	99.52201594
165	3.5000E+00	3.6000E+00	3.599517	134.0619	98.5966762
166	3.4000E+00	3.5000E+00	3.573628	131.3555	97.53222063
167	3.3000E+00	3.4000E+00	3.545838	128.4601	96.30243381
168	3.2000E+00	3.3000E+00	3.517978	125.4897	95.00917182
169	3.1000E+00	3.2000E+00	3.490299	122.5022	93.68797693
170	3.0000E+00	3.1000E+00	3.462958	118.9765	92.35413948
171	2.9000E+00	3.0000E+00	3.435419	115.0609	90.76551874
172	2.8000E+00	2.9000E+00	3.407949	111.2695	89.02547356
173	2.7000E+00	2.8000E+00	3.381418	107.5785	87.37151704
174	2.6000E+00	2.7000E+00	3.356308	103.6466	85.76901333
175	2.5000E+00	2.6000E+00	3.32892	99.83511	83.96172406
176	2.4000E+00	2.5000E+00	3.311813	96.11607	82.27735384
177	2.3000E+00	2.4000E+00	3.30334	92.44197	80.6761621
178	2.2000E+00	2.3000E+00	3.297371	88.87327	79.1151403
179	2.1000E+00	2.2000E+00	3.295216	85.34364	77.62508379
180	2.0000E+00	2.1000E+00	3.294805	81.92402	76.13316667
181	1.9000E+00	2.0000E+00	3.30693	78.69069	74.76712649
182	1.8000E+00	1.9000E+00	3.337992	75.57986	73.61286106
183	1.7000E+00	1.8000E+00	3.375011	72.85775	72.47708238
184	1.6000E+00	1.7000E+00	3.435006	70.25755	71.66204299
185	1.5000E+00	1.6000E+00	3.502824	68.04988	70.87145382
186	1.4000E+00	1.5000E+00	3.597043	66.15967	70.39258717
187	1.3000E+00	1.4000E+00	3.710927	64.42605	70.17353698
188	1.2000E+00	1.3000E+00	3.846838	62.57152	70.07001114
189	1.1000E+00	1.2000E+00	3.984873	61.03186	69.77732402
190	1.0000E+00	1.1000E+00	4.172892	59.89667	69.93502203
191	9.6000E-01	1.0000E+00	4.322477	59.14966	70.06497797
192	9.2000E-01	9.6000E-01	4.410211	58.41629	70.00729929
193	8.8000E-01	9.2000E-01	4.502726	57.59902	69.97919942
194	8.4000E-01	8.8000E-01	4.598038	56.74971	69.84339927
195	8.0000E-01	8.4000E-01	4.703776	55.82237	69.72284176
196	7.6000E-01	8.0000E-01	4.811644	54.84565	69.49990339
197	7.2000E-01	7.6000E-01	4.92181	53.98345	69.19035158
198	6.9000E-01	7.2000E-01	5.025134	53.21802	68.92693318
199	6.6000E-01	6.9000E-01	5.118239	52.4083	68.65547602
200	6.3000E-01	6.6000E-01	5.212889	51.52209	68.3148426
201	6.0000E-01	6.3000E-01	5.309917	50.6176	67.87972396
202	5.7500E-01	6.0000E-01	5.388134	49.8003	67.30699229
203	5.5000E-01	5.7500E-01	5.471592	48.97418	66.79000713
204	5.2500E-01	5.5000E-01	5.565547	48.08909	66.27791202

Energy Bin #	Lower Energy Bound [MeV]	Upper Energy Bound [MeV]	Total Cross Section [b]	NRT Damage Energy [MeV-mb]	1-MeV(GaAs)-Eqv. Damage Energy [MeV-mb]
205	5.0000E-01	5.2500E-01	5.663743	47.0947	65.68702754
206	4.7500E-01	5.0000E-01	5.754036	46.03836	64.93524864
207	4.5000E-01	4.7500E-01	5.854427	44.8963	64.12331025
208	4.2500E-01	4.5000E-01	5.960082	43.71304	63.20903871
209	4.0000E-01	4.2500E-01	6.069267	42.50098	62.23391592
210	3.8000E-01	4.0000E-01	6.164258	41.33552	61.15567281
211	3.6000E-01	3.8000E-01	6.255457	40.15747	60.07595076
212	3.4000E-01	3.6000E-01	6.348374	38.89014	58.97740799
213	3.2000E-01	3.4000E-01	6.44768	37.60432	57.74294581
214	3.0000E-01	3.2000E-01	6.554046	36.28896	56.48510683
215	2.8000E-01	3.0000E-01	6.668703	35.2232	55.16183665
216	2.7000E-01	2.8000E-01	6.759046	34.23779	54.04349517
217	2.5500E-01	2.7000E-01	6.834737	32.98027	52.9738633
218	2.4000E-01	2.5500E-01	6.928498	31.86123	51.56550633
219	2.3000E-01	2.4000E-01	7.01466	30.96151	50.23825256
220	2.2000E-01	2.3000E-01	7.084094	30.06179	49.16551969
221	2.1000E-01	2.2000E-01	7.153507	29.16177	48.09347859
222	2.0000E-01	2.1000E-01	7.222991	28.19254	47.02026864
223	1.9000E-01	2.0000E-01	7.306112	27.1659	45.79580124
224	1.8000E-01	1.9000E-01	7.403111	26.13906	44.44061457
225	1.7000E-01	1.8000E-01	7.50009	25.11243	43.08423521
226	1.6000E-01	1.7000E-01	7.597068	24.08559	41.72857146
227	1.5000E-01	1.6000E-01	7.694046	23.12318	40.37338479
228	1.4250E-01	1.5000E-01	7.790256	22.22639	39.06712243
229	1.3500E-01	1.4250E-01	7.885674	21.32821	37.8138634
230	1.2750E-01	1.3500E-01	7.981102	20.41169	36.55845751
231	1.2000E-01	1.2750E-01	8.077602	19.64087	35.26605426
232	1.1500E-01	1.2000E-01	8.158476	19.02474	34.17657597
233	1.1000E-01	1.1500E-01	8.223041	18.40872	33.305146
234	1.0500E-01	1.1000E-01	8.287624	17.7927	32.43493258
235	1.0000E-01	1.0500E-01	8.352239	16.52418	31.56397969
236	9.6000E-02	1.0000E-01	8.079481	16.02397	29.49558584
237	9.2000E-02	9.6000E-02	8.153351	15.52037	28.76944986
238	8.8000E-02	9.2000E-02	8.227892	14.99865	28.03496502
239	8.4000E-02	8.8000E-02	8.306892	14.47405	27.2597139
240	8.0000E-02	8.4000E-02	8.386633	13.93754	26.47730661
241	7.6000E-02	8.0000E-02	8.469202	13.38804	25.66887474
242	7.2000E-02	7.6000E-02	8.555702	12.90344	24.82752452
243	6.9000E-02	7.2000E-02	8.633762	12.47204	24.07901359
244	6.6000E-02	6.9000E-02	8.703996	12.03634	23.3999771
245	6.3000E-02	6.6000E-02	8.775837	11.59794	22.70843163

Energy Bin #	Lower Energy Bound [MeV]	Upper Energy Bound [MeV]	Total Cross Section [b]	NRT Damage Energy [MeV-mb]	1-MeV(GaAs)-Eqv. Damage Energy [MeV-mb]
246	6.0000E-02	6.3000E-02	8.850569	11.20004	22.00920521
247	5.7500E-02	6.0000E-02	8.933589	10.84304	21.36872375
248	5.5000E-02	5.7500E-02	9.024446	10.48423	20.78840177
249	5.2500E-02	5.5000E-02	9.117624	10.12358	20.20270789
250	5.0000E-02	5.2500E-02	9.213371	9.74955	19.61189021
251	4.7500E-02	5.0000E-02	9.31284	9.362482	18.99163921
252	4.5000E-02	4.7500E-02	9.416386	8.973403	18.34150408
253	4.2500E-02	4.5000E-02	9.523563	8.581727	17.68531245
254	4.0000E-02	4.2500E-02	9.634781	8.21885	17.02236778
255	3.8000E-02	4.0000E-02	9.739828	7.884035	16.40074042
256	3.6000E-02	3.8000E-02	9.837927	7.547222	15.81974338
257	3.4000E-02	3.6000E-02	9.940178	7.208728	15.23313829
258	3.2000E-02	3.4000E-02	10.04758	6.868014	14.64171233
259	3.0000E-02	3.2000E-02	10.16027	6.52407	14.04377903
260	2.8000E-02	3.0000E-02	10.30109	6.265064	13.432676
261	2.7000E-02	2.8000E-02	10.42781	6.045988	12.96667613
262	2.5500E-02	2.7000E-02	10.5383	5.782613	12.57209239
263	2.4000E-02	2.5500E-02	10.67488	5.563588	12.09635775
264	2.3000E-02	2.4000E-02	10.79387	5.386991	11.70010424
265	2.2000E-02	2.3000E-02	10.89216	5.209564	11.37867797
266	2.1000E-02	2.2000E-02	10.99495	5.031187	11.05534577
267	2.0000E-02	2.1000E-02	11.10044	4.847312	10.7277652
268	1.9000E-02	2.0000E-02	11.23672	4.658197	10.38237055
269	1.8000E-02	1.9000E-02	11.4017	4.467813	10.01992276
270	1.7000E-02	1.8000E-02	11.57218	4.276879	9.653345865
271	1.6000E-02	1.7000E-02	11.74936	4.084615	9.284192749
272	1.5000E-02	1.6000E-02	11.93484	3.91589	8.911847984
273	1.4250E-02	1.5000E-02	12.10482	3.770744	8.584317505
274	1.3500E-02	1.4250E-02	12.2563	3.624848	8.301396168
275	1.2750E-02	1.3500E-02	12.41379	3.478202	8.015013632
276	1.2000E-02	1.2750E-02	12.58007	3.356236	7.723981976
277	1.1500E-02	1.2000E-02	12.72526	3.257859	7.481726735
278	1.1000E-02	1.1500E-02	12.84674	3.158802	7.286036654
279	1.0500E-02	1.1000E-02	12.97273	3.058995	7.087362453
280	1.0000E-02	1.0500E-02	13.10452	3.086517	6.886302863
281	9.6000E-03	1.0000E-02	13.80231	3.319689	6.965645641
282	9.2000E-03	9.6000E-03	15.46469	3.495921	7.50720745
283	8.8000E-03	9.2000E-03	16.99177	2.538813	7.924034932
284	8.4000E-03	8.8000E-03	12.79815	3.161236	5.758467531
285	8.0000E-03	8.4000E-03	16.69523	2.508621	7.184175813
286	7.6000E-03	8.0000E-03	13.88861	2.235694	5.70753234

Energy Bin #	Lower Energy Bound [MeV]	Upper Energy Bound [MeV]	Total Cross Section [b]	NRT Damage Energy [MeV-mb]	1-MeV(GaAs)-Eqv. Damage Energy [MeV-mb]
287	7.2000E-03	7.6000E-03	12.92449	2.449059	5.09764109
288	6.9000E-03	7.2000E-03	14.86407	1.733643	5.58782164
289	6.6000E-03	6.9000E-03	10.87041	2.995486	3.95982768
290	6.3000E-03	6.6000E-03	19.8596	2.312583	6.846371467
291	6.0000E-03	6.3000E-03	16.07128	2.165385	5.289927222
292	5.7500E-03	6.0000E-03	15.56725	3.006287	4.953041251
293	5.5000E-03	5.7500E-03	22.65435	1.400253	6.891548332
294	5.2500E-03	5.5000E-03	10.67369	2.634319	3.204069949
295	5.0000E-03	5.2500E-03	21.59185	3.288431	6.037512613
296	4.7500E-03	5.0000E-03	27.9216	1.466616	7.532819362
297	4.5000E-03	4.7500E-03	13.0438	1.260602	3.350969302
298	4.2500E-03	4.5000E-03	11.61853	1.028351	2.879805066
299	4.0000E-03	4.2500E-03	10.14627	1.903873	2.35253197
300	3.8000E-03	4.0000E-03	19.42509	1.452464	4.34068828
301	3.6000E-03	3.8000E-03	15.76737	4.054121	3.312807864
302	3.4000E-03	3.6000E-03	46.07861	0.5978173	9.240451888
303	3.2000E-03	3.4000E-03	6.844732	0.8439564	1.352893595
304	3.0000E-03	3.2000E-03	10.05612	0.8790135	1.899323265
305	2.8000E-03	3.0000E-03	11.68768	1.879378	1.974659784
306	2.7000E-03	2.8000E-03	25.97413	0.951868	4.206059363
307	2.5500E-03	2.7000E-03	13.27074	1.811672	2.127311262
308	2.4000E-03	2.5500E-03	27.90104	0.475641	4.04508622
309	2.3000E-03	2.4000E-03	7.047716	0.2998908	1.052220677
310	2.2000E-03	2.3000E-03	5.014559	0.3054485	0.661454991
311	2.1000E-03	2.2000E-03	5.610708	0.4749004	0.669819593
312	2.0000E-03	2.1000E-03	7.898108	1.497989	1.03579895
313	1.9000E-03	2.0000E-03	27.78267	1.293323	3.21234486
314	1.8000E-03	1.9000E-03	22.03988	0.3467158	2.782607659
315	1.7000E-03	1.8000E-03	7.569213	2.168767	0.729918014
316	1.6000E-03	1.7000E-03	43.1889	1.234325	4.539443584
317	1.5000E-03	1.6000E-03	25.53358	1.25861	2.535953762
318	1.4250E-03	1.5000E-03	21.94059	0.7395322	2.620887889
319	1.3500E-03	1.4250E-03	12.37884	1.306218	1.522871339
320	1.2750E-03	1.3500E-03	29.53784	0.1546463	2.587721453
321	1.2000E-03	1.2750E-03	4.460852	0.153543	0.291391373
322	1.1500E-03	1.2000E-03	5.095152	0.5031696	0.274989206
323	1.1000E-03	1.1500E-03	8.173228	0.1685113	1.014838306
324	1.0500E-03	1.1000E-03	5.79045	0.167162	0.286182401
325	1.0000E-03	1.0500E-03	6.285567	0.1826502	0.268044626
326	9.6000E-04	1.0000E-03	7.106645	2.028716	0.283489059
327	9.2000E-04	9.6000E-04	40.56082	0.695301	3.819333093

Energy Bin #	Lower Energy Bound [MeV]	Upper Energy Bound [MeV]	Total Cross Section [b]	NRT Damage Energy [MeV-mb]	1-MeV(GaAs)-Eqv. Damage Energy [MeV-mb]
328	8.8000E-04	9.2000E-04	10.43702	0.1879984	1.381663045
329	8.4000E-04	8.8000E-04	6.829768	0.1774986	0.281663045
330	8.0000E-04	8.4000E-04	7.884208	0.2513202	0.222497191
331	7.6000E-04	8.0000E-04	10.8523	5.457706	0.304611194
332	7.2000E-04	7.6000E-04	124.22	2.65158	9.284130729
333	6.9000E-04	7.2000E-04	59.5415	2.136339	4.429095532
334	6.6000E-04	6.9000E-04	32.8884	0.1354103	4.007172862
335	6.3000E-04	6.6000E-04	5.261858	0.1679684	0.150685298
336	6.0000E-04	6.3000E-04	6.904832	0.1652048	0.163626768
337	5.7500E-04	6.0000E-04	8.620038	0.3081101	0.09012466
338	5.5000E-04	5.7500E-04	14.55116	7.824156	0.203422149
339	5.2500E-04	5.5000E-04	253.8188	0.3673263	9.503247706
340	5.0000E-04	5.2500E-04	11.28731	1.900583	0.473241671
341	4.7500E-04	5.0000E-04	18.70537	1.429665	3.868543649
342	4.5000E-04	4.7500E-04	16.87643	0.1198157	2.763274088
343	4.2500E-04	4.5000E-04	7.24886	0.1435506	0.050200158
344	4.0000E-04	4.2500E-04	9.398675	0.4119523	0.052857099
345	3.8000E-04	4.0000E-04	23.43724	2.322094	0.290041243
346	3.6000E-04	3.8000E-04	106.934	0.2298422	2.408512019
347	3.4000E-04	3.6000E-04	12.47762	8.024226	0.224640105
348	3.2000E-04	3.4000E-04	110.7185	6.982711	15.98477884
349	3.0000E-04	3.2000E-04	109.1103	5.369696	13.87120336
350	2.8000E-04	3.0000E-04	376.95	0.7746775	5.298171123
351	2.7000E-04	2.8000E-04	50.48507	0.2236164	0.91753141
352	2.5500E-04	2.7000E-04	11.66549	2.508277	0.340220744
353	2.4000E-04	2.5500E-04	20.44638	0.05215432	5.420975671
354	2.3000E-04	2.4000E-04	4.44084	0.0369523	0.078001593
355	2.2000E-04	2.3000E-04	4.285107	0.02749421	0.054939041
356	2.1000E-04	2.2000E-04	4.289133	0.02080887	0.043491445
357	2.0000E-04	2.1000E-04	4.363814	0.0159066	0.036565518
358	1.9000E-04	2.0000E-04	4.472341	0.01386186	0.032062955
359	1.8000E-04	1.9000E-04	4.597996	0.0128801	0.029116047
360	1.7000E-04	1.8000E-04	4.733547	0.012517	0.027329129
361	1.6000E-04	1.7000E-04	4.877272	0.0127579	0.026594119
362	1.5000E-04	1.6000E-04	5.031621	0.01372976	0.02711931
363	1.4250E-04	1.5000E-04	5.181095	0.01579856	0.029186392
364	1.3500E-04	1.4250E-04	5.333214	0.0208365	0.033567634
365	1.2750E-04	1.3500E-04	5.535869	0.03785048	0.04421801
366	1.2000E-04	1.2750E-04	5.903088	0.1170026	0.08014403
367	1.1500E-04	1.2000E-04	6.896231	12.22259	0.247206114
368	1.1000E-04	1.1500E-04	90.11565	1.039	25.7943223

Energy Bin #	Lower Energy Bound [MeV]	Upper Energy Bound [MeV]	Total Cross Section [b]	NRT Damage Energy [MeV-mb]	1-MeV(GaAs)-Eqv. Damage Energy [MeV-mb]
369	1.0500E-04	1.1000E-04	10.99697	0.1360729	2.192870552
370	1.0000E-04	1.0500E-04	6.409558	2.364276	0.286671883
371	9.6000E-05	1.0000E-04	28.14851	14.3	4.897509416
372	9.2000E-05	9.6000E-05	113.2995	1.256662	30.38185292
373	8.8000E-05	9.2000E-05	11.42512	0.08030572	2.743988226
374	8.4000E-05	8.8000E-05	5.47328	0.04427222	0.17218721
375	8.0000E-05	8.4000E-05	5.492048	0.03373623	0.094717773
376	7.6000E-05	8.0000E-05	5.581619	0.03032044	0.072253834
377	7.2000E-05	7.6000E-05	5.686302	0.03041884	0.065096238
378	6.9000E-05	7.2000E-05	5.788815	0.03271246	0.065486727
379	6.6000E-05	6.9000E-05	5.891471	0.03771173	0.070616909
380	6.3000E-05	6.6000E-05	6.017637	0.04741347	0.081648017
381	6.0000E-05	6.3000E-05	6.188073	0.06452692	0.102963749
382	5.7500E-05	6.0000E-05	6.420272	0.09671726	0.140491628
383	5.5000E-05	5.7500E-05	6.777673	0.1746357	0.211071707
384	5.2500E-05	5.5000E-05	7.508444	0.453894	0.381838371
385	5.0000E-05	5.2500E-05	9.744335	5.785752	0.993791073
386	4.7500E-05	5.0000E-05	44.90358	55.42768	12.6778104
387	4.5000E-05	4.7500E-05	341.0631	0.8738932	121.4561124
388	4.2500E-05	4.5000E-05	9.372419	0.2669044	1.914234088
389	4.0000E-05	4.2500E-05	6.484992	0.1449193	0.584061791
390	3.8000E-05	4.0000E-05	6.039646	0.1000554	0.316748048
391	3.6000E-05	3.8000E-05	5.925041	0.07585701	0.218434923
392	3.4000E-05	3.6000E-05	5.890817	0.06133385	0.16540591
393	3.2000E-05	3.4000E-05	5.889642	0.05201878	0.133575387
394	3.0000E-05	3.2000E-05	5.904017	0.04577328	0.11314876
395	2.8000E-05	3.0000E-05	5.926264	0.042391	0.099449118
396	2.7000E-05	2.8000E-05	5.945652	0.04021972	0.092025147
397	2.5500E-05	2.7000E-05	5.963274	0.03818831	0.087255158
398	2.4000E-05	2.5500E-05	5.985342	0.0368867	0.082786634
399	2.3000E-05	2.4000E-05	6.004253	0.03606321	0.079918467
400	2.2000E-05	2.3000E-05	6.019736	0.03539121	0.07809918
401	2.1000E-05	2.2000E-05	6.035508	0.03489769	0.076611938
402	2.0000E-05	2.1000E-05	6.051581	0.03453588	0.075516091
403	1.9000E-05	2.0000E-05	6.067843	0.03430145	0.074702912
404	1.8000E-05	1.9000E-05	6.084425	0.0341944	0.074169277
405	1.7000E-05	1.8000E-05	6.101247	0.03421582	0.073914183
406	1.6000E-05	1.7000E-05	6.11835	0.03436814	0.073936511
407	1.5000E-05	1.6000E-05	6.135852	0.03459306	0.074244106
408	1.4250E-05	1.5000E-05	6.151454	0.03488769	0.074709114
409	1.3500E-05	1.4250E-05	6.165168	0.035264	0.075330651

Energy Bin #	Lower Energy Bound [MeV]	Upper Energy Bound [MeV]	Total Cross Section [b]	NRT Damage Energy [MeV-mb]	1-MeV(GaAs)-Eqv. Damage Energy [MeV-mb]
410	1.2750E-05	1.3500E-05	6.179221	0.0357177	0.076127466
411	1.2000E-05	1.2750E-05	6.193505	0.0361763	0.077092188
412	1.1500E-05	1.2000E-05	6.20578	0.03659535	0.078070293
413	1.1000E-05	1.1500E-05	6.215836	0.03707168	0.078964265
414	1.0500E-05	1.1000E-05	6.226201	0.03760779	0.079984137
415	1.0000E-05	1.0500E-05	6.236806	0.0381419	0.081131604
416	9.6000E-06	1.0000E-05	6.246641	0.03866193	0.08227597
417	9.2000E-06	9.6000E-06	6.255548	0.03923965	0.083390543
418	8.8000E-06	9.2000E-06	6.264813	0.03985725	0.084628917
419	8.4000E-06	8.8000E-06	6.274239	0.04054734	0.085955503
420	8.0000E-06	8.4000E-06	6.284085	0.0413051	0.087436161
421	7.6000E-06	8.0000E-06	6.294291	0.04213675	0.089062519
422	7.2000E-06	7.6000E-06	6.304835	0.04293561	0.090849842
423	6.9000E-06	7.2000E-06	6.314491	0.04367549	0.092566129
424	6.6000E-06	6.9000E-06	6.323068	0.04448465	0.09415723
425	6.3000E-06	6.6000E-06	6.332004	0.04534501	0.095895677
426	6.0000E-06	6.3000E-06	6.34121	0.04622016	0.097744592
427	5.7500E-06	6.0000E-06	6.350157	0.04704261	0.099626401
428	5.5000E-06	5.7500E-06	6.358442	0.04795045	0.101395142
429	5.2500E-06	5.5000E-06	6.367239	0.04893607	0.103348942
430	5.0000E-06	5.2500E-06	6.376395	0.05000876	0.105468049
431	4.7500E-06	5.0000E-06	6.386091	0.05116254	0.107774338
432	4.5000E-06	4.7500E-06	6.396216	0.05243618	0.11025662
433	4.2500E-06	4.5000E-06	6.407062	0.05382958	0.112997431
434	4.0000E-06	4.2500E-06	6.418517	0.05518221	0.115994599
435	3.8000E-06	4.0000E-06	6.429412	0.05653463	0.118905894
436	3.6000E-06	3.8000E-06	6.440008	0.05794853	0.121816735
437	3.4000E-06	3.6000E-06	6.450884	0.0595239	0.124859942
438	3.2000E-06	3.4000E-06	6.462679	0.06126462	0.128250366
439	3.0000E-06	3.2000E-06	6.475464	0.06318829	0.131996594
440	2.8000E-06	3.0000E-06	6.489288	0.06474536	0.136136554
441	2.7000E-06	2.8000E-06	6.500294	0.06618276	0.139488358
442	2.5500E-06	2.7000E-06	6.51029	0.06804246	0.142583304
443	2.4000E-06	2.5500E-06	6.523005	0.0697069	0.146585913
444	2.3000E-06	2.4000E-06	6.53431	0.0711682	0.150169744
445	2.2000E-06	2.3000E-06	6.544036	0.07271478	0.153315499
446	2.1000E-06	2.2000E-06	6.554301	0.07438812	0.156645119
447	2.0000E-06	2.1000E-06	6.565318	0.07616913	0.160247102
448	1.9000E-06	2.0000E-06	6.576883	0.0781112	0.164081566
449	1.8000E-06	1.9000E-06	6.589388	0.08021513	0.168262316
450	1.7000E-06	1.8000E-06	6.602862	0.082519	0.17279577

Energy Bin #	Lower Energy Bound [MeV]	Upper Energy Bound [MeV]	Total Cross Section [b]	NRT Damage Energy [MeV-mb]	1-MeV(GaAs)-Eqv. Damage Energy [MeV-mb]
451	1.6000E-06	1.7000E-06	6.617477	0.08505132	0.17774848
452	1.5000E-06	1.6000E-06	6.633361	0.08746545	0.183203672
453	1.4250E-06	1.5000E-06	6.648475	0.08971204	0.188413216
454	1.3500E-06	1.4250E-06	6.662358	0.09219997	0.19324241
455	1.2750E-06	1.3500E-06	6.677693	0.09482805	0.198596462
456	1.2000E-06	1.2750E-06	6.693776	0.0972304	0.204258633
457	1.1500E-06	1.2000E-06	6.70841	0.09931583	0.209430035
458	1.1000E-06	1.1500E-06	6.721096	0.1015439	0.213916521
459	1.0500E-06	1.1000E-06	6.734631	0.1039444	0.218728755
460	1.0000E-06	1.0500E-06	6.749095	0.1062529	0.223893263
461	9.6000E-07	1.0000E-06	6.762939	0.1084329	0.228855491
462	9.2000E-07	9.6000E-07	6.776034	0.1107826	0.233556375
463	8.8000E-07	9.2000E-07	6.790049	0.113267	0.238607744
464	8.4000E-07	8.8000E-07	6.804903	0.1159354	0.243966996
465	8.0000E-07	8.4000E-07	6.820796	0.1188492	0.249711726
466	7.6000E-07	8.0000E-07	6.838071	0.1219557	0.255988159
467	7.2000E-07	7.6000E-07	6.856493	0.1249053	0.262666053
468	6.9000E-07	7.2000E-07	6.873906	0.1276046	0.269015002
469	6.6000E-07	6.9000E-07	6.88983	0.130524	0.274844413
470	6.3000E-07	6.6000E-07	6.907003	0.1335659	0.281122039
471	6.0000E-07	6.3000E-07	6.924907	0.1366079	0.287670406
472	5.7500E-07	6.0000E-07	6.9428	0.1395736	0.2942307
473	5.5000E-07	5.7500E-07	6.960193	0.1427542	0.300612568
474	5.2500E-07	5.5000E-07	6.978846	0.1461577	0.307459824
475	5.0000E-07	5.2500E-07	6.998767	0.1498418	0.314800617
476	4.7500E-07	5.0000E-07	7.020339	0.1537627	0.322733464
477	4.5000E-07	4.7500E-07	7.043231	0.158039	0.331164857
478	4.2500E-07	4.5000E-07	7.068151	0.1627141	0.340380326
479	4.0000E-07	4.2500E-07	7.09539	0.1672715	0.350442132
480	3.8000E-07	4.0000E-07	7.12196	0.1717	0.360261343
481	3.6000E-07	3.8000E-07	7.1477	0.1765037	0.369800749
482	3.4000E-07	3.6000E-07	7.17569	0.1817401	0.380135442
483	3.2000E-07	3.4000E-07	7.206088	0.1874813	0.391419044
484	3.0000E-07	3.2000E-07	7.239485	0.1938098	0.403780124
485	2.8000E-07	3.0000E-07	7.27618	0.1989444	0.417416434
486	2.7000E-07	2.8000E-07	7.305979	0.2036311	0.428473662
487	2.5500E-07	2.7000E-07	7.333179	0.2096844	0.438563376
488	2.4000E-07	2.5500E-07	7.368305	0.215137	0.451599522
489	2.3000E-07	2.4000E-07	7.399892	0.2198477	0.463335154
490	2.2000E-07	2.3000E-07	7.427182	0.2248804	0.473489274
491	2.1000E-07	2.2000E-07	7.456402	0.2302809	0.484330624

Energy Bin #	Lower Energy Bound [MeV]	Upper Energy Bound [MeV]	Total Cross Section [b]	NRT Damage Energy [MeV-mb]	1-MeV(GaAs)-Eqv. Damage Energy [MeV-mb]
492	2.0000E-07	2.1000E-07	7.487649	0.2360774	0.495949134
493	1.9000E-07	2.0000E-07	7.521247	0.2423487	0.508440696
494	1.8000E-07	1.9000E-07	7.557612	0.2491638	0.521947956
495	1.7000E-07	1.8000E-07	7.597097	0.2565808	0.53662167
496	1.6000E-07	1.7000E-07	7.640021	0.2647206	0.552599715
497	1.5000E-07	1.6000E-07	7.687202	0.2724645	0.570120868
498	1.4250E-07	1.5000E-07	7.732065	0.2797115	0.586809281
499	1.3500E-07	1.4250E-07	7.774059	0.2875555	0.602415444
500	1.2750E-07	1.3500E-07	7.819452	0.2961241	0.619290156
501	1.2000E-07	1.2750E-07	7.869143	0.3038361	0.637755684
502	1.1500E-07	1.2000E-07	7.913815	0.3105023	0.654351306
503	1.1000E-07	1.1500E-07	7.952481	0.3176273	0.668726847
504	1.0500E-07	1.1000E-07	7.993825	0.3252762	0.684063222
505	1.0000E-07	1.0500E-07	8.038158	0.3326743	0.700537189
506	9.6000E-08	1.0000E-07	8.081022	0.3396743	0.716479453
507	9.2000E-08	9.6000E-08	8.121616	0.3471334	0.731556299
508	8.8000E-08	9.2000E-08	8.164869	0.3551042	0.747620218
509	8.4000E-08	8.8000E-08	8.211142	0.3636629	0.764769011
510	8.0000E-08	8.4000E-08	8.260763	0.3728654	0.783205675
511	7.6000E-08	8.0000E-08	8.314234	0.3827968	0.803023241
512	7.2000E-08	7.6000E-08	8.37187	0.3921232	0.824424465
513	6.9000E-08	7.2000E-08	8.42601	0.4006919	0.844497029
514	6.6000E-08	6.9000E-08	8.475761	0.4098864	0.86295063
515	6.3000E-08	6.6000E-08	8.529251	0.4197548	0.882768195
516	6.0000E-08	6.3000E-08	8.586579	0.4294252	0.904011746
517	5.7500E-08	6.0000E-08	8.642828	0.4388666	0.924842863
518	5.5000E-08	5.7500E-08	8.697666	0.4489419	0.94516613
519	5.2500E-08	5.5000E-08	8.756334	0.459761	0.966870061
520	5.0000E-08	5.2500E-08	8.81929	0.4714139	0.990164568
521	4.7500E-08	5.0000E-08	8.887075	0.4839904	1.01525241
522	4.5000E-08	4.7500E-08	8.960347	0.4976237	1.042357813
523	4.2500E-08	4.5000E-08	9.039717	0.5124318	1.071714545
524	4.0000E-08	4.2500E-08	9.125975	0.5269598	1.103601459
525	3.8000E-08	4.0000E-08	9.210712	0.5410071	1.134882722
526	3.6000E-08	3.8000E-08	9.29273	0.556244	1.165138508
527	3.4000E-08	3.6000E-08	9.381657	0.5728545	1.197955484
528	3.2000E-08	3.4000E-08	9.478641	0.5910415	1.233727002
529	3.0000E-08	3.2000E-08	9.584871	0.6110731	1.272894835
530	2.8000E-08	3.0000E-08	9.702055	0.6274247	1.316042689
531	2.7000E-08	2.8000E-08	9.79764	0.6422327	1.351254118
532	2.5500E-08	2.7000E-08	9.884268	0.6613496	1.383152958

Energy Bin #	Lower Energy Bound [MeV]	Upper Energy Bound [MeV]	Total Cross Section [b]	NRT Damage Energy [MeV-mb]	1-MeV(GaAs)-Eqv. Damage Energy [MeV-mb]
533	2.4000E-08	2.5500E-08	9.996325	0.6786619	1.424311875
534	2.3000E-08	2.4000E-08	10.09766	0.6935798	1.461605271
535	2.2000E-08	2.3000E-08	10.1854	0.7095195	1.493723328
536	2.1000E-08	2.2000E-08	10.27868	0.7266219	1.528057173
537	2.0000E-08	2.1000E-08	10.37917	0.745017	1.564894959
538	1.9000E-08	2.0000E-08	10.48719	0.7648796	1.60449908
539	1.8000E-08	1.9000E-08	10.60382	0.7864648	1.647272428
540	1.7000E-08	1.8000E-08	10.73063	0.8098914	1.693728099
541	1.6000E-08	1.7000E-08	10.86887	0.8356335	1.744266362
542	1.5000E-08	1.6000E-08	11.02069	0.8602689	1.799667238
543	1.4250E-08	1.5000E-08	11.16516	0.8832037	1.852616413
544	1.3500E-08	1.4250E-08	11.30095	0.907962	1.902007781
545	1.2750E-08	1.3500E-08	11.44712	0.9350986	1.955548532
546	1.2000E-08	1.2750E-08	11.60776	0.9596041	2.013904427
547	1.1500E-08	1.2000E-08	11.75271	0.9807314	2.066624604
548	1.1000E-08	1.1500E-08	11.87736	1.003266	2.112130891
549	1.0500E-08	1.1000E-08	12.01091	1.027462	2.160623206
550	1.0000E-08	1.0500E-08	12.15446	1.050723	2.212735587
551	9.6000E-09	1.0000E-08	12.2924	1.072884	2.263002154
552	9.2000E-09	9.6000E-09	12.42436	1.096446	2.310597564
553	8.8000E-09	9.2000E-09	12.56421	1.12165	2.361421834
554	8.4000E-09	8.8000E-09	12.71405	1.148722	2.415723047
555	8.0000E-09	8.4000E-09	12.87549	1.177811	2.473945599
556	7.6000E-09	8.0000E-09	13.04873	1.20924	2.53665268
557	7.2000E-09	7.6000E-09	13.23606	1.238889	2.604292744
558	6.9000E-09	7.2000E-09	13.41339	1.265969	2.668140041
559	6.6000E-09	6.9000E-09	13.57533	1.295132	2.7265248
560	6.3000E-09	6.6000E-09	13.74957	1.32634	2.789239037
561	6.0000E-09	6.3000E-09	13.9362	1.357015	2.856361472
562	5.7500E-09	6.0000E-09	14.12013	1.386831	2.922524981
563	5.5000E-09	5.7500E-09	14.29947	1.418711	2.986763482
564	5.2500E-09	5.5000E-09	14.491	1.452904	3.055348159
565	5.0000E-09	5.2500E-09	14.69642	1.489724	3.129030411
566	4.7500E-09	5.0000E-09	14.91815	1.5295	3.208420897
567	4.5000E-09	4.7500E-09	15.15796	1.57257	3.294022933
568	4.2500E-09	4.5000E-09	15.41836	1.619522	3.386738197
569	4.0000E-09	4.2500E-09	15.70176	1.665469	3.487881036
570	3.8000E-09	4.0000E-09	15.98006	1.709879	3.586841245
571	3.6000E-09	3.8000E-09	16.24946	1.758083	3.682480994
572	3.4000E-09	3.6000E-09	16.54235	1.810584	3.786219136
573	3.2000E-09	3.4000E-09	16.86184	1.868065	3.899226896

Energy Bin #	Lower Energy Bound [MeV]	Upper Energy Bound [MeV]	Total Cross Section [b]	NRT Damage Energy [MeV-mb]	1-MeV(GaAs)-Eqv. Damage Energy [MeV-mb]
574	3.0000E-09	3.2000E-09	17.21181	1.931429	4.023061932
575	2.8000E-09	3.0000E-09	17.59908	1.983415	4.159515671
576	2.7000E-09	2.8000E-09	17.91747	2.030062	4.271585973
577	2.5500E-09	2.7000E-09	18.20346	2.090726	4.372008425
578	2.4000E-09	2.5500E-09	18.57603	2.145641	4.502620349
579	2.3000E-09	2.4000E-09	18.91381	2.192799	4.620930826
580	2.2000E-09	2.3000E-09	19.2047	2.243245	4.722514962
581	2.1000E-09	2.2000E-09	19.5159	2.29733	4.831093056
582	2.0000E-09	2.1000E-09	19.85038	2.355365	4.947590639
583	1.9000E-09	2.0000E-09	20.20955	2.418147	5.072480016
584	1.8000E-09	1.9000E-09	20.59922	2.486329	5.207867487
585	1.7000E-09	1.8000E-09	21.02287	2.560499	5.354649956
586	1.6000E-09	1.7000E-09	21.48571	2.641867	5.514358843
587	1.5000E-09	1.6000E-09	21.99423	2.719776	5.689591836
588	1.4250E-09	1.5000E-09	22.48186	2.792316	5.857480219
589	1.3500E-09	1.4250E-09	22.9379	2.870785	6.013637264
590	1.2750E-09	1.3500E-09	23.43143	2.956542	6.182622925
591	1.2000E-09	1.2750E-09	23.97205	3.034151	6.367228108
592	1.1500E-09	1.2000E-09	24.46328	3.100894	6.534522529
593	1.1000E-09	1.1500E-09	24.88623	3.172164	6.678108578
594	1.0500E-09	1.1000E-09	25.33878	3.248634	6.831710872
595	1.0000E-09	1.0500E-09	25.82581	3.322394	6.996333659
596	9.6000E-10	1.0000E-09	26.29585	3.392395	7.155305461
597	9.2000E-10	9.6000E-10	26.74321	3.466965	7.305997581
598	8.8000E-10	9.2000E-10	27.22065	3.546623	7.466589062
599	8.4000E-10	8.8000E-10	27.73177	3.63219	7.63819865
600	8.0000E-10	8.4000E-10	28.28179	3.724185	7.82244841
601	7.6000E-10	8.0000E-10	28.87469	3.823498	8.020550118
602	7.2000E-10	7.6000E-10	29.51588	3.917353	8.234512272
603	6.9000E-10	7.2000E-10	30.12317	4.00311	8.436647671
604	6.6000E-10	6.9000E-10	30.67939	4.095135	8.621183677
605	6.3000E-10	6.6000E-10	31.27759	4.193838	8.819476216
606	6.0000E-10	6.3000E-10	31.92048	4.290913	9.031961815
607	5.7500E-10	6.0000E-10	32.55367	4.385277	9.241036308
608	5.5000E-10	5.7500E-10	33.17046	4.48608	9.444266601
609	5.2500E-10	5.5000E-10	33.83115	4.594221	9.661305905
610	5.0000E-10	5.2500E-10	34.54062	4.710679	9.894322538
611	4.7500E-10	5.0000E-10	35.30677	4.836425	10.14508407
612	4.5000E-10	4.7500E-10	36.1355	4.972628	10.41594489
613	4.2500E-10	4.5000E-10	37.0354	5.121028	10.70929991
614	4.0000E-10	4.2500E-10	38.01789	5.266379	11.02898008

Energy Bin #	Lower Energy Bound [MeV]	Upper Energy Bound [MeV]	Total Cross Section [b]	NRT Damage Energy [MeV-mb]	1-MeV(GaAs)-Eqv. Damage Energy [MeV-mb]
615	3.8000E-10	4.0000E-10	38.98218	5.406851	11.3419096
616	3.6000E-10	3.8000E-10	39.91628	5.55915	11.64439589
617	3.4000E-10	3.6000E-10	40.93125	5.725155	11.97251794
618	3.2000E-10	3.4000E-10	42.0395	5.906986	12.32994926
619	3.0000E-10	3.2000E-10	43.2556	6.107272	12.72150833
620	2.8000E-10	3.0000E-10	44.59848	6.271938	13.1529153
621	2.7000E-10	2.8000E-10	45.70383	6.419408	13.50755572
622	2.5500E-10	2.7000E-10	46.69582	6.611187	13.82501747
623	2.4000E-10	2.5500E-10	47.9882	6.784869	14.23813329
624	2.3000E-10	2.4000E-10	49.16074	6.934049	14.61216214
625	2.2000E-10	2.3000E-10	50.16842	7.093516	14.93341905
626	2.1000E-10	2.2000E-10	51.24757	7.264521	15.27692209
627	2.0000E-10	2.1000E-10	52.40591	7.44801	15.6451783
628	1.9000E-10	2.0000E-10	53.65032	7.646637	16.04029159
629	1.8000E-10	1.9000E-10	54.99889	7.862188	16.46809663
630	1.7000E-10	1.8000E-10	56.46564	8.096955	16.9324148
631	1.6000E-10	1.7000E-10	58.06334	8.354325	17.43779743
632	1.5000E-10	1.6000E-10	59.81699	8.6003	17.99175848
633	1.4250E-10	1.5000E-10	61.49936	8.829678	18.52189667
634	1.3500E-10	1.4250E-10	63.06638	9.07778	19.01693148
635	1.2750E-10	1.3500E-10	64.76365	9.349107	19.55102703
636	1.2000E-10	1.2750E-10	66.62017	9.594771	20.13462892
637	1.1500E-10	1.2000E-10	68.30396	9.805564	20.66331202
638	1.1000E-10	1.1500E-10	69.7517	10.03107	21.11837727
639	1.0500E-10	1.1000E-10	71.29883	10.27283	21.60332189
640	1.0000E-10	1.0500E-10	72.95992	336.1373	22.12437413

DISTRIBUTION

Email—Internal

Name	Org.	Sandia Email Address
Michael Gregson	00512	mwgregs@sandia.gov
Daniel Dorsey	00513	djdorse@sandia.gov
Patrick Griffin	01000	pjgriff@sandia.gov
J. Charles Barbour	01300	jcbarbo@sandia.gov
E. Frederick Hartman	01340	efhart@sandia.gov
Bryan Oliver	01340	bvolive@sandia.gov
Joseph Castro	01341	jpcastr@sandia.gov
Donald Bruss	01341	dbruss@sandia.gov
K. Russell DePriest	01341	krdepris@sandia.gov
Michael McLain	01343	mlmclai@sandia.gov
Jeffrey Black	01343	jefblac@sandia.gov
James Bryson	01344	jwbryso@sandia.gov
Dolores Black	01344	dablack@sandia.gov
J. Kyle McDonald	01344	jkmcdon@sandia.gov
Arlen Heger	01354	aheger@sandia.gov
Biliana Paskaleva	01356	bspaska@sandia.gov
Matthew Burger	01380	mjburge@sandia.gov
William Martin	01384	wjmarti@sandia.gov
Andrew Tonigan	01384	amtonig@sandia.gov
David Epp	01390	dsepp@sandia.gov
Edward Bielejec	01866	esbiele@sandia.gov
Rodney Keith	08841	rlkeithsandia.gov
Technical Library	01177	libref@sandia.gov

This page left blank

This page left blank

Sandia National Laboratories

Sandia National Laboratories is a multimission laboratory managed and operated by National Technology & Engineering Solutions of Sandia LLC, a wholly owned subsidiary of Honeywell International Inc. for the U.S. Department of Energy's National Nuclear Security Administration under contract DE-NA0003525.